A mining research contract report
SEPTEMBER 1983

ADAPTIVE-NOISE-CANCELLATION TECHNIQUES FOR THROUGH-THE-EARTH ELECTROMAGNETICS

VOLUME II

Contract No. J0318070

Green Mountain Radio Research Company

Bureau of Mines Open File Report 189-84

BUREAU OF MINES
UNITED STATES DEPARTMENT OF THE INTERIOR

REPORT DOCUMENTATION PAGE	1. REPORT NO. BuMines OFR 189-84	2.	3. Recipient's Accession No. PB85 111409
4. Title and Subtitle Adaptive-Noise-Cancellation Techniques for Through-the-Earth Electromagnetics. Volume II			5. Report Date Sept. 1983 6.
7. Author(s) Frederick H. Raab			8. Performing Organization Rept. No.
9. Performing Organization Name and Address Green Mountain Radio Research Co. 50 Vermont Ave., Fort Ethan Allen Winooski, VT 05404			10. Project/Task/Work Unit No. 11. Contract(C) or Grant(G) No. (C) J0318070 (G)
12. Sponsoring Organization Name and Address Office of Assistant Director--Mining Research Bureau of Mines U.S. Department of the Interior Washington, DC 20241			13. Type of Report & Period Covered Contract research, 6/4/82--6/30/83 14.

15. Supplementary Notes
Supplements BuMines OFR 175-82 (PB 83-1227454).
Approved for release August 9, 1984.

16. Abstract (Limit: 200 words)

An electromagnetic (EM) system to locate trapped miners at coal mine depths was investigated. The use of such a system in deep mines requires transmission at extremely low frequencies (ELF) and a reduction in the effective noise level beyond that which can be obtained by acceptable integration times. Automatic-noise-cancellation (ANC) techniques reduce the effective noise level by combining several received signals that contain correlated noise. The signals can be obtained either from a remote magnetic antenna or a local electric antenna. This report presents the results of a simulation of the use of ANC techniques in a through-the-earth EM system. A multicomponent ELF noise model that incorporates impulsivity, direction of arrival, and ground characteristics was developed. Nonlinear processors (NLP) for ELF noise were compared and the adaptive clipper was found to be preferable. Direct-matrix-inversion (DMI) and least-mean-square ANC techniques were compared and the DMI algorithm was preferable. The performance of the combined NLP-ANC system was evaluated by simulation and effective noise reductions between 5 and 30 dB were obtained for typical ELF-noise conditions. While improvements of the individual systems were not additive, maximum noise reduction was obtained when both were included.

17. Document Analysis a. Descriptors
Mining research
Electromagnetic direction finding
Trapped-miner location
Trapped-miner communications
Near-field location systems
Adaptive noise cancellation
Extremely low-frequency noise
Adaptive clipper
Nonlinear processing

b. Identifiers/Open-Ended Terms

c. COSATI Field/Group 08I

18. Availability Statement	19. Security Class (This Report)	21. No. of Pages
Release unlimited by NTIS.	Unclassified	121
	20. Security Class (This Page) Unclassified	22. Price

(See ANSI-Z39.18) See Instructions on Reverse OPTIONAL FORM 272 (4-77) (Formerly NTIS-35) Department of Commerce

DISCLAIMER NOTICE

The views and conclusions contained in this document are those of the author and should not be interpreted as necessarily representing the official policies or recommendations of the Interior Department's Bureau of Mines or of the U.S. Government.

FOREWARD

This report was prepared by Green Mountain Radio Research Company, Winooski, Vermont under contract J0318070. This contract was initiated under the Coal Mine Health and Safety Program. It was administered under the technical direction of the U.S. Bureau of Mines with Steve Shope and Harry Dobroski acting as Technical Project Officers. Karen Hatters was the contract administrator for the Bureau of Mines. This report is a summary of the work recently completed as a part of this contract during the period June 1982 to June 1983. This report was submitted by the author in September 1983.

The manuscript and artwork were prepared by Patricia L. Scott.

CONTENTS

ILLUSTRATIONS

PAGE

TABLES

CHAPTER 1. INTRODUCTION

1.1 BACKGROUND

Electromagnetic (EM) techniques and apparatus for the subsurface location of trapped mine workers have been developed during the past decade. The "first-generation" system [1 - 4] transmits signals in the 600 - 3000 Hz range to maximize the signal-to-noise ratio. Physical movement of the receiver and detection by human ear is required, and the accuracy can be degraded by irregularities in the conducting ground.

The elements of the "second-generation" EM location system [5] are shown in Figure 1-1. The subsurface beacon transmitter is similar to that of the first-generation system, but uses a lower transmitting frequency. Uplink signals are received by three three-axis magnetic-field antennas (called "search coils"). The amplitudes of the nine field components are forwarded to a computer in the electronics van. The computer processes the signals and determines the position of the subsurface transmitter. Note that the requirements for physical movement and detection by human ear are eliminated by this system.

The deep-mine (1-km depth) application of electromagnetic (EM) trapped-miner location techniques [5] and the desire to reduce the effects of the conducting ground [6 - 9] mandate the use of lower uplink frequencies. At such frequencies (1 - 30 Hz), the ambient-noise levels [5,7,10] are considerably greater than those in the 600-to-3000-Hz band used by the first-generation EM location system. However, intrinsic-safety considerations prevent significant increases in the output of the beacon transmitter, and the link analysis [5] clearly shows that simple signal integration alone does not produce adequate signal-to-noise ratio in an acceptable length of time.

The primary receiving antenna is a three-axis magnetic-field sensor, and receives both the uplink signal and noise. Since the uplink signal is a quasi-static magnetic field, it decays very rapidly and has an insignificant associated electric field. In contrast, propagating atmospheric-noise fields decay very slowly and include both electric- and magnetic-field components. An electric-field antenna or a remote magnetic-field sensor therefore receives the atmospheric noise, but not the beacon signal.

Since the noises received by the primary and reference antennas are in general highly correlated, significant improvement in the signal-to-noise ratio (SNR) can be achieved by combining their outputs. Since the correlation characteristics of the antenna outputs change with time and are therefore not known *a priori*, an adaptive-noise-cancellation (ANC) algorithm is required to combine the outputs to obtain a signal with minimum noise.

A preliminary investigation of ANC techniques for through-the-earth (TTE) EM systems was conducted during Phase I of this program [11]. This report presents the results of Phase II, in which candidate techniques were evaluated and compared by simulation.

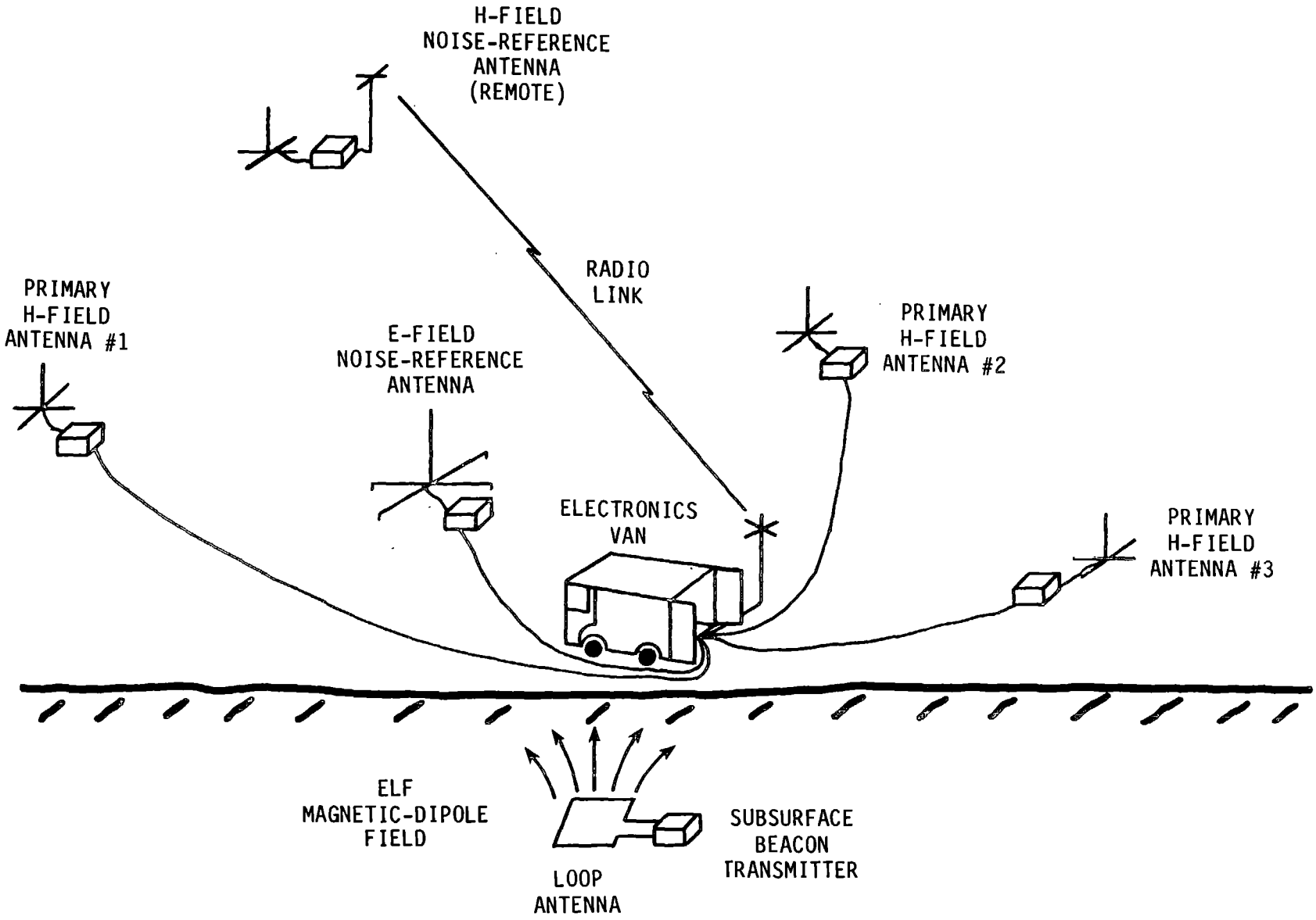

Figure 1-1. Elements of electromagnetic location system.

1.2 ANC CONCEPT

A simplified example of an automatic-noise-cancellation technique is shown in Figure 1-2. The output of the primary receiving antenna is represented by x and contains the desired signal corrupted by a significant amount of noise. The signal-to-noise ratio (SNR) in this example is about -10 dB.

Waveform y represents the output of a noise-reference antenna; in the present application, this antenna could be either a remote magnetic-field sensor or a local electric-field sensor. This received signal contains little or nothing of the desired signal, but contains noise that is highly correlated with that in the output of the primary antenna (e.g., $a \approx 1$ and $b \ll 1$).

The output signal z is a linear combination of the primary and noise-reference signals. If the constant c is set properly, much of the noise is cancelled, producing the +10 dB SNR shown in Figure 1-2b.

In general, the noise statistics (hence constant c) are not known *a priori* and are time varying. It is therefore necessary to use an adaptive technique to set the value of c for maximum noise cancellation. A variety of such techniques have been developed for other applications [1].

The transmitters in through-the-earth electromagnetic systems use electrically small loop antennas and can therefore be regarded as magnetic-dipole sources. The use of extremely low excitation frequencies to reduce the effects of the conducting ground also guarantees that the electric field produced by the subsurface transmitter will be negligible within its region of operation. Consequently, the field produced is essentially a pure quasi-static magnetic dipole field having a free-space structure with an inverse-distance-cubed amplitude variation.

Atmospheric noise at extremely low frequencies is produced primarily by thunderstorms. Nearby thunderstorms produce distinct noise impulses, while the aggregate of distant thunderstorms produces a Gaussian background noise. Since much of the received noise power is contained in the impulses, it is necessary to include processing that edits (blanks) or cancels individual impulses.

Because the attenuation rates for ELF signals are very low (e.g., 0.2 dB/Mm), most of the received noise power (especially after editing) is due to distant sources. Since the wavelengths of the signals of interest are 6 Mm (3600 mi) or more, noise waveforms tend to be similar at points separated by significant distance (15 km). The primary causes of differences in the noise waveforms are local geological features (e.g., changes in ground conductivity). Nonetheless, noise waveforms with correlations from 0.9 to 0.9999 (10 to 40 dB) can be found at sites separated by as much as 15 km. (This correlation is the basis of remote-reference magnetotellurics). Since the amplitude of the desired signal decreases by 60 dB as distance is increased from 1 km to 10 km, it is apparent that a remote magnetic-field sensor can provide an essentially signal-free source of correlated noise.

A propagating electromagnetic signal contains both electric and magnetic-

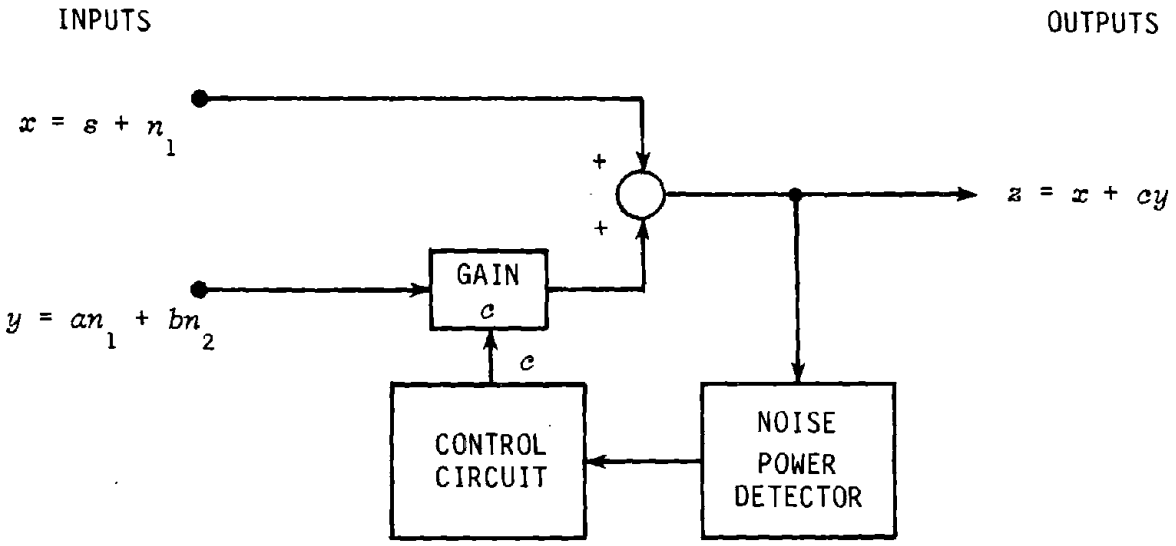

(a) Block diagram

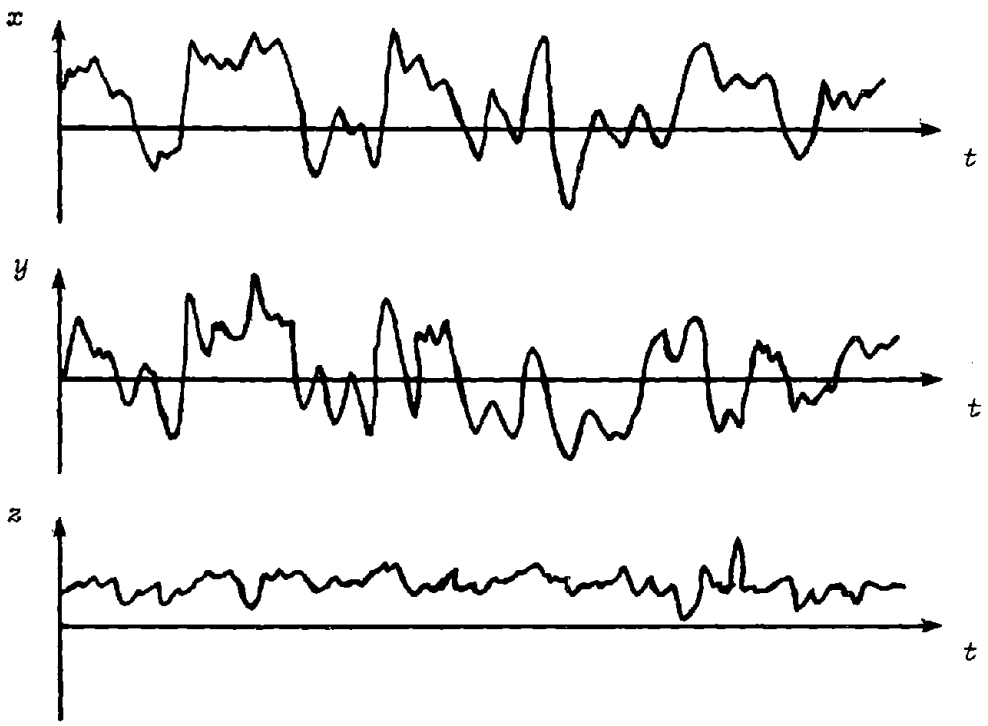

(b) Waveforms

Figure 1-2. Example adaptive noise-reduction technique.

field components, which are related by the free-space impedance (377 Ω). Propagation over conducting ground produces the well-known phenomenon called "E-field tilt," which causes the electric-field to tilt in the direction of propagation. This implies that the horizontal electric-field components are strongly correlated with the opposite horizontal magnetic-field components. Since the beacon transmitter produces little, if any, electric field, it is apparent that a local electric-field antenna can also be used as a source of correlated noise. The magnetotelluric technique for geophysical prospecting is based upon this phenomenon. A noise-cancellation technique based upon electric- and magnetic-field correlation has been proposed for use with trolley phones [12].

1.3 PHASE-I RESULTS

The objective of Phase I was to conduct a preliminary investigation and feasibility assesment of ANC techniques for TTE EM systems [1]. The two principal areas of investigation were:

- ELF-noise characteristics, and
- ANC algorithms.

Phase I work also included analysis of correlation estimators.

The TTE EM location system involves reception of all three magnetic-field components and (if ANC is used) possibly all three electric-field components. The incident field includes the vertical electric and horizontal magnetic components. The Field-Lewinstein-Modestino model represents single-channel ELF noise as the sum of Gaussian and power-Rayleigh random-variables. Direction-of-arrival characteristics are accommodated by using multiple noise sources positioned to correspond to the major thunderstorm areas of the world. Horizontal-electric and vertical-magnetic field components are generated by a "geology filter" that accounts for the electromagnetic characteristics of the ground.

The limited amount of published empirical data for the frequencies of interest show correlations of both the electric- and magnetic-field components ranging from 0.9 to 0.9999. These correlation levels suggest the possibility of noise reductions from 10 to 40 dB through ANC.

Candidate ANC algorithm including direct-matrix-inversion (DMI), gradient (least-mean-square - LMS), and recursive (Kalman-filter) techniques are identified. The DMI and LMS techniques have the most potential in the TTE EM application.

1.4 PHASE-II OBJECTIVES AND ORGANIZATION

The objectives of Phase II are a thorough comparison and evaluation by simulation of ANC techniques for the TTE EM application. The specific areas of investigation include:

- The Field-Lewinstein-Modestino (FLM) ELF-noise model,
- Direction-of-arrival (DOA) characteristics,
- The geology filter,
- Effects of reception bandwidth,
- Nonlinear-processing techniques,
- ANC algorithms, and
- The combination of nonlinear processing and ANC.

Chapter 2 develops the basic software for random-noise generation, including subroutines for uniform, Gaussian, and power-Rayleigh random-variables. The Gaussian and power-Rayleigh random variables are obtained by nonlinear transformation of the uniform random variable. Proper operation is verified by moment and histogram tests.

The multicomponent ELF-noise simulation model is developed in Chapter 3. The output from individual noise sources is obtained by summing Gaussian and power-Rayleigh random variables as specified by the FLM model. The vertical-electric-field component is obtained by summing the outputs from several such sources. The horizontal-magnetic-field components are obtained by transforming the outputs of individual sources into X and Y components and then summing the results. The unit-pulse response of a homogeneous ground is derived and used to implement a geology filter. Proper operation is verified by moment, amplitude-histogram, and DOA-histogram tests.

The FLM model characterizes ELF noise by power, impulsivity, and spikiness. However, values of the impulsivity and spikiness parameters are published for only a limited number of bandwidths. The effect of bandwidth upon these parameters is therefore analyzed, and a two-moment method for conversion is shown to be suitable.

A considerable portion of the power in ELF noise is contained in discrete impulses. Nonlinear processing can therefore be used to reduce the effective received noise power. Nonlinear processors based upon editing, clipping, adaptive editing, and adaptive clipping are compared by simulation. The adaptive clipper is found to be most effective and is operable at all signal levels.

Narrowband DMI and LMS ANC algorithms are implemented and compared by simulation with Gaussian noise. In this application, the DMI algorithm must both estimate the noise-covariance matrix and the weighting matrix. Since errors in one estimate produce errors in the other, it is effective to apply the DMI algorithm recursively. (Two iterations are sufficient). The simulations show a gain of 0.1 to produce the greatest noise reduction by the LMS algorithm. The simulations also show the DMI algorithm to produce significantly greater noise reduction than does the LMS algorithm.

The DMI algorithm is modified to operate on complex inputs that represent the narrowband outputs of the nonlinear processor (NLP). The DMI ANC and NLP algorithms are then combined; proper operation of both subsystems is verified by simulation. The combined algorithm is then tested under a variety of conditions. The benefits obtained with one algorithm alone are not additive, but the inclusion of both algorithms is nonetheless desirable. Under typical atmospheric conditions, the total noise reduction ranges from 5 to 30 dB, depending upon the local-noise level.

1.5 REFERENCES

1. H. K. Sacks, "Trapped-miner location and communication systems," *Underground Mine Communications, Part 4, Section-to-Place Communications*, U.S. Bureau of Mines Information Circular 8745, 1977.

2. R. G. Olsen and A. J. Farstad, "Electromagnetic direction finding experiments for location of trapped miners," *IEEE Transactions on Geoscience Electronics*, vol. GE-11, no. 4, pp. 178 - 185, October 1973.

3. J. Durkin, "Assessment of present techniques for the location of trapped miners," *Proceedings of the Fifth WVU Conference on Coal Mine Electrotechnology*, Morgantown, WV, pp. 1-1 - 1-16, July 30 - August 1, 1980.

4. R. Gabillard, J. P. Dubus, and F. Cherperell, "Electromagnetic survey method applicable to underground quarries," *Proceedings of the Thru-the-Earth Electromagnetic Workshop*, Golden, CO, (NTIS PB 231,154), pp. 121 - 129, August 15 - 17, 1973.

5. L. H. Rorden, T. C. Moore, E. C. Fraser, and L. R. Bulduc, "Phase I Development of a system concept for location of trapped miners in deep mines by an electromagnetic method," Phase I Report, contract J0199009, Develco, Inc., Sunnyvale, CA, October 1979.

6. T. W. H. Caffey, "Locating a buried magnetic dipole," *Proceedings of the Electromagnetic Guided Waves Workshop*, Boulder, CO, March 28 - 30, 1978.

7. F. H. Raab and P. K. Hansen, "Electromagnetic retransmission system for locating trapped mine workers," Final Report, contract H0188071, (PB81-215329) Polhemus Navigation Sciences, Inc., Essex Junction, VT, February 1980.

8. F. H. Raab and P. K. Hansen, "Electromagnetic technique for subsurface position determination," *Proceedings of the IEEE Industry Applications Society Annual Meeting*, Philadelphia, PA, pp. 111 - 118, October 5 - 9, 1981.

9. F. H. Raab, "Quasi-static magnetic-field technique for determining position and orientation," *IEEE Transactions on Geoscience and Remote Sensing*, vol.GE-19, no. 4, pp. 235 - 243, October 1981.

10. E. L. Maxwell, "Atmospheric noise from 20 Hz to 30 kHz," *Radio Science*, vol. 2, (new series), no. 6, pp. 637 - 644, June 1967.

11. F. H. Raab, "Adaptive-noise-cancellation techniques for through-the-earth electromagnetics, Volume I," Final Report GMRR-TR82-1, Green Mountain Radio Research Company, Burlington, VT, January 1982.

12. R. L. Lagace, D. A. Curtis, J. D. Foulkes, J. L. Rothery, "Technical service for mine communications research; Transmit antennas for portable VLF to MF wireless mine communications," Contract No. H0346045-Task Order No. 1, Arthur D. Little, Inc., Cambridge, MA, May 1974 - May 1977.

CHAPTER 2. NOISE GENERATORS

This chapter develops software algorithms for the generation of the uniform, Gaussian, and power-Rayleigh random variables that are used in the subsequent atmospheric-noise generators and ANC simulators. The uniform random variable is generated by a shift register, and the Gaussian and power-Rayleigh random variables are obtained from a nonlinear function of the uniform random variable. Satisfactory performance is verified by simulation. Both the uniform and Gaussian random variables developed here are considerably faster than those developed in [1].

2.1 UNIFORM RANDOM-VARIABLE GENERATOR

A random integer with equally likely values in the range of -32767 to +32767 is a satisfactory uniform random variable. A random integer with suitable characteristics is produced by a linear-feedback shift-register generator (LFSRG) based upon a length-32 primitive polynomial [2].

The LFSRG produces a pseudorandom binary sequence of length

$$L_{binary} = 2^{32}-1 = 4,294,967,303 \quad . \tag{1}$$

Random integers are formed from consecutive but nonoverlapping sets of 16 random bits. The number of independent pseudorandom integers is therefore

$$L_{integer} = L_{binary}/16 \cong 2.68 \cdot 10^{8} \quad . \tag{2}$$

Because the length of the binary sequence is not an integer multiple of 16, the sequence of integers does not repeat immediately. However, integers separated in the sequence by $L_{integer}$ will be well correlated with each other. Nonetheless, a total of 268 million random integers is more than sufficient for current simulation needs.

Two integers (four bytes of memory) are used as the shift register (See Appendix B). Prior to shifting, masks are applied to each integer and the number of 1s in the result is counted and saved.

Shifting is accomplished by division by 2. The high bit of each integer is masked to produce a positive number prior to division. The lower integer IR1 is shifted first. The low bit of the higher integer IR2 is then placed in the high bit of IR1. Integer IR2 is then shifted by division by 2.

Feedback is accomplished by setting the high bit of IR2 according to the parity of the total 1s count for the masked original integers. The value of IR1 = 1ØØØØØØØB = 8ØØØH is decoded into -32768 decimal. Since the corresponding positive integer does not exist, a new random integer is computed when this value occurs.

The feedback taps for the LFSRG are derived from the nineteenth length-32 primitive polynomial given by Peterson [2, Appendix C]. Conversion to in-

teger masks is accomplished as follows:

Octal code from [2]	4	1	7	6	0	4	2	7	6	0	7
Corresponding binary code	100	001	111	110	000	100	010	111	110	000	111
Reverse-order binary code	1	1100	0011	1110	1000	1000	0111	1110	0001		
Corresponding hexadecimal code	-	C	3	E	8	8	7	E	1		

$$M1' = 1 \cdot 1 + 14 \cdot 16 + 7 \cdot 256 + 8 \cdot 4096 - 65536 = 34785 - 65536 = -30751 \quad (3)$$

$$M2' = 8 \cdot 1 + 14 \cdot 16 + 3 \cdot 256 + 12 \cdot 4096 - 65536 = 50152 - 65536 = -15384 \quad . \quad (4)$$

Satisfactory performance of the random-integer generator was verified by simulation programs that tested for repetition, compiled histograms, and estimated moments. Typical results are shown in Table 2-1 and Figure 2-1.

2.2 NONLINEAR CONVERSION OF RANDOM VARIABLES

The nonlinear conversion of random variable u into random variable y is

$$y = f(u) \quad , \quad (5)$$

where f is a nonlinear function. The relationship between the p.d.f.s of the two random variables can be found by observing [3] that the corresponding cumulative distributions must be equal; i.e.,

$$\int_{-\infty}^{y} p_y(y')\, dy' = \int_{-\infty}^{u} p_u(u')\, du' \quad . \quad (6)$$

In the present application, $0 \leq u < k$ is a uniform random variable and $y > 0$. For this case, (6) becomes

$$\int_{0}^{y} p_y(y')\, dy' = \int_{0}^{u} p_u(u')\, du' = u/k \quad . \quad (7)$$

In the present application, the p.d.f. of y is known and the nonlinear function $f(u)$ required to convert uniform random variable u into y must be determined. This can be accomplished by inserting $p_y(y)$ into (7) and solving for f. The nonzero uniform random variable u is obtained by taking the absolute value of a random integer generated as described in Section 2.1. If negative values of y are desired, the sign of y is determined from the sign of the random integer from which u is obtained.

Variable	Spikiness	Mean	Variance	Correlation
Uniform	---	.2329E-02	.9928	.9427E-04
		-.9349E-03	1.007	-.9709E-04
		.2329E-02	.9928	.9427E-04
		-.1794E-02	1.012	-.9449E-04
		.2708E-02	.9907	.5671E-04
		.3440E-02	.9909	-.7106E-05
Gaussian	---	-.1048E-01	1.014	-.1155E-03
		-.5752E-02	.9988	.7855E-06
		-.1048E-01	1.014	-.1155E-03
		.4016E-02	1.004	.3518E-04
		.1094E-01	1.002	.4370E-04
		-.6682E-04	1.008	.2339E-04
Power Rayleigh	0.25	.9894E-03	.7668	-.9789E-10
	0.5	.3093E-02	.9616	-.9566E-09
	1.0	-.1031E-01	1.017	-.1062E-07
	2.0	-.9626E-02	1.008	-.9266E-08

True mean = 0.0 and true variance = 1.0 for all tests.
Total number of sample pairs for each test = 10,000.

Table 2-1. Results of moment estimates.

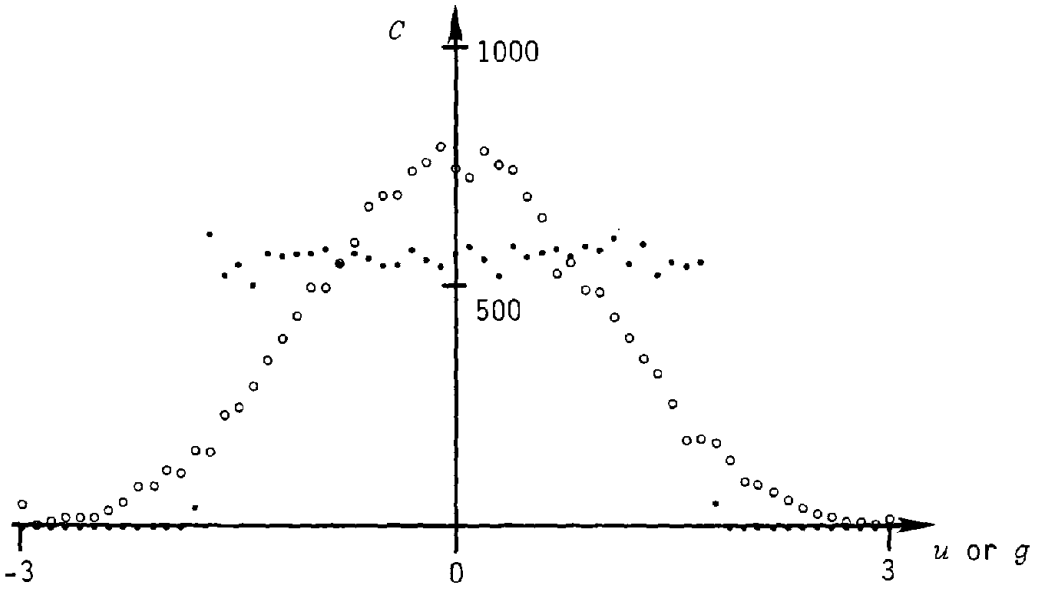

• Uniform ∘ Gaussian

Total number of samples = 20,000

Figure 2-1. Histogram of uniform and Gaussian random variables.

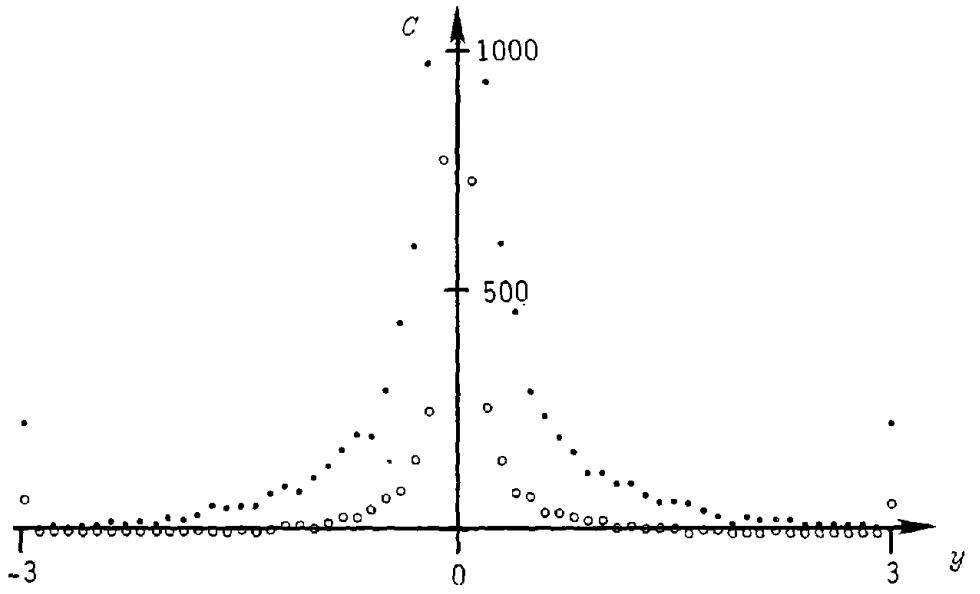

• α = 0.5 ∘ α = 0.25

Total number of samples = 20,000

Figure 2-2. Histogram of power-Rayleigh random variables.

2.3 GAUSSIAN-NOISE GENERATOR

Insertion of a Gaussian p.d.f. [1] with zero mean and unity variance into (7) yields

$$\int_0^g (1/2\pi)^{1/2} \exp(-z^2/2)\, dz = u/k \quad , \tag{8}$$

from which

$$(1/8\pi)^{1/2} \operatorname{erf}(g/2^{1/2}) = u/k \quad . \tag{9}$$

The form of $f(u)$ is therefore an inverse error function.

The inverse error function is readily generated by neither formula nor iteration. Subroutine GAUSS (Appendix B) therefore uses a 28-point conversion table with linear interpolation between points. The required values of u and g are given in a number of references (e.g., [4]). Note that values of u are scaled prior to entry in the table by multiplication by k=32767, which corresponds to the maximum value of a random integer. Finally, g is scaled and translated to obtain the specified mean and variance.

The results of histogram (Figure 2-1) and correlation (Table 2-1) tests show satisfactory performance of subroutine GAUSS.

2.4 POWER-RAYLEIGH-NOISE GENERATOR

The power-Rayleigh random variable is used to generate both wideband impulsive noise and the envelope of narrowband impulsive noise. Setting a=2 produces a conventional Rayleigh random variable. Substitution of its p.d.f. ([1], Chapter 2, (3)) into (7) and imposing $u \geq 0$ and $y \geq 0$ yields

$$u/2k = \int_0^y (a/2R^a)\, z^{a-1} \exp[-(z/R)^a]\, dz \tag{10}$$

$$u/k = \int_0^{y/R} a\, v^{a-1} \exp[-v^a]\, dv \tag{11}$$

$$= \int_0^{(y/R)^a} \exp(-w)\, dw = 1 - \exp[-(y/R)^a] \quad , \tag{12}$$

where

$$w = v^a = (y/R)^a \tag{13}$$

is used to simplify the integral.

Rearrangement of (13) then yields

$$y = f(u) = R[-\ln(1 - u/k)]^{(1/a)} \quad . \tag{14}$$

Subroutine PWRRAY (Appendix B) uses this formula to generate an always-positive power-Rayleigh random variable from a random integer u. Constant k= 32767 corresponds to the maximum value of u, and u=32767 is not used to avoid zero in the argument of the logarithm.

The results of histogram (Figure 2-2) and moment (Table 2-1) tests show satisfactory operation of subroutine PWRRAY. The estimated variance of 0.7668 is not a cause for alarm, as the variance of this estimate increases rapidly as spikiness increases. Similar deviations (both high and low) were observed in other runs.

2.5 REFERENCES

1. F. H. Raab, "Adaptive-noise cancellation techniques for through-the-earth electromagnetics, Volume I," Final Report No. GMRR-TR82-1, Green Mountain Radio Research Company, Burlington, VT, January 1982.

2. W. W. Peterson, *Error Correcting Codes*, New York: John Wiley and Sons, 1961.

3. P. Beckman, *Probability in Communication Engineering*, New York: Harcourt, Brace, and World, Inc., 1967.

4. C. D. Hodgman, Ed., *Standard Mathematical Tables*, Ohio: Chemical Rubber Publishing Company, 1954.

CHAPTER 3. ELF NOISE

Simulation software for generating multicomponent ELF noise fields is developed in this chapter. Impulsive ELF noise is generated by summing Gaussian and power-Rayleigh random variables. Incident noise fields (horizontal magnetic and vertical electric components) are obtained from impulsive noise sources at various azimuths. The remaining field components (horizontal electric and vertical magnetic) are produced by the response of a geology filter to the incident field components.

3.1 WIDEBAND ELF NOISE

Wideband ELF noise is generally regarded as the sum of Gaussian and impulsive components [1]. The Field-Lewinstein-Modestino ELF-noise model [2,3] represents the impulsive component as a two-sided power-Rayleigh random variable and allows adjustment of both impulsivity and impulse energy to fit observed statistics. Furthermore, it is tractable and has been shown to provide a good fit to observed ELF-noise data.

ELF Noise

The Gaussian and power-Rayleigh random variables are obtained from subroutines GAUSS and PWRRAY (Chapter 2). ELF-noise characteristics are most conveniently described in terms of total noise power P_n, impulsivity γ, and the power-Rayleigh p.d.f. shape factor a. However, the noise-generator subroutines require the rms voltage σ_x of the Gaussian noise and the impulse energy R in addition to the shape factor a.

Impulsivity is the ratio of the powers of the Gaussian and power-Rayleigh components. From (4) and (5) of Chapter 2 of [1],

$$\sigma_x^2 = P_n/(1 + \gamma^2) \tag{1}$$

and

$$\sigma_y^2 = \gamma^2 \sigma_x^2 \quad . \tag{2}$$

The relationship among impulsivity, impulse power, and impulse energy is given by (5) of Chapter 2 of [1]. Rearrangement yields

$$R^2 = \sigma_y^2/\Gamma(1 + 2/a) \quad , \tag{3}$$

where $\Gamma(n) = (n - 1)!$ is the well-known Gamma function.

Equations (1) - (3) convert the more convenient specifications to the parameters needed by subroutines GAUSS and PWRRAY, and are implemented in subroutine ELFPRM.

Histograms corresponding to Gaussian, low-level, moderate-level, and high-level noise (Table 3-1) are shown in Figures 3-1 to 3-4. These histo-

Noise Conditions	γ	α	λ, Hz
High-level atmospheric (Saipan)	4.4	0.25	12.8
Moderate-level atmospheric (Malta)	2.6	0.25	10.2
Low-level atmospheric (Norway)	1.2	0.50	8.0
Gaussian	0.0	--	--

Table 3-1. Noise parameters for 300-Hz bandwidth [3].

INDEX	LOCATION	AZIMUTH
1	Africa	45°
2	South America	135°
3	Indonesia	-70°
4	Random	$\psi_{min} < \psi < \psi_{max}$

Table 3-2. Noise sources.

TEST	NOISE-SOURCE PARAMETERS										COMMENTS
	AFRICA 45°		S.A. 135°		INDONESIA -70°		RANDOM				
	P	γ	P	γ	P	γ	P	γ	ψ_{min}	ψ_{max}	
1	0	-	0	-	1.0	4.4	0	-	-	-	Single source, high impulsivity
2	0	-	0	-	0	-	1.0	4.4	-110°	-160°	Single source, random azimuth
3	0	-	0.5	4.4	0.5	4.4	0	-	-	-	Two sources, high impulsivity
4	0.5	4.4	0.5	4.4	0	-	0	-	-	-	Two sources, high impulsivity
5	0.5	4.4	0	-	0.5	4.4	0	-	-	-	Two sources, high impulsivity
6	0.33	4.4	0.33	4.4	0.33	4.4	0	-	-	-	Three sources, high impulsivity
7	0.33	2.6	0.33	2.6	0.33	2.6	0	-	-	-	Three sources, mod. impulsivity
8	0.33	1.2	0.33	1.2	0.33	1.2	0	-	-	-	Three sources, low impulsivity
9	0.33	0	0.33	0	0.33	0	0	-	-	-	Three sources, Gaussian noise
10	0.33	2.6	0.33	1.2	0.33	4.4	0	-	-	-	Three sources, varying impulsivity
11	0.22	2.6	0.07	2.6	0.71	2.6	0	-	-	-	Three sources, 5-dB power variation
12	0.09	2.6	0.01	2.6	0.90	2.6	0	-	-	-	Three sources, 10-dB power variation

Noise Conditions: High level $\gamma = 4.4$, $\alpha = 0.25$
Mod. level $\gamma = 2.6$, $\alpha = 0.25$
Low level $\gamma = 1.2$, $\alpha = 0.5$
Gaussian $\gamma = 0.0$

Table 3-3. Test conditions.

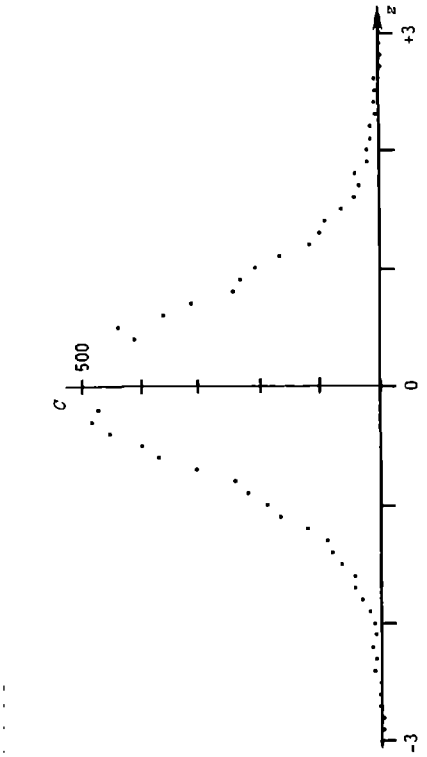

Figure 3-1. Histogram for Gaussian noise.

Figure 3-2. Histogram for low-level atmospheric noise.

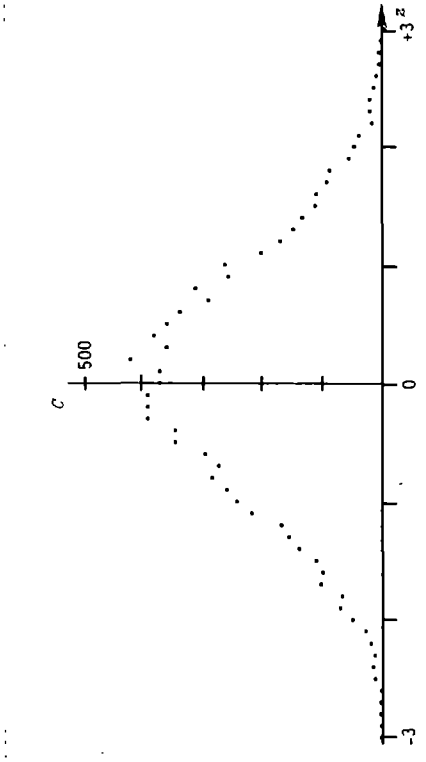

Figure 3-3. Histogram for moderate-level atmospheric noise.

Figure 3-4. Histogram for high-level atmospheric noise.

grams are in good agreement with plots of the corresponding p.d.f.s (Figure 2-5 of [1]). Satisfactory performance was also verified by moment tests.

The incident ELF signals at a given location are the two horizontal magnetic-field components (H_x and H_y) and the vertical electric-field component (E_z). The incident ELF fields are simulated by using the ELF-noise generator described previously to produce noise fields corresponding to several sources of fixed and random azimuths. The operation of the ELF incident-noise generator was tested thoroughly by compiling several statistics, including time series, amplitude histograms, and direction-of-arrival data.

Incident Noise

The noise sources included in the ELF incident-noise generator are listed in Table 3-2. The three fixed-azimuth sources correspond approximately to the earth's three principal areas of thunderstorm activity, as seen from California. The azimuth of the fourth noise source is uniformly distributed between two specified azimuths; a new random azimuth is determined for each noise sample. The noise power P_n, impulsivity γ, and impulse energy a are independently specified for each source, but remain constant throughout a particular simulation.

The total incident fields are the sum of the incident fields from all four noise sources. The magnetic fields are summed according to direction of arrival, as defined in Section 2.3 of [1], thus

$$H_x = - \sum_{i=1}^{4} n_i \sin \psi_i \tag{4}$$

and

$$H_y = + \sum_{i=1}^{4} n_i \cos \psi_i \quad . \tag{5}$$

The vertical electric field has no directionality and is therefore simply

$$E_z = + \sum_{i=1}^{4} n_i \quad . \tag{6}$$

Tests

The test program generates histograms of the amplitudes of all three incident components of the incident ELF noise. The mean and variance (noise power) of each component is also computed. The program optionally allows output of a set of time series (actual samples) of all three components.

The direction of arrival of each noise sample is determined by conventional radio-direction-finding techniques in which the polarity of the vertical electric field is assumed to be the polarity of the noise source. The

estimated direction of arrival is therefore given by

$$\hat{\psi} = \arctan\left[(H_x \operatorname{sgn} E_z)/(H_y \operatorname{sgn} E_z)\right] \quad . \tag{7}$$

The software implementation (subroutine DF) uses the four-quadrant inverse tangent ATAN2, which provides correct quadrant resolution except when $H_x = 0$. In that case, $\psi = 0$ or π, depending upon whether $H_y \operatorname{sgn} E_z$ is positive or negative. If $E_z = 0$ or both $H_x = 0$ and $H_y = 0$, the direction of arrival is indeterminate, which subroutine DF indicates by setting $\hat{\psi} = 10$.

The test program compiles several statistics related to direction of arrival. The most straightforward is a simple histogram of ψ in sectors of 6° widths. Since this histogram gives equal weight to both large and strong signals, additional histograms are compiled for signals exceeding 1, 4, and 9 times the total noise power.

The received energy is also sorted by 6° sectors of the direction of arrival. Since instantaneous electric- and magnetic-field energies are not necessarily the same when there are multiple noise sources [1], they are sorted separately. The power accumulated in each sector is normalized by the number of samples.

Test Results

The performance of the ELF noise generator was evaluated through a set of 12 different tests (Table 3-3) that provide various sources, powers, and impulsivities. Each test included 10,000 samples.

Figure 3-5 presents amplitude histograms for the H_x, H_y, and E_z signals produced in test #6. The statistics of all three incident signals are quite similar.

The time series for two sources with highly impulsive noise (test #3) is shown in Figure 3-6. Each graph depicts 600 sequential noise samples. For a sampling rate of 300 Hz (as in [3]), each graph corresponds to 2-s of data. The rate of impulse occurrence is therefore approximately 10 Hz, which also corresponds to the data [3] from which impulsivity and spikiness parameters were taken.

Direction-of-Arrival Histograms

Direction-of-arrival (DOA) statistics are shown in histogram form in Figures 3-7 - 3-14. The left graph in each figure is a radial histogram of DOA in 6° sectors. The solid dots (.) are histograms of all samples, while the open dots (°) are histograms of those samples exceeding the rms power level (1 σ). The right graph represents the average received magnetic-field energy, again divided into 6° sectors. (In all cases, the received electric-field energy graph was quite similar to the magnetic-field energy graph.)

The DOA data for single sources are not especially interesting, and pri-

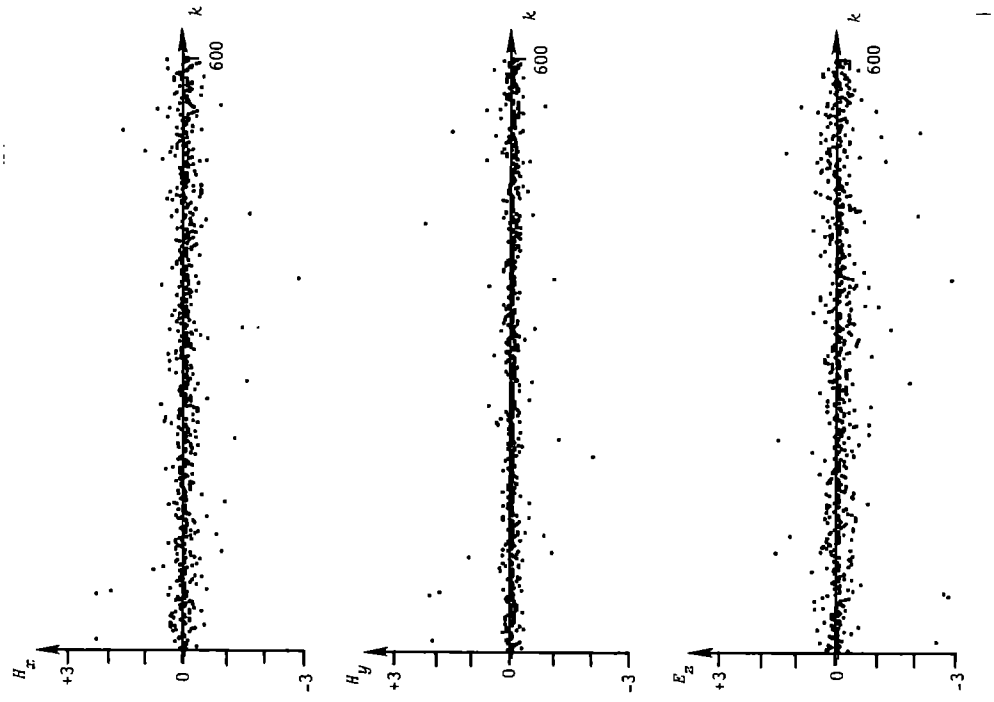

Figure 3-6. Time series for two sources with high impulsivity (Test #3).

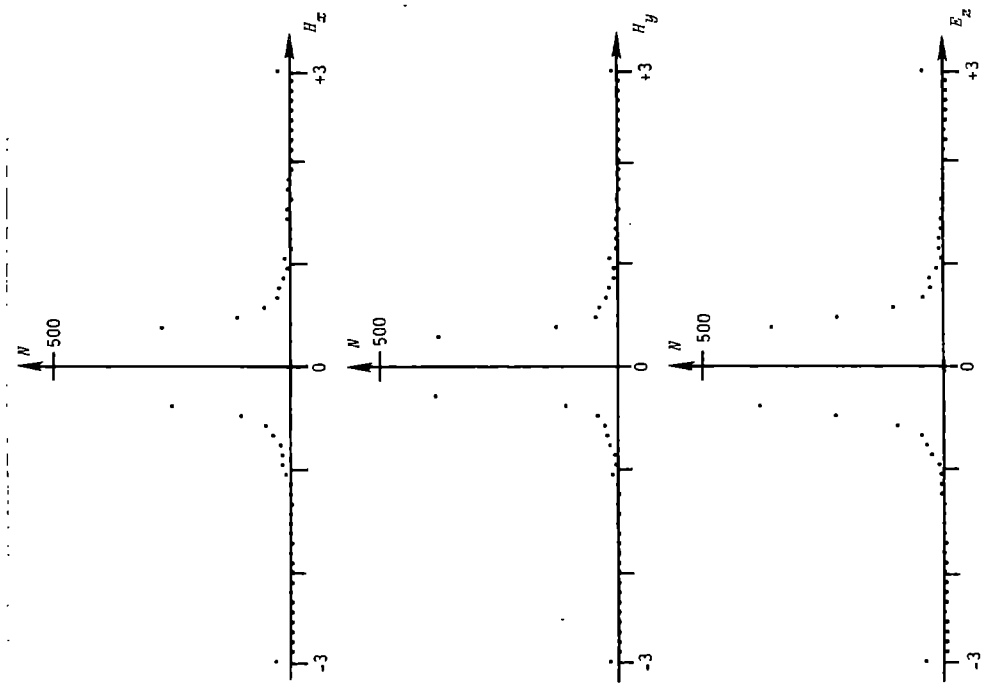

Figure 3-5. Amplitude histograms for three sources with high impulsivity (Test #6).

· All points ° $E > \sigma^2$

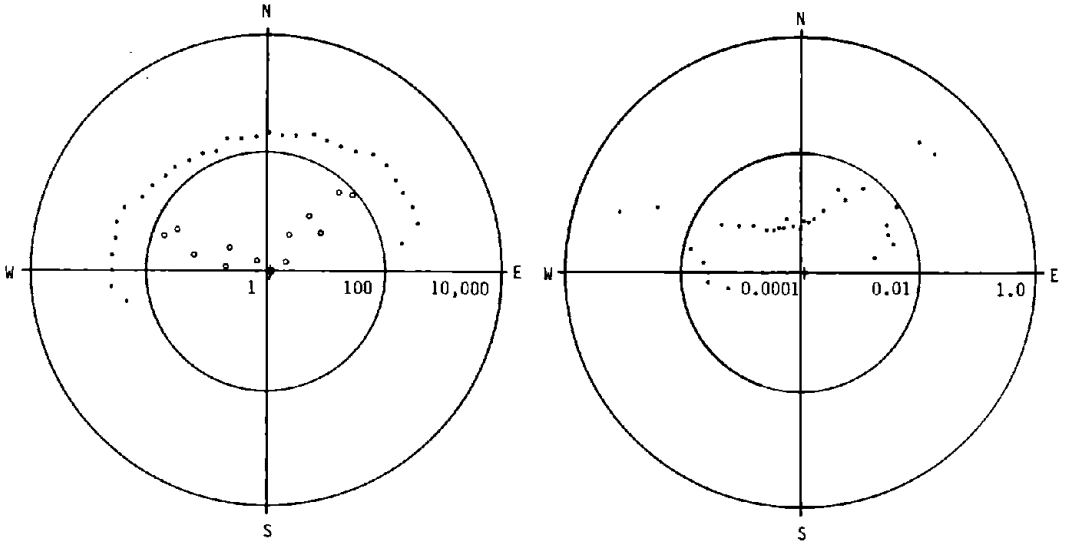

(a) DOA count (b) Magnetic-field energy

Figure 3-7. Directional histograms for two sources with high impulsivity (Test #5).

· All points ° $E > \sigma^2$

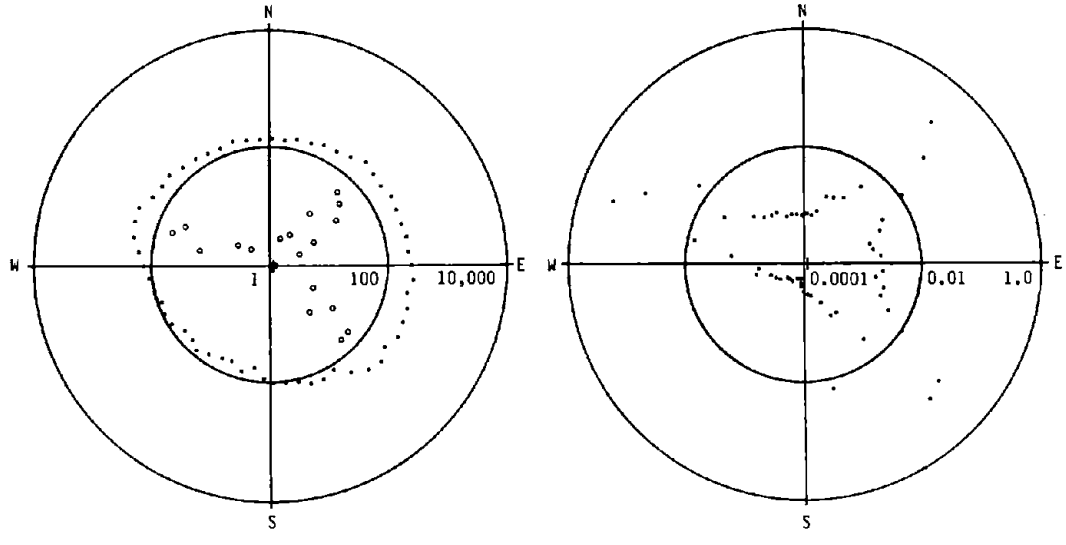

(a) DOA count (b) Magnetic-field energy

Figure 3-8. Directional histograms for three sources with high impulsivity (Test #6).

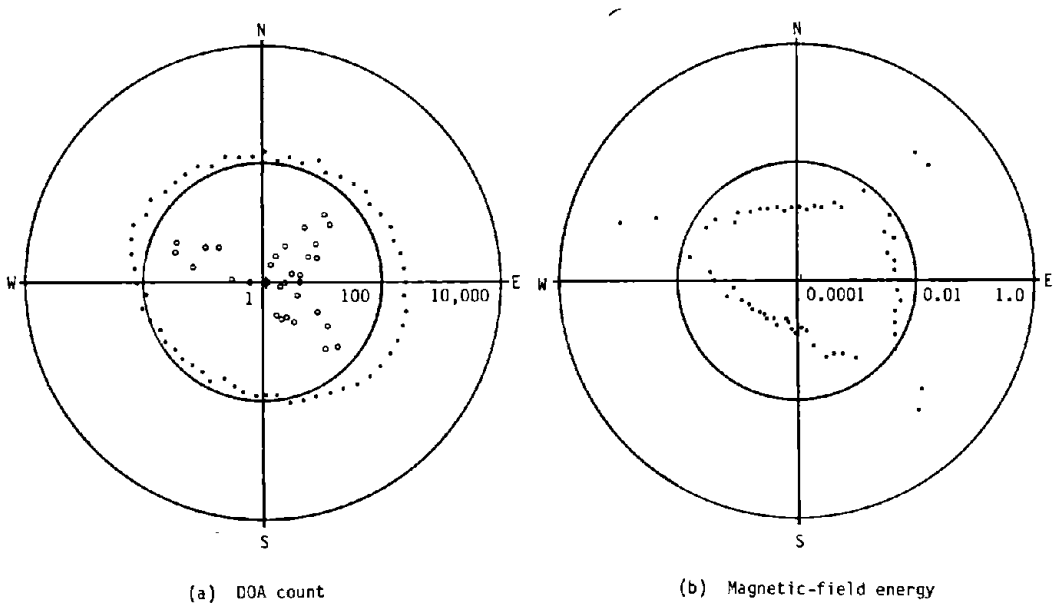

(a) DOA count (b) Magnetic-field energy

Figure 3-9. Directional histograms for three sources with moderate impulsivity (Test #7).

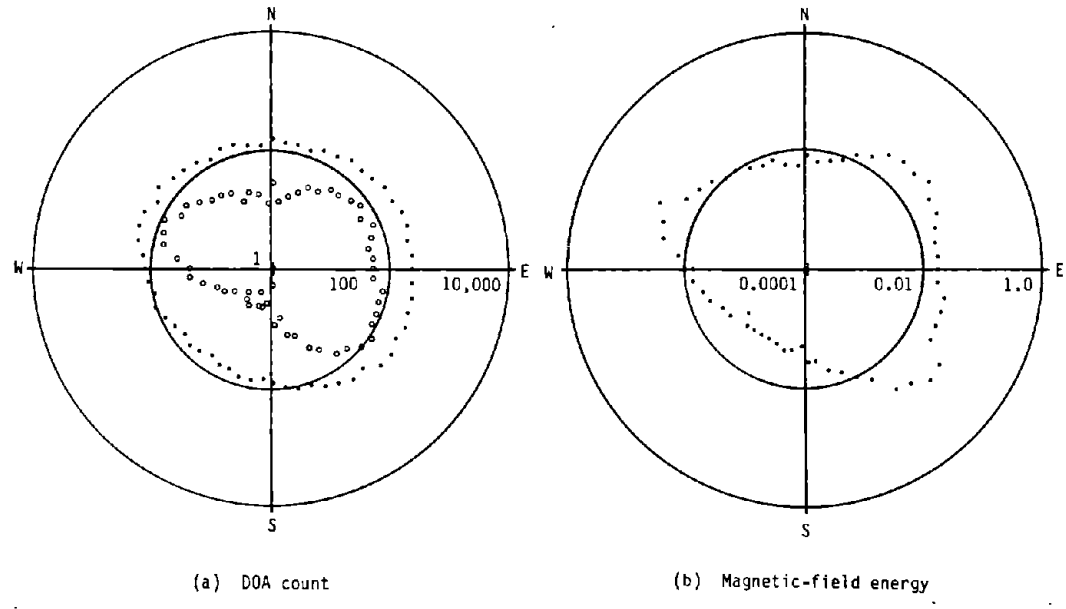

(a) DOA count (b) Magnetic-field energy

Figure 3-10. Directional histograms for three sources with low impulsivity (Test #8).

· All points ° $E > \sigma^2$

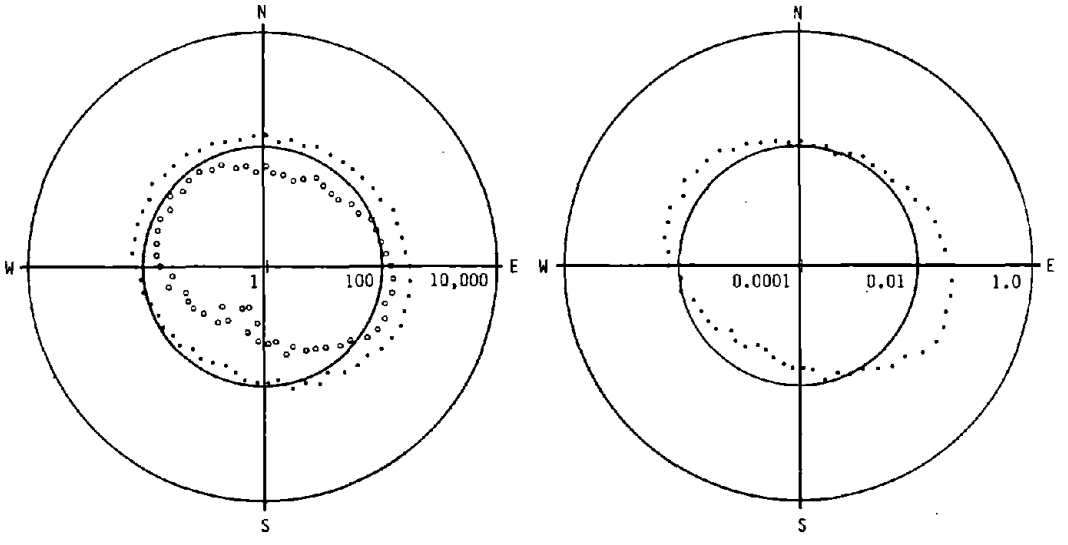

(a) DOA count (b) Magnetic-field energy

Figure 3-11. Directional histograms for three Gaussian sources (Test #9).

· All points ° $E > \sigma^2$

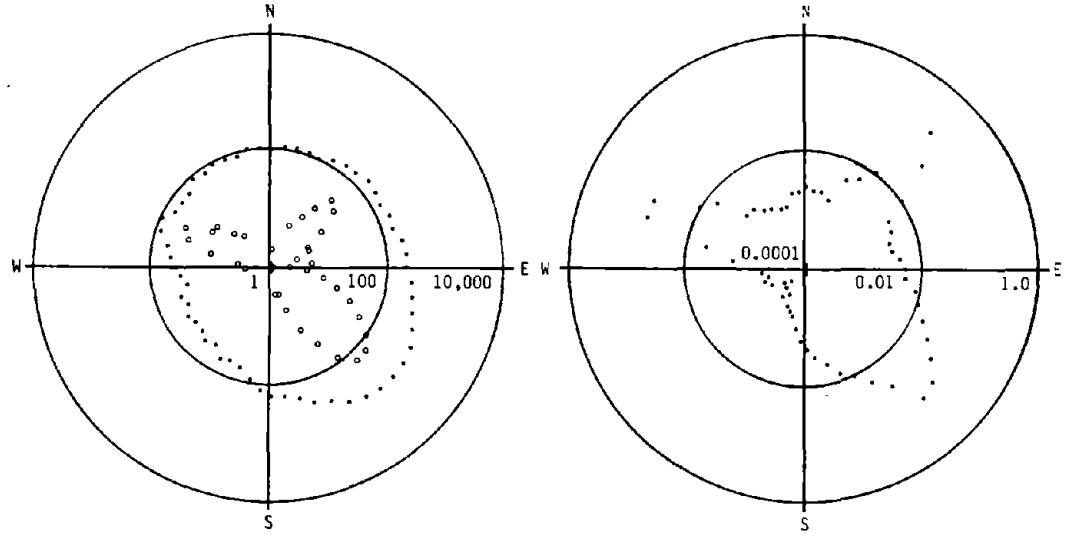

(a) DOA count (b) Magnetic-field energy

Figure 3-12. Directional histograms for three sources with different impulsivities (Test #10).

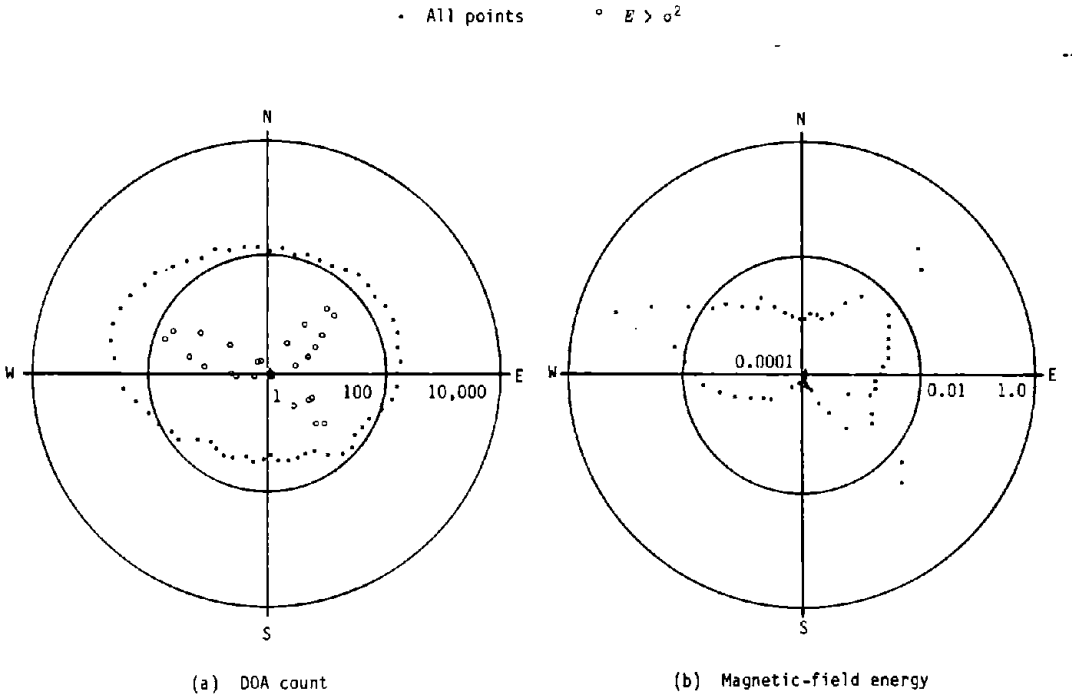

(a) DOA count (b) Magnetic-field energy

Figure 3-13. Directional histograms for three sources with 5-dB difference in power (Test #11).

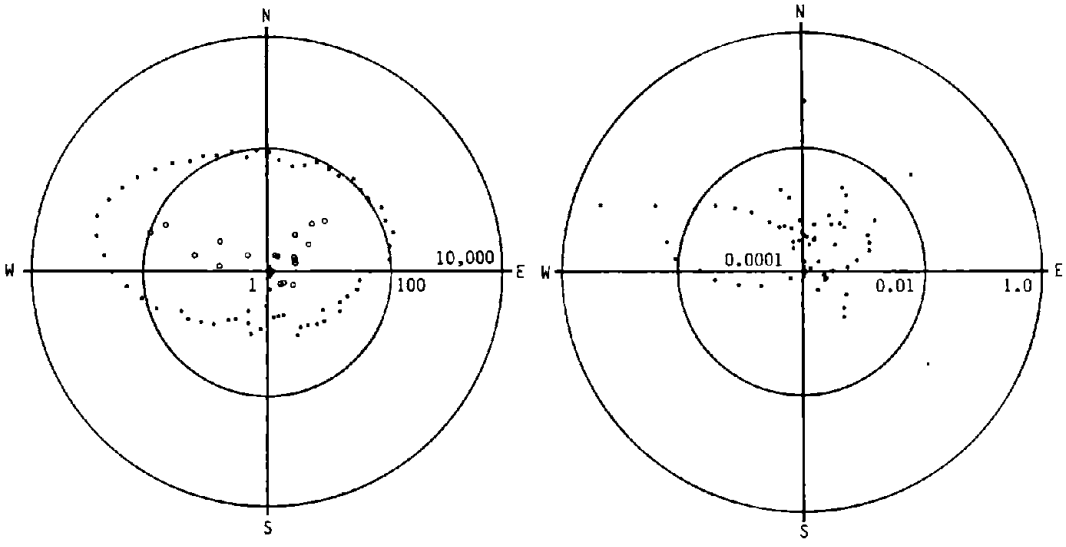

(a) DOA count (b) Magnetic-field energy

Figure 3-14. Directional histograms for three sources with 10-dB difference in power (Test #12).

marily verify proper operation of the software. The statistics for two highly impulsive sources are plotted in Figure 3-7. It is interesting to observe that the DOA counts for many sectors are identically zero. It is also interesting to note that while the overall DOA count is a rather broad curve, the locations of the two sources are apparent in the 1-σ and energy plots.

Figures 3-8 - 3-11 present statistics for three sources with the same impulsivities. It is apparent that the overall DOA count is largely independent of the source directions, even for highly impulsive noise. The 1-σ and energy plots, however, clearly indicate source azimuth for high and moderate impulsivities.

The effects of differences in the impulsivity and noise power of the three sources are shown in Figures 3-12 - 3-14. The source with the greatest impulsivity is clearly indicated by the data in Figure 3-12; however, the two sources of lesser impulsivity are also distinguishable in the 1-σ and energy data. All three sources are clearly visible when the difference in their powers are 5 dB (Figure 3-13). However, with differences of 10 dB (i.e., South America is 20 dB weaker than Indonesia), the weakest source begins to disappear (Figure 3-14).

3.2 GEOLOGY FILTER

The incident field at a given location includes horizontal magnetic components (H_x and H_y) and a vertical electric component (E_z). The horizontal electric-field components (E_x and E_y) and the vertical magnetic-field component (H_z) are produced [1] by the application of the incident field components to a "geology filter" based upon the characteristics of the local ground.

The horizontal electric-field components are directly associated with the horizontal magnetic-field components through an impedance sensor or surface impedance; this relationship is the basis of magnetotellurics [4]. It is therefore possible to derive a somewhat universal means of producing the horizontal electric-field components in an ANC simulation. This note uses the well-known frequency-response characteristics to drive a nonrecursive filter for time-domain processing.

In contrast, there is no simple, universally applicable relationship between the vertical magnetic-field component and the incident horizontal magnetic-field components [5]. Therefore, the most feasible method for generating H_z in a simulation is to use a linear combination of the two incident magnetic-field components and perhaps the three electric-field components as well.

Desired Frequency Response

The relationship between E_x and H_y for single-frequency excitation is given [1, (2.37)] by

$$\overline{E}_x(\omega) = Z_{xy}(\omega)\ \overline{H}_y(\omega) \quad , \tag{8}$$

where

$$Z_{xy}(\omega) \cong (j\omega\mu\rho)^{1/2} = \frac{1 + j}{2}\ (\omega\mu\rho)^{1/2} \tag{9}$$

and $\rho = 1/\sigma$ represents ground resistivity. This approximation is valid for $\omega\varepsilon\rho \ll 1$. For the worst case of poorly conducting ground, this implies that $f \ll 10$ kHz, which clearly includes the ELF band of interest here. The relationship between E_y and H_x is similar, except that $Z_{yx} = -Z_{xy}$.

Equation (9) implies a 45° phase shift and a 10 dB/decade high-pass response. Aside from being rather unusual (from the viewpoint of filter theory), such a frequency response is by itself clearly unrealizable, since its gain is unbounded as frequency increases. Nature overcomes this inconsistancy by flattening the response and eliminating the phase shift for frequencies for which $\omega\varepsilon\rho \gg 1$. Since such frequencies are well beyond the ELF band, the use of (9) should not cause any difficulties.

Temporal Waveform

Nonlinear processing of wideband ELF noise requires waveforms rather than frequency spectra. The time and frequency domains are related by the Fourier and inverse Fourier transforms, which are defined [6] by

$$\overline{H}_y(\omega) = F[H_y(t)] = \int_{-\infty}^{+\infty} H_y(t)\ e^{-j\omega t}\ dt \tag{10}$$

and

$$E_x(t) = F^{-1}[\overline{E}_x(\omega)] = \frac{1}{2\pi} \int_{-\infty}^{+\infty} \overline{E}_x(\omega)\ e^{+j\omega t}\ d\omega \quad . \tag{11}$$

Note the use of the overscore to differentiate a frequency-domain function from a time-domain function.

The relationship between the waveforms of the horizontal electric field and the corresponding horizontal magnetic field is determined by applying the Fourier-transform relationships to the geology-filter frequency response (9), thus

$$E_x(t) = F^{-1}\ \{\overline{E}_x(\omega)\} = F^{-1}\ \{Z_{xy}(\omega)\ \overline{H}_y(\omega)\} \tag{12}$$

$$= F^{-1}\ \{Z_{xy}(\omega)\ F[H_y(t)]\} = F^{-1}\ \{(j\omega\mu\rho)^{1/2}\ F[H_y(t)]\} \tag{13}$$

Such a relationship could be simulated by the use of fast-Fourier transforms; however, the computational requirements would be excessive. Equation (13) has the same general form as a differentiation relationship, but the meaning of a half-order derivative is not at all clear.

Conversion of (13) to a pure time-domain relationship is facilitated by converting the Laplace transform of $t^{-1/2}$ [6, Table A-3, (3.1)] into a Fourier transform, thus

$$F[G(t)] = F[(\pi t)^{-1/2}] = (j\omega)^{-1/2} = \overline{G}(\omega) \quad . \tag{14}$$

Rewriting (13) to include $\overline{G}(\omega)$ and using the differentiation principle [6, (6.23)] yields

$$E_x(t) = (\mu\rho)^{1/2}\ F^{-1}\ \{(j\omega)^{-1/2}\ [(j\omega)\ \overline{H}_y(\omega)]\} = (\mu\rho)^{1/2}\ F\{\overline{G}(\omega)\ \overline{H}_y'(\omega)\} \tag{15}$$

where

$$\overline{H}_y'(t) = dH_y(t)/dt \quad . \tag{16}$$

The waveform of the horizontal electric field is now given as the inverse-Fourier transform of the product of two frequency-domain functions. The convolution principle [6, (6.28)] allows (15) to be expressed directly in terms of time-domain functions, thus

$$E_x(t) = (\mu\rho)^{1/2} \int_0^t G(\tau)\ H_y'(t - \tau)\ d\tau \tag{17}$$

$$= (\mu\rho/\pi)^{1/2} \int_0^t \frac{H_y'(t - \tau)}{\tau^{1/2}}\ d\tau \quad . \tag{18}$$

A similar relationship is given by Cagniard [7].

Sampled-Data Implementation

Continuous integrals such as (18) must be converted to discrete summations for use in time-domain simulations. Insertion of $t=k\Delta t$ and $t=i\Delta t$ into (18) yields

$$E_x(k\Delta t) = (\mu\rho/\pi)^{1/2} \sum_{i\,=\,1}^{k} \frac{H_y'(k\Delta t - i\ \Delta t)}{(i\ \Delta t)^{1/2}}\ \Delta t \quad , \tag{19}$$

where Δt is the sampling period. In the more usual sampled-data notation, (19) becomes

$$E_x(k) = C\ \Delta t \sum_{i\,=\,1}^{k} \frac{H_y'(k - i)}{i^{1/2}} \quad , \tag{20}$$

where

$$C = (\mu\rho/\pi\ \Delta t)^{1/2} \quad . \tag{21}$$

The derivative of the magnetic-field waveform is simply

$$H_y'(k) = [H_y(k) - H_y(k - 1)]/\Delta t \quad . \tag{22}$$

Insertion of this relationship into (20) produces

$$E_x(k) = C \sum_{i=1}^{k} \frac{H_y(k - i) - H_y(k - i - 1)}{i^{1/2}} \quad . \tag{23}$$

Equation (23) expresses E_x directly in terms of previous H_y samples. However, the convolution summation implies an ever-increasing computational load.

The coefficients of a nonrecursive digital filter can be found from the response of the filter to a unit pulse [8]. The unit pulse function (analogous to the impulse function in the analysis of continuous systems) is defined by

$$H_y(k) = \begin{cases} 1, & k = 0 \\ 0, & k \neq 0 \end{cases} \quad . \tag{24}$$

The unit-pulse response of the geology filter is shown in Figure 3-15. The decay of $p(k)$ with increasing k is very slow, assymptotically approaching $k^{-3/2}$.

Since the output at sample k can be represented as the sum of the individual responses to each previous input sample,

$$p(k) = \begin{cases} 0, & k \leq 0 \\ C, & k = 1 \\ C[k^{-1/2} - (k - 1)^{-1/2}], & k \geq 2 \end{cases} \tag{25}$$

$$\begin{aligned} E_x(k) &= p(0)\ H_y(k) + p(1)\ H_y(k - 1) + p(2)\ H_y(k - 2) + \ldots \\ &= \sum_{i=0}^{k} p(i)\ H_y(k - i) \quad . \end{aligned} \tag{26}$$

In practice, it is necessary to include only a finite number (I) of terms. Since $p(0)=0$, the nonrecursive digital implementation of the geology filter has the form

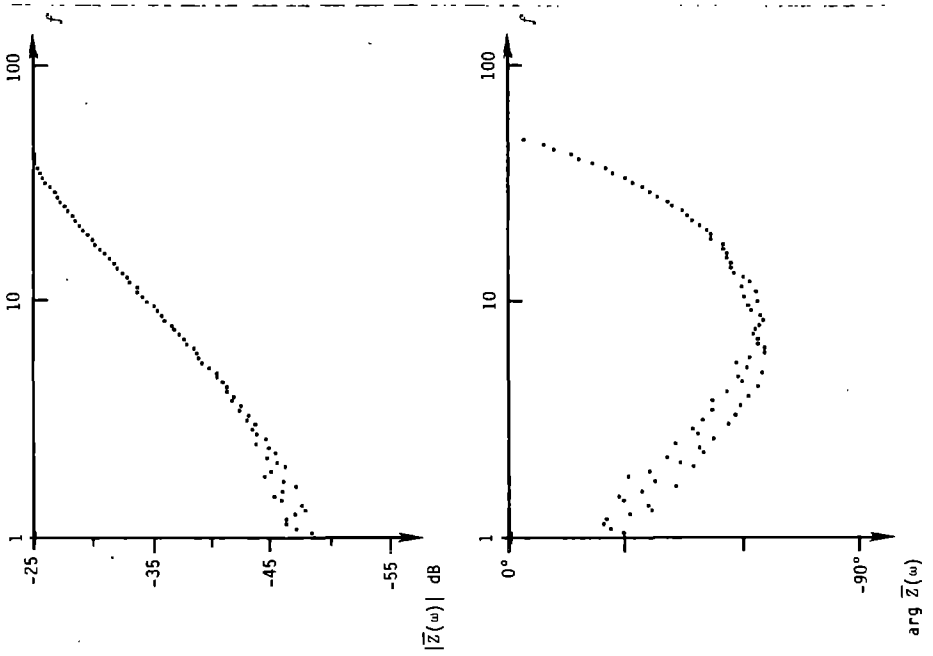

Figure 3-16. Frequency response of 100-element ground filter with 100-Hz sampling frequency.

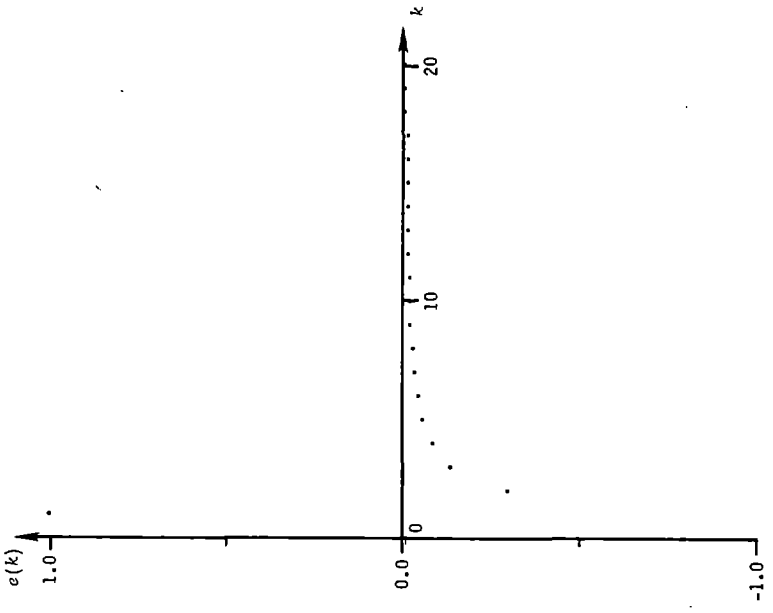

Figure 3-15. Unit-pulse response of ideal ground.

$$E_x(k) \cong \sum_{i=1}^{I} p(i)\, H_y(k - i) \quad . \tag{27}$$

Digital filters can in general be implemented in either recursive or nonrecursive forms (or hybrid forms). However, the coefficients in a recursive implementation of this filter decay even more slowly than those in the nonrecursive implementation, making the recursive implementation the less desirable.

Test Results

The frequency response of the geology filter was tested by time-domain simulation with cosinusoidal input signals. After adequate settling time ($1/f_{min}$), the frequency response was calculated by a numerical Fourier integration. The accuracy of this method was tested by setting the filter length to 1 to produce an (ideally) flat response. The results show errors of less than 1 dB and less than 2°, which are consistant with the accuracy of the simulation.

Frequency responses were determined for sampling frequencies (f_s) of 100 and 300 Hz and filter lengths (N_f) of 100, 200, and 300 elements. The primary effect of increased filter length is better low-frequency response. While the frequency response curves (e.g., Figure 3-16) leave something to be desired, they do provide the desired general tendencies. Since the impulse response of this filter decays very slowly, it is doubtful that a significant improvement can be attained without a tremendous increase in the number of terms in the filter.

3.3 REFERENCES

1. F. H. Raab, "Adaptive-noise-cancellation techniques for through-the-earth electromagnetics, Volume 1," Final Report GMRR TR82-1, Green Mountain Radio Research Company, Burlington, VT, January 1982.

2. E. C. Field, Jr. and M. Lewinstein, "Amplitude-probability distribution model for VLF/ELF atmospheric noise," *IEEE Transactions on Communications*, vol. COM-26, no. 1, pp. 83 - 87, January 1978.

3. J. W. Modestino, "A model for ELF atmospheric noise," Technical Report 493 (AD 737,368), MIT Lincoln Laboratory, Lexington, MA, December 1971.

4. G. V. Keller and F. C. Frischknecht, *Electrical Methods in Geophysical Prospecting*, London: Pergamon Press, 1966.

5. D. A. Hill and J. R. Wait, "Theoretical noise and propagation models for through-the-earth communication," Final Report, Contract No. J0113058, National Telecommunications and Information Admin., Boulder, CO, May

1982.

6. R. G. Brown and J. W. Nilson, *Introduction to Linear Systems Analysis*, New York: John Wiley and Sons, Inc, 1966.

7. L. Cagniard, "Basic theory of the magneto-telluric method of geophysical prospecting," *Geophysics*, vol. 18, no. 3, pp. 605 - 635, 1953.

8. S. M. Bozic, *Digital and Kalman Filtering*, New York: John Wiley and Sons, 1979.

CHAPTER 4. RECEPTION BANDWIDTH

The Field-Lewinstein-Modestino model represents ELF noise as a sum of Gaussian and impulsive components. This model has proven to be accurate and is especially convenient for analysis and simulation. However, the parameters of the model are bandwidth dependent and have been measured for only a few specific bandwidths. No method of calculating the parameters for other bandwidths has been presented. This chapter derives such a method by equating the moments of the impulsive component of the ELF noise at the input and output of the filter.

The per-second rate λ of occurrence of ELF-noise impulses is a natural parameter that varies from 9 to 13 Hz, depending upon atmospheric conditions (Table 3-1). In contrast, the per-sample rate of occurrence of impulses in noise simulated using the Field-Lewinstein-Modestion (FLM) model is determined completely by the parameters α (or R) and γ. Furthermore, the per-sample and per-second impulse rates are directly related by the sampling frequency. It is therefore obvious that some modification must be made to the values of α and γ if the sampling frequency used in a simulation is not the same as that used to collect the data from which α and γ were extracted.

The data presented by Modestino [1] and subsequently used by Field and Lewinstein [2] were collected with a bandwidth of 300 Hz. Neither paper suggests a method of converting α and γ for one bandwidth into α and γ for another bandwidth. It is, of course, possible simply to generate simulated ELF noise at a 300-Hz rate and apply it to a low-pass filter to obtain ELF noise with the desired bandwidth. However, doing so requires the generation of a larger number of random numbers than is really necessary, resulting in a slower-running simulation.

One approach to determining the parameters of interest is to calculate the p.d.f. of the filter output and find the best fit between it and the p.d.f. of the FLM model. Calculation of the p.d.f. by either direct convolution or transformation to the characteristic function involves unmanageble integrals and must therefore be accomplished numerically. The erratic nature of impulsive noise makes simulation impractical because of the extremely large number of samples required for adequate accuracy. The approach presented here avoids the both lengthly numerical calculations and lengthly simulations by matching the moments of FLM noise to the moments of the filter output.

4.1 GENERAL FORMULATION

A general idea of how filtering affects ELF noise can be obtained by considering the effects of the "box-car" average

$$Z = \frac{G}{N} \sum_{n=1}^{N} z_n \quad , \tag{1}$$

where each z_n is a "wideband" noise sample. According to the FLM model

ELF noise is a sum of Gaussian and impulsive components, thus

$$z_n = x_n + y_n \quad . \tag{2}$$

The objective here is to fit the FLM model to the filter output, thus by analogy to (2),

$$Z \cong X + Y \quad . \tag{3}$$

For convenience, the filter gain is set at

$$G = N^{1/2} \tag{4}$$

so that both output power and input power can be normalized to unity.

4.2 CONSTANT-IMPULSIVITY APPROACH

Individual wideband noise samples (including both the Gaussian and impulsive components) are assumed to have zero means and be mutually independent. Furthermore, both the Gaussian and impulsive components are assumed to be white over the bandwidth of interest. Consequently, the filter reduces the power in each component by the same amount.

Implications

The impulsivity (ratio of impulsive-noise power to Gaussian-noise power) of the filter output is therefore unchanged by the filter; i.e.,

$$\gamma_o = \gamma_i = \sigma_y^2/\sigma_x^2 = \sigma_y^2/\sigma_x^2 \quad . \tag{5}$$

This implies that the Gaussian and impulsive components of the filter output correspond directly to the Gaussian and impulsive components of the input, thus

$$X = \frac{G}{N} \sum_{n=1}^{N} x_n \tag{6}$$

and

$$Y = \frac{G}{N} \sum_{n=1}^{N} y_n \quad . \tag{7}$$

The summation of Gaussian random variables produces a Gaussian random variable, hence X is Gaussian. As long as the rate of occurrence of large impulses in the input is relatively low, it is unlikely that two or more impulses occur during one averaging interval. Under such conditions, Y is relatively impulsive compared to X.

Moments of Input

The FLM model assumes a two-sided power-Rayleigh p.d.f. for the impulsive component of ELF noise:

$$p_y(y) = (|y|^{a-1}/2\ R^a)\ \exp[-(y/R)^a] \quad . \tag{8}$$

The symmetry of this p.d.f. implies that all odd-order moments of y are zero. The even-order moments are given by

$$\mu_{Ky} = \int_{-\infty}^{+\infty} y^k\ p_y(y)\ dy = R^k \int_0^{\infty} u^{k/a}\ e^{-u}\ du = R^k\ \Gamma(1 + k/a) \quad , \tag{9}$$

which is obtained from (8) by use of the substitution $u = (y/R)^a$.

Moments of Output

The second moment of the impulsive component of the output is

$$\mu_{2Y} = E[Y^2] = \frac{G^2}{N^2}\ E[y_1^2 + y_2^2 + \ldots + 2y_1\ y_2 + \ldots] \quad . \tag{10}$$

The independence of different samples and (4) imply that

$$\mu_{2Y} = \frac{G^2 N}{N}\ E[y_n^2] = \mu_{2y} \quad . \tag{11}$$

The fourth moment of Y is similarly

$$\mu_{4Y} = E[Y^4] = \frac{G^4}{N^4}\ E[y_1^4 + y_2^4 + \ldots + 4y_1\ y_2^3 + \ldots + 6y_1^2\ y_2^2 + \ldots] \tag{12}$$

$$= \frac{N^2}{N^4}\ \{N\mu_{4y} + 3\ N(N - 1)\ \mu_{2y}\} \tag{13}$$

$$= \frac{1}{N}\ \{\mu_{4y} + 3\ (N - 1)\ \mu_{2y}\} \quad . \tag{14}$$

Fitting

The power-Rayleigh random variable to be fitted to the impulsive component of the filter output is characterized completely by two parameters, a_o and R_o. Fitting is accomplished by choosing a_o and R_o to produce the second and fourth moments of the output. This ensures that the FLM model produces the power, and to a first approximation, the spikiness that occur in the filter output.

Inspection of (9) shows that unknown R_o can be eliminated by dividing the fourth moment by square of the second moment, producing

$$f(a_o) = \frac{\mu_{4Y}}{\mu_{2Y}^2} = \frac{\Gamma(1 + 4/a_o)}{\Gamma(1 + 2/a_o)} \quad . \tag{15}$$

The value of $f(a_o)$ is determined from N and input moments μ_{2Y}^2 and μ_{4Y}; which are obtained from (9) by insertion of a and R for the wideband input noise. Unknown a_o is obtained by solving (15) numerically. Unknown R_o is then determined from a_o and the second moment (power) by

$$R_o^2 = \mu_{2Y}/\Gamma(1 + 2/a_o) \quad . \tag{16}$$

The numerical solution of (15) is readily implemented by rearranging it into

$$0 = \Gamma(1 + 2\beta) - (\mu_{4Y}/\mu_{2Y})\ \Gamma(1 + \beta) \quad , \tag{17}$$

finding $\beta = 2/a_o$ numerically, and then calculating a_o.

Results

The variation of a_o with N is shown in Figure 4-1 for several values of a. As expected, increasing the integration time (decreasing the bandwidth) produces increasing values of a_o, implying decreasing "spikiness" of the noise.

Figure 4-2 compares the histograms of filtered moderate-level FLM noise and FLM noise with a_o and R_o determined by this method. For $N = 10$, it is apparent that the agreement is excellent. Excellent agreement is also obtained for high- and low-level noise.

These relationships are expected to be valid for values of $a_o \leq 1$. As $a_o \to 2$, the power-Rayleigh p.d.f. tends toward the nonimpulsive Rayleigh p.d.f. of the envelope of narrowband Gaussian noise.

4.3 VARIABLE-IMPULSIVITY APPROACH

The two-moment bandwidth-conversion method presented previously is convenient and easy to use. However, it does not allow for eventual convergence of the FLM random variable to a Gaussian random variable for very large values of N. This note develops a three-moment technique for matching impulsivity as well as power and spikiness.

The three-moment method is formulated by deriving the second, fourth, and sixth moments of the wideband and averaged ELF noise z, as well as those

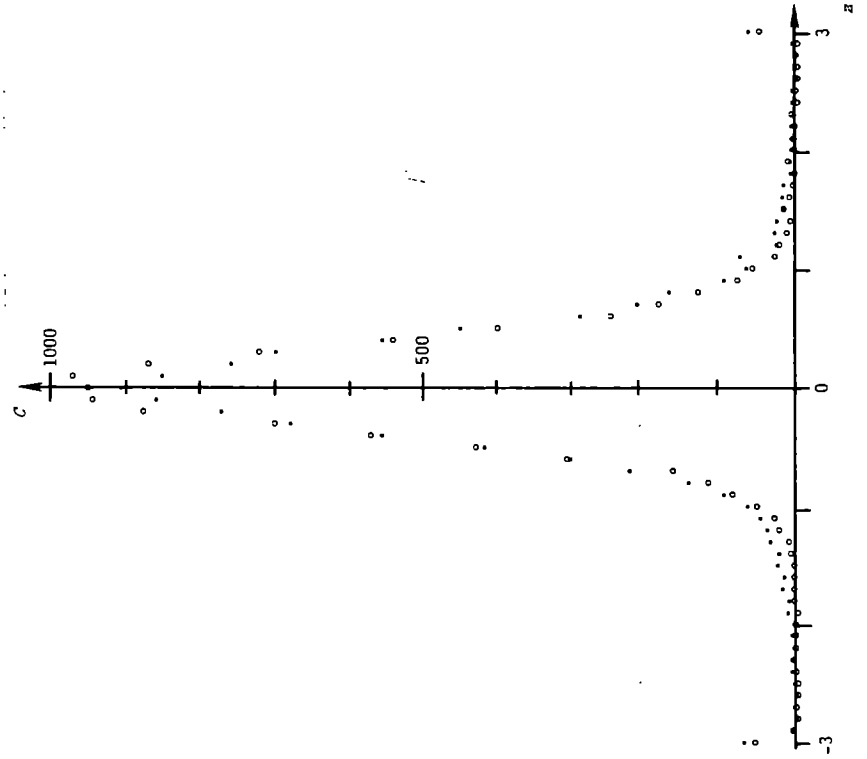

Figure 4-2. Histogram for moderate-level noise, two-moment method.

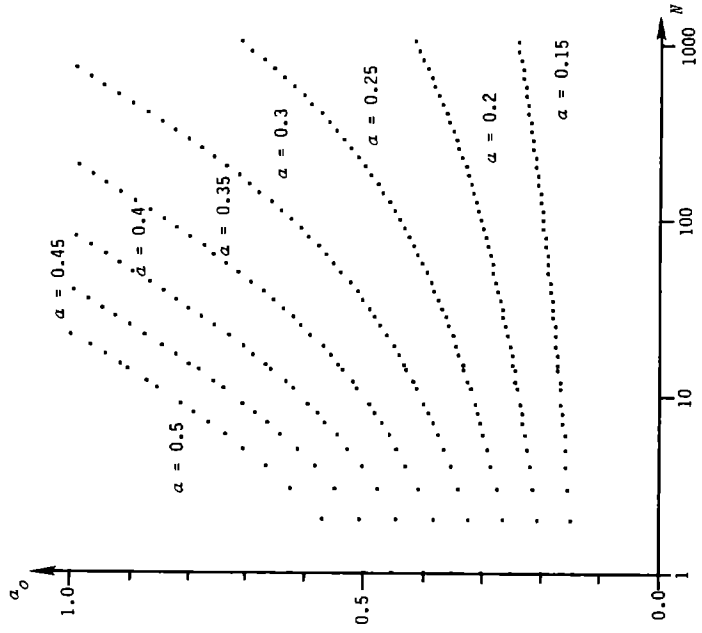

Figure 4-1. Effect of averaging on spikiness.

of its Gaussian and impulsive components x and y. Matching the moments of a single sample to those of the average is accomplished by solving a system of three nonlinear equations.

Moments of Wideband Noise

The moments of the impulsive component y are given in Section 4.2. From (1-4) of [3], the even (nonzero) moments of the Gaussian component x are

$$\mu_{Kx} = 1 \cdot 3 \cdot 5 \cdot \ldots \cdot (K - 1)\ \sigma_x^K \quad . \tag{18}$$

The moments of the FLM ELF noise are then obtained by expanding z^K, taking its expectation, dropping terms containing odd (zero) moments, and substituting the moments of the two components:

$$\mu_{2z} = E[z^2] = E[x^2 + 2\,xy + y^2] \tag{19}$$

$$= \mu_{2x} + \mu_{2y} \tag{20}$$

$$= \sigma_x^2 + R^2\ \Gamma(1 + 2/a) \tag{21}$$

$$\mu_{4z} = E[x^4] + E[y^4] + 6\ E[x^2]\ E[y^2] \tag{22}$$

$$= \mu_{4x} + \mu_{4y} + 6\ \mu_{2x}\ \mu_{2y} \tag{23}$$

$$= 3\ \sigma_x^4 + R^4\ \Gamma(1 + 4/a) + 6\ \sigma_x^2\ R^2\ \Gamma(1 + 2/a) \tag{24}$$

$$\mu_{6z} = E[x^6] + E[y^6] + 15\ E[x^4]\ E[y^2] + 15\ E[x^2]\ E[y^4] \tag{25}$$

$$= \mu_{6x} + \mu_{6y} + 15\ \mu_{4x}\ \mu_{2y} + 15\ \mu_{2x}\ \mu_{4y} \tag{26}$$

$$= 15\ \sigma_x^6 + R^6\ \Gamma(1 + 6/a) + 45\ \sigma_x^4\ R^2\ \Gamma(1 + 2/a) + 15\ \sigma_x^2\ R^4\ \Gamma(1 + 4/a) \quad . \tag{27}$$

Moments of Averaged Noise

By analogy to Section 4.2, the second and fourth moments of the averaged noise are

$$\mu_{2Z} = \frac{1}{N}\ \{N\ E[z]\} = \mu_{2z} \tag{28}$$

and

$$\mu_{4Z} = \frac{1}{N}\left\{\mu_{4z} + 3(N-1)\,\mu_{2z}^2\right\} \quad . \tag{29}$$

The sixth moment of the averaged noise is found by expanding the sum and determing the total number of each type of term as a function of N, thus

$$\begin{aligned}\mu_{6Z} = \frac{G^6}{N^6} E[&z_1^6 + z_2^6 + \ldots \\ &+ 15\, z_1^4 z_2^2 + \ldots \\ &+ 15\, z_1^2 z_2^4 + \ldots \\ &+ 90\, z_1^2 z_2^2 z_3^2 + \ldots] \end{aligned} \tag{30}$$

$$\begin{aligned}= \frac{1}{N^3}\{&N\,E[z^6] \\ &+ 2(15/2!)\,N(N-1)\,E[z^4]\,E[z^2] \\ &+ (90/3!)\,N(N-1)(N-2)\,E^3[z^2]\}\end{aligned} \tag{31}$$

$$= \frac{1}{N^2}\left\{\mu_{6z} + 15(N-1)\,\mu_{4z}\,\mu_{2z} + 15\,(N-1)(N-2)\,\mu_{2z}^3\right\} \quad . \tag{32}$$

Inspection of (28), (29), and (30) shows that they converge to the moments of a Gaussian random variable as $N \to \infty$. Furthermore, for Gaussian wideband noise ($\gamma = 0$), they produce the moments of Gaussian noise for all values of N.

Solution

Equating the moments of a single FLM random variable [(21), (24), and (27)] to the moments of a sum of FLM random varaibles [(28), (29), and (32)] produces a system of three nonlinear equations in three unknowns. Simplification of this system of equations appears impossible.

A numerical solution can be implemented using the linearized form

$$\boldsymbol{p} = \boldsymbol{C}\,\Delta\boldsymbol{v} \quad , \tag{33}$$

where

$$\Delta\boldsymbol{v} = \begin{bmatrix} \Delta\sigma_x \\ \Delta R \\ \Delta\alpha \end{bmatrix} \tag{34}$$

represents the differences between σ_x, R, and α for an assumed solution and

those for the true solution. The vector

$$p = \begin{bmatrix} \mu_{2Z} - \mu_{2\hat{z}} \\ \mu_{4Z} - \mu_{4\hat{z}} \\ \mu_{6Z} - \mu_{6\hat{z}} \end{bmatrix} \tag{35}$$

represents the differences between the moments of the average and the moments of a single FLM random variable with the assumed values of σ_x, R, and a. The rates of change for the assumed parameter values are contained in matrix C, which has the form

$$C = \begin{bmatrix} \partial\mu_{2z}/\partial\sigma_x & \partial\mu_{2z}/\partial R & \partial\mu_{2z}/\partial a \\ \partial\mu_{4z}/\partial\sigma_x & \partial\mu_{4z}/\partial R & \partial\mu_{4z}/\partial a \\ \partial\mu_{6z}/\partial\sigma_x & \partial\mu_{6z}/\partial R & \partial\mu_{6z}/\partial a \end{bmatrix} , \tag{36}$$

and must be calculated numerically.

The solution for the difference vector is then

$$\Delta v = C^{-1} p \quad . \tag{37}$$

The solution is most readily implemented by changing N in small increments and using the previous solution for σ_x, R, and a as the assumed initial set of values in the subsequent solution. It is desirable to allow for up to 10 iterations. Stability can be assured (in all but a few anomolous cases) by multiplying Δv by a constant in the range of 0.5 to 0.75 prior to updating the assumed values of σ_x, R, and a.

Results

The variations of impulsivity and spikiness with the number of samples averaged are shown in Figure 4-3. The rapid decrease in impulsivity with increases in N is apparent.

The histogram plots of Figure 4-4 compare a single FLM random variable with parameters calculated by the three-parameter method to the average of 10 FLM random variables. For N=10, it is apparent that the decrease in impulsivity predicted by the three-parameter method is excessive.

4.4 PREFERRED METHOD

Comparison of histogram plots (e.g., Figures 4-2 and 4-4) shows that the two-moment method gives more accurate results for the bandwidth conversions of interest. Parameters for various bandwidths of interest (calculated by the two-moment method) are given in Table 4-1.

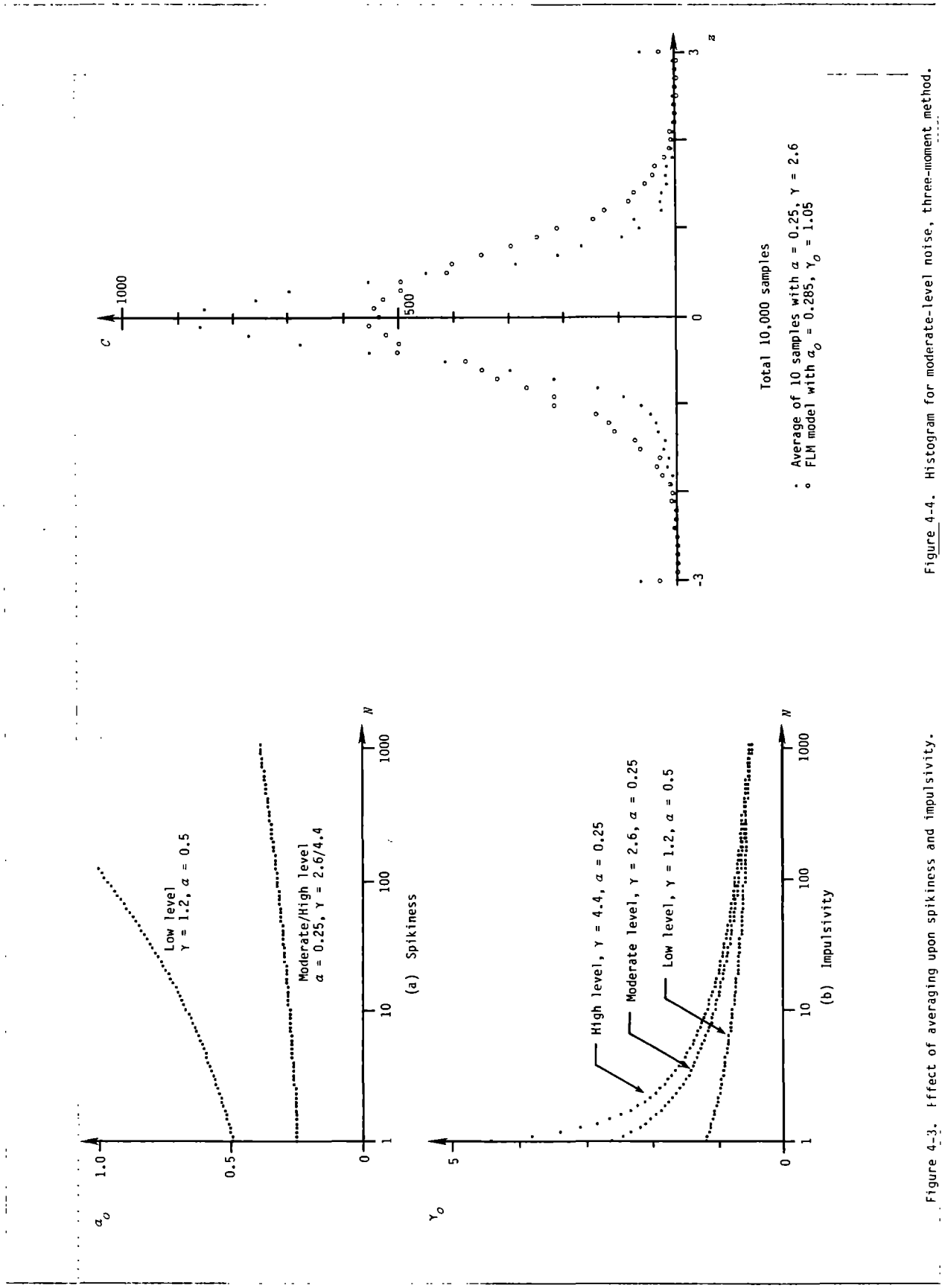

Figure 4-3. Effect of averaging upon spikiness and impulsivity.

Figure 4-4. Histogram for moderate-level noise, three-moment method.

4.5 REFERENCES

1. J. W. Modestino, "A model for ELF noise," ESD-TR-71-322 (AD-737,368), Lincoln Laboratory, M.I.T., Lexington, MA, December 16, 1971.

2. E. C. Field, Jr. and M. Lewinstein, "Amplitude-probability distribution model for VLF/ELF atmospheric noise," *IEEE Transactions on Communications*, vol. COM-26, no. 1, pp. 83 - 87, January 1978.

3. N. M. Blachman, *Noise and its Effect on Communication*, New York: McGraw-Hill, 1966.

NOISE CONDITION	BANDWIDTH					
	300 Hz		100 Hz		30 Hz	
	γ	α	γ	α	γ	α
HIGH LEVEL	4.4	0.25	4.4	0.28	4.4	0.32
MODERATE LEVEL	2.6	0.25	2.6	0.28	2.6	0.32
LOW LEVEL	1.2	0.5	1.2	0.63	1.2	0.83
GAUSSIAN	0.0	-	0.0	-	0.0	-

Note: Based upon two-moment method and data from Table 3-1.

Table 4-1. Parameters for ELF noise of various bandwidths.

CHAPTER 5. NONLINEAR PROCESSING

Atmospheric noise at extremely low frequencies is in general a combination of Gaussian and impulsive components. Because a significant fraction of the total noise power is concentrated in readily discernible impulses, significant improvement in the effective signal-to-noise ratio can usually be achieved by nonlinear processing of the noisy signal.

There are many possible approaches to nonlinear processing. The theoretically optimum approach [1] is to pass the noisy signal through a nonlinearity that converts the impulsive noise into Gaussian noise. However, such an approach is not practical unless the specific p.d.f. of the impulsive noise is known *a priori*. In this application, it is therefore necessary to use a more straightforward nonlinear processing method such as clipping or editing.

This chapter addresses several key issues in the nonlinear processing of ELF noise, including:

- Clipping vs. editing,
- Adaptively setting the threshold,
- Implementation of a signal-nulling loop, and
- Statistics of the output of the nonlinear processor.

5.1 ADAPTIVE CLIPPER/EDITOR

The block diagram of an adaptive nonlinear processor is shown in Figure 5-1. This processor includes both nonlinear impulse processing and coherent signal detection.

Wideband noise from the analog portion of the receiver is applied to a bandpass filter and then sampled and digitized. It is desirable to leave the input bandwidth as large as possible (up to about 1 kHz) to preserve the sharpness of the impulses. However, it is also necessary to eliminate 50- and 60-Hz power-line noise. The probable cut-off frequency of the input filter is therefore 30 Hz.

The adaptive nonlinear processor shown in Figure 5-1 may be either a clipper or an editor. The threshold for clipping or editing is derived from the estimated total input power. This concept is discussed in greater detail in the next section.

After nonlinear processing, the received signal is applied to a coherent detector. Coherent detection is accomplished by mixing the signal separately with cosine and sine waves of the signal frequency. Integration of the mixer outputs yields estimates of the in-phase and phase-quadrature components of the signal. Signal amplitude and phase are readily derived from $\hat{s}_I$ and $\hat{s}_Q$. Alternatively, a low-pass filter may be used in place of the integrator. In either case, the combination of the mixers and integrators (or low-pass filters) acts as a bandpass filter at the signal frequency.

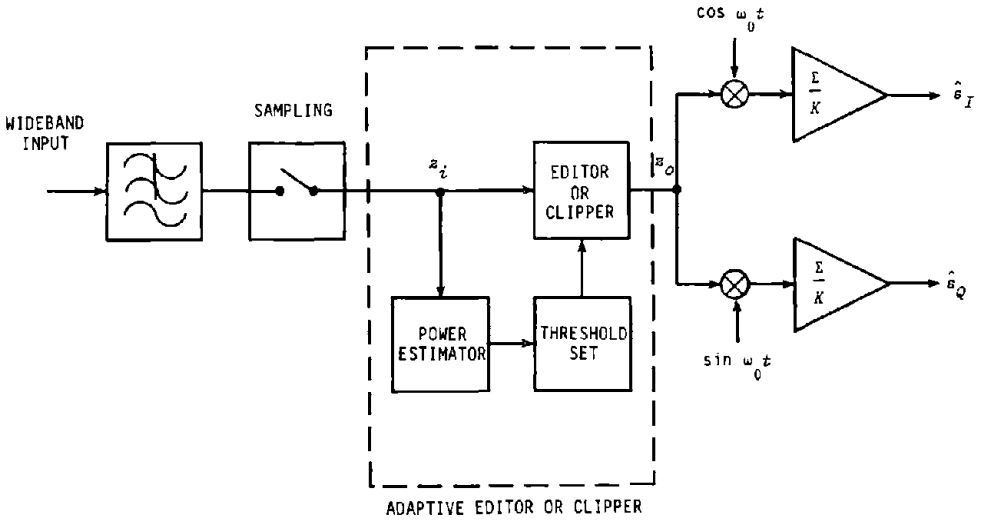

Figure 5-1. Adaptive nonlinear processor without signal nulling.

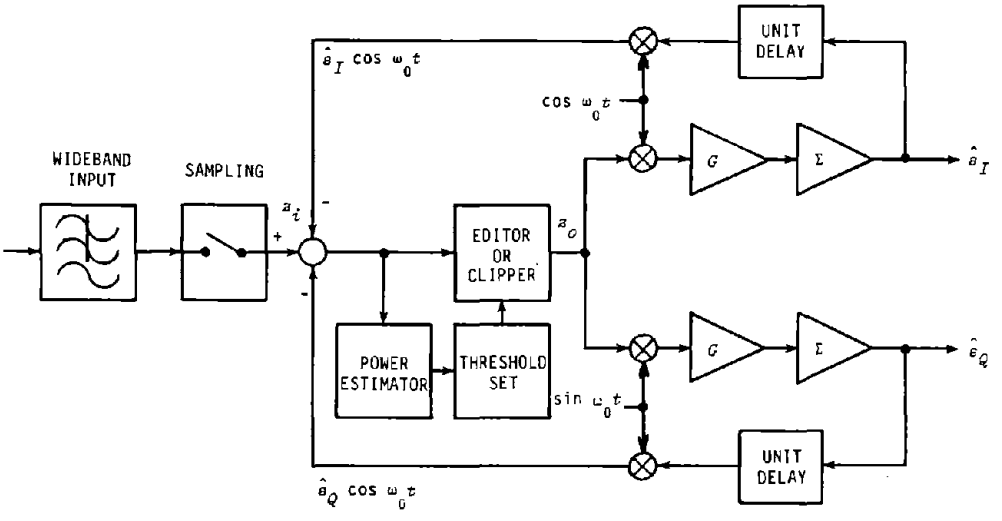

Figure 5-2. Acaptive nonlinear processor with signal nulling.

5.2 THRESHOLD DETERMINATION

The two nonlinear processing techniques considered practical for this application are clipping and editing. Clipping limits the maximum positive and negative values of the signal, and is therefore characterized by

$$z_o = \begin{cases} +\tau, & z_i > \tau \\ z_i, & -\tau \leq z_i \leq +\tau \\ -\tau, & z_i < -\tau \end{cases} , \tag{1}$$

where z_i and z_o represent its input and output, respectively. The editor (also called a "hole puncher") discards data (zeros its output) whenever its input exceeds a threshold. The editor is therefore characterized by

$$z_o = \begin{cases} 0, & z_i > \tau \\ z_i, & -\tau \leq z_i \leq +\tau \\ 0, & z_i < -\tau \end{cases} . \tag{2}$$

Since neither the power nor the impulsivity of the noise is known *a priori* the threshold τ must be set adaptively. A review of the works of Field, Lewinstein, and Modestino [2,3] suggests that the optimum threshold is readily determined from knee of the probability distribution. However, accurate estimation of the distribution function requires a very large number of samples. Furthermore, considerable memory is required.

In contrast, the estimated noise power $\hat{P}$ is a relatively easy statistic to utilize. It is obtained from

$$\hat{P} = \frac{1}{K} \sum_{k=1}^{K} z_i^2(k) \tag{3}$$

and is easily updated as new samples are received. The threshold is conveniently specified in terms of the estimated rms noise power, thus

$$\tau = c\, \hat{P}^{1/2} . \tag{4}$$

This method of adaptively determining the clipping/editing threshold is therefore preferred.

5.3 SIGNAL-NULLING LOOP

The principal problem in using clippers or editors is distortion of strong signals. The threshold should in general be set to no more than the

rms level to achieve effective impulse suppression. However, the peak of a pure sinewave is 1.414 times its rms level. Since position is derived from signal amplitudes, the potential for distortion is a serious consideration in the selection of a processing technique.

Concept

The optimum processor for a signal corrupted by impulsive noise estimates both the signal and the impulsive component of the noise [4]. A practical variation upon this concept is the signal-nulling loop [5].

Figure 5-2 presents the block diagram of a signal-nulling loop incorporated into the adaptive nonlinear processor/detector of Figure 5-1. The input low-pass filter, adaptive nonlinear processor, and mixers are the same as those discussed in Section 5.1.

An estimated replica of the received signal is obtained by multiplying the estimates $\hat{s}_I$ and $\hat{s}_Q$ by cosine and sine waves, respectively. The estimated signal is then subtracted from the sampled/digitized input signal, ideally leaving only noise. The adaptive nonlinear processor then processes only noise and does not distort the signal, regardless of its amplitude.

Loop Analysis

In the absence of clipping or editing, the signal-nulling loop shown in Figure 5-2 is equivalent to a single-pole digital filter. This allows determination of its temporal- and frequency-response characteristics by standard techniques.

A set of equivalent network topologies for the loop are shown in Figure 5-3. Since the cosine and sine functions are orthogonal, the I and Q loops act independently (neglecting numerical errors) and can be analyzed separately. The resultant equivalent carrier-frequency loop is shown in Figure 5-3a. The error signal X has the form

$$X = x(k) \cos \omega_0 t \quad , \tag{5}$$

where

$$x(k) = z(k) - \hat{s}_I(k) \tag{6}$$

is the difference between the envelopes of the input and estimated signals.

Mixing produces the product signal

$$Y = x(k)(1/2)(1 + \cos 2\,\omega_0 t) \quad , \tag{7}$$

whose baseband component is clearly the difference envelope $x(k)/2$. Since the loop acts upon the signal envelope, it is convenient to replace the carrier-frequency block diagram of (a) with the baseband block diagram of (b). In making this conversion, gain G must be halved to allow for the factor of 1/2 introduced in the mixing process (7).

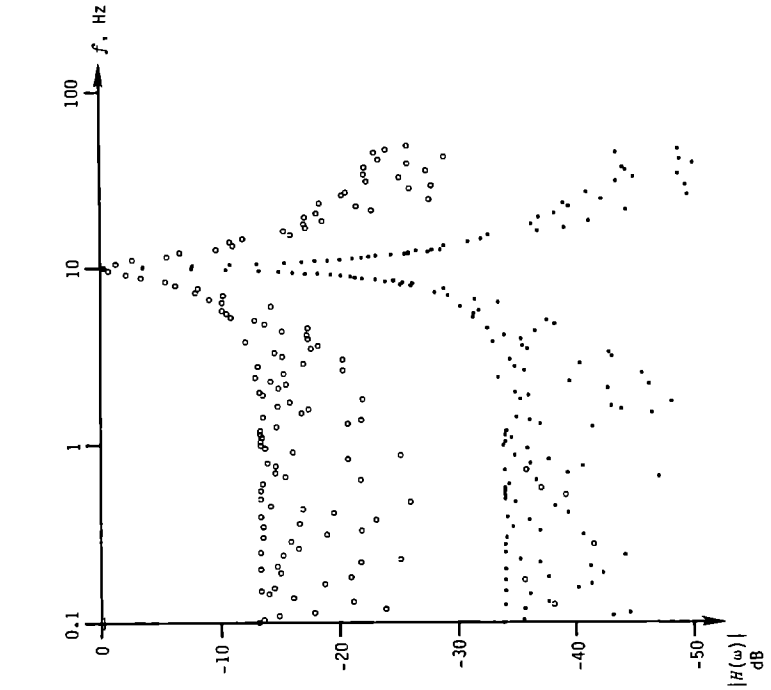

Figure 5-4. Frequency response.

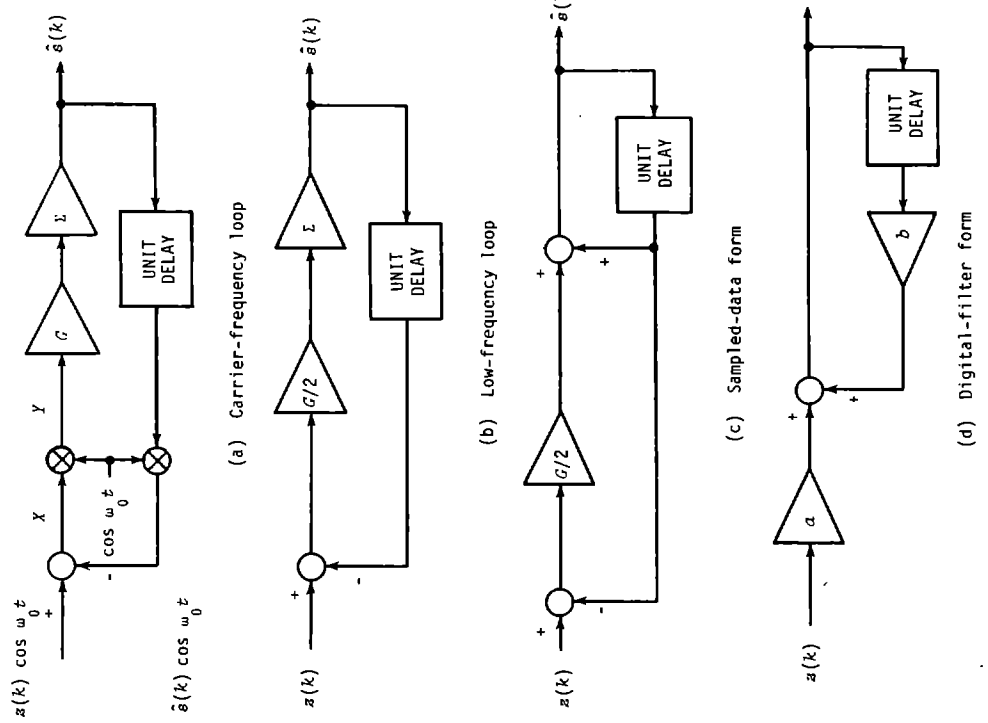

Figure 5-3. Equivalent filter topologies.

The integrator (summation) block can be represented as a simple loop that accumulates its output, allowing transformation of the signal-nulling loop into sampled-data form, as shown in Figure 5-3c. This form is in turn readily converted into the standard recursive digital-filter form shown in Figure 5-3d. Equivalence of (c) and (d) requires that

$$a = G/2 \tag{8}$$

and

$$b = 1 - G/2 \quad . \tag{9}$$

The response (estimate) $\hat{s}(k)$ is related to the current input sample and the previous estimate by

$$\hat{s}(k) = a\, z(k) + b\, \hat{s}(k - 1) \tag{10}$$

$$= a\, z(k) + b[a\, z(k - 1) + b\, \hat{s}(k - 2)] \tag{11}$$

$$= a[z(k) + b\, z(k - 1)] + b^2\, \hat{s}(k - 2) \quad . \tag{12}$$

The obvious generalization of the above is

$$\hat{s}(k) = a[z(k) + b\, z(k - 1) + b^2\, z(k - 2) + \ldots$$

$$+ b^{n-1}\, z(k - n + 1)] + b^n\, \hat{s}(k - n) \quad . \tag{13}$$

Unit-step excitation is described by

$$z(k) = \begin{cases} 1, & k \leq 0 \\ 0, & k > 0 \end{cases} \quad . \tag{14}$$

Insertion of this into (13) then yields

$$y(k) = a[1 + b + b^2 + \ldots + b^k] = a\,\frac{b^k - 1}{b - 1} \quad , \tag{15}$$

which eventually converges to

$$y(\infty) = a/(1 - b) = 1 \quad . \tag{16}$$

It is obvious from (16) that achieving both convergence and stability requires that $0 < b < 1$ and $0 < a < 1$. The gain G in the signal-nulling loop is therefore limited to the range

$$0 < G < 2 \quad . \tag{17}$$

The frequency response of a single-pole digital filter is [6, §2.3]

$$H(\omega) = a/(1 - be^{-j\omega T}) \quad , \tag{18}$$

where $T=1/f_s$. Use of the identity

$$e^{j\omega T} = \cos \omega T - j \sin \omega T \tag{19}$$

yields

$$|H(\omega)|^2 = H(\omega)\, H^*(\omega) = \frac{a^2}{1 + b^2 - 2\, b \cos \omega T} \quad . \tag{20}$$

When $\omega = 0$, $\cos \omega t = 1$, hence $|H(\omega)|^2 = 1$ as expected.

In the current application, the bandwidth is considerably smaller than the sampling frequency. The approximation

$$\cos \omega T \cong 1 - (\omega T)^2/2 \tag{21}$$

can therefore be inserted into (20), producing

$$|H|^2 \cong \frac{a^2}{1 + b^2 - 2\, b[1 - (\omega T)]^2/2} = \frac{a^2}{a^2 + b(\omega T)^2} \tag{22}$$

The cut-off frequency f_c is the frequency at which the filter produces an attenuation of 3 dB. Insertion of $|H(\omega)|^2 = 1/2$ into (22) produces

$$(\omega_c T)^2 = a^2/b \cong a^2 \quad . \tag{23}$$

This relationship is quite useful, since it relates a (hence b and G) directly to the desired bandwidth.

The frequency-response characteristics of the signal-nulling loop are verified by simulation. Both responses shown in Figure 5-4 are as desired, if the numerical errors are neglected.

Start Up

The initial power estimate for an adaptive clipper or editor without a signal-nulling loop can be set to zero. As samples are processed, the power estimate becomes more accurate and the threshold is set properly. The initial power estimate for an adaptive clipper with a signal-nulling loop can also be set initially at zero. Upon processing the first sample, the power estimate becomes nonzero, allowing a nonzero output of the clipper, hence eventual convergence of the power estimate.

However, setting the initial power estimate to zero in an adaptive editor with a signal-nulling loop causes the first-sample editing threshold to be set at zero. Consequently, the editor produces a zero output in response to the first sample. Since the power estimate remains at zero, the processor never produces a nonzero output. One solution to the start-up problem is to set the initial power estimate somewhat above the anticipated input power level. The other solution is to inhibit editing for a short time period so that the processor can establish a nonzero editing threshold. The second solution is preferred, since it produces more accurate power es-

timates under varied conditions.

5.4 COMPARISON OF PROCESSORS

The noise-reduction capabilities of several nonlinear processors are compared by simulation. The specific processors tested are:

- Bandpass filter only,
- Clipper followed by bandpass filter,
- Editor followed by bandpass filter,
- Signal-nulling loop with clipper, and
- Signal-nulling loop with editor.

In all cases, the sampling frequency, signal frequency, and bandwidth are 100 Hz, 10 Hz, and 1 Hz, respectively.

The simulations include a variety of signal levels, signal-to-noise ratios, thresholds, and noise conditions. The parameters shown in Table 3-1 for a 100-Hz bandwidth are used to define the four noise conditions.

There are many ways by which the nonlinear processors can be compared. In communication applications where absolute signal amplitude is not important, the ratio output SNR to input SNR is most commonly used. However, the TTE EM location system derives position from signal amplitude. It is therefore more appropriate to define the improvement produced by a nonlinear processor as the ratio

$$\xi = \overline{\varepsilon^2_{NLP}} / \overline{\varepsilon^2_{LP}} \quad . \tag{24}$$

The instantaneous squared error for the output of the nonlinear processor is defined by

$$\overline{\varepsilon^2_{NLP}} = (\hat{\varepsilon}_{I,NLP} - \varepsilon)^2 + (\hat{\varepsilon}_Q - \varepsilon_Q)^2 \quad ; \tag{25}$$

the instantaneous squared error $\overline{\varepsilon^2_{LP}}$ for the output of a purely linear filter is similarly defined.

The effect of the choice of threshold τ upon the improvement ratio is shown in Figures 5-5 - 5-7 for various SNRs. For -20 dB SNR (Figures 5-5), low values of τ appear to produce dramatic improvements. These improvements are, however, illusory, as the best estimate of a weak signal is simply zero, which can be obtained by setting $\tau = 0$.

True improvements in the SNR can be observed for SNRs of 0 and +20 dB (Figures 5-6 and 5-7). Drastic degradation of the SNR by conventional clipping and editing is apparent when $\tau < 1$. In contrast, the signal-nulling clipper and editor improve the SNR for all reasonable threshold settings. It appears that the maximum improvement occurs for $0.1 \leq \tau \leq 0.316$. The "best" setting for τ appears to be approximately 0.178, which produces maximum improvement and is safely removed from the erratic results obtained when

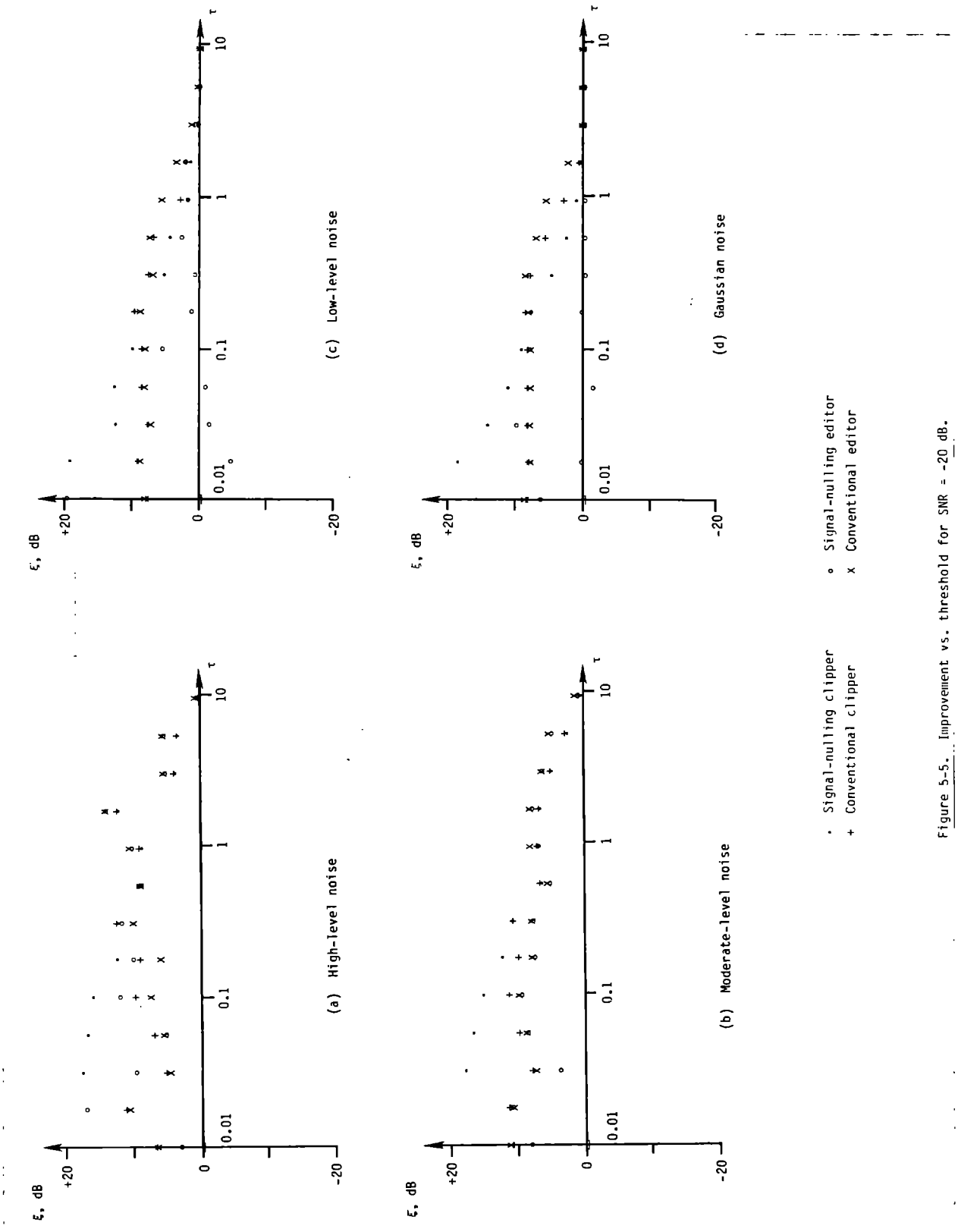

Figure 5-5. Improvement vs. threshold for SNR = -20 dB.

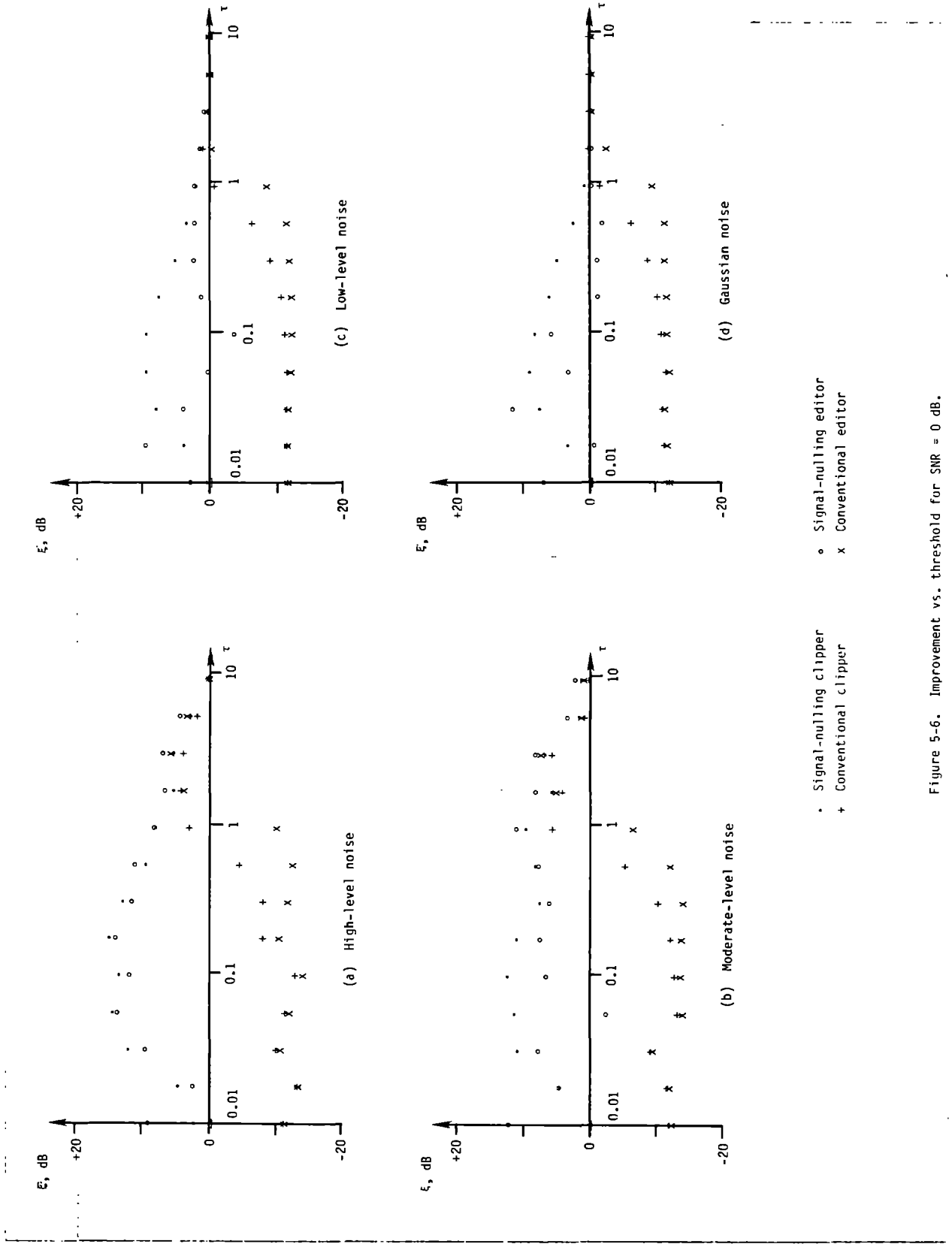

Figure 5-6. Improvement vs. threshold for SNR = 0 dB.

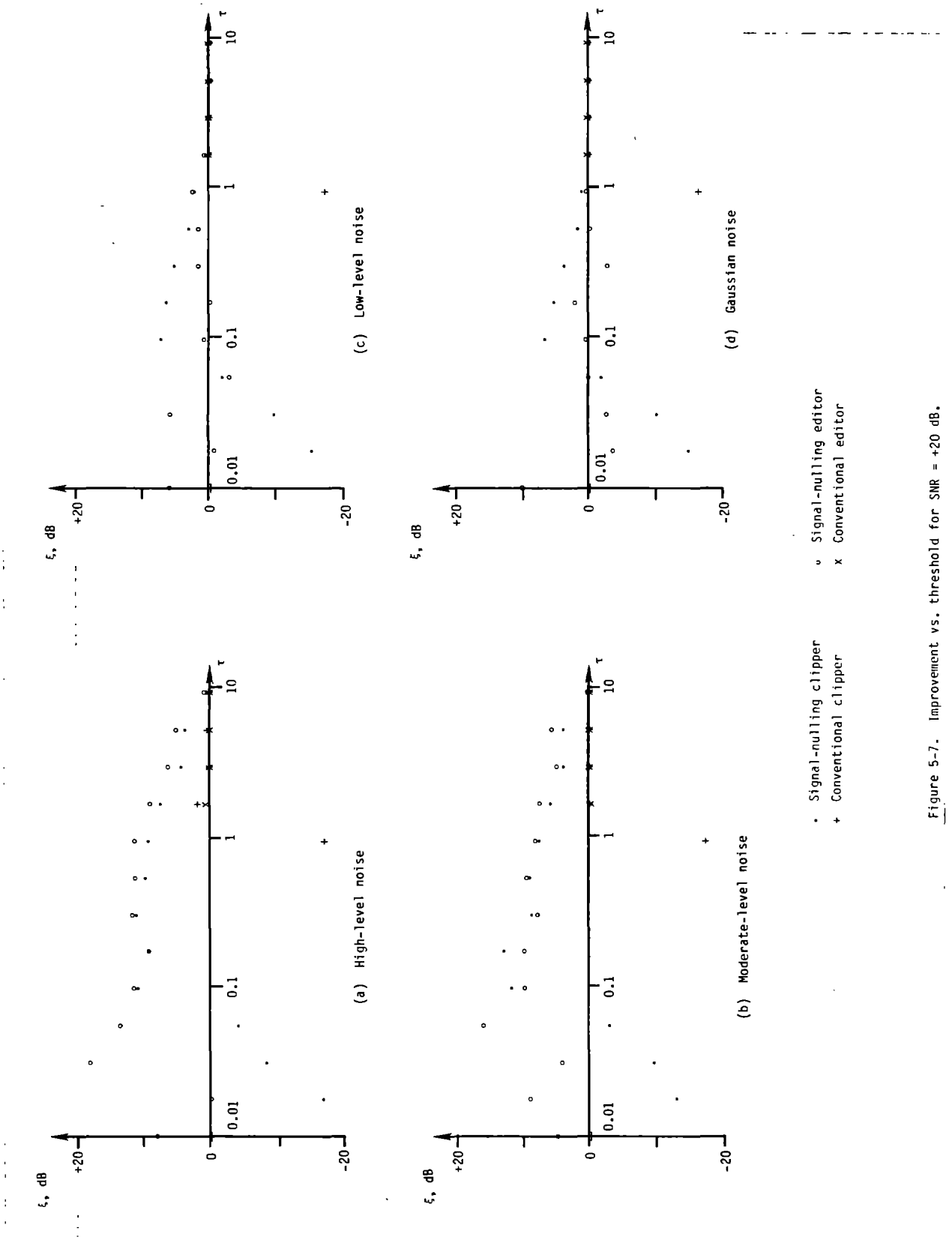

Figure 5-7. Improvement vs. threshold for SNR = +20 dB.

$\tau < 0.1$.

The signal-nulling clipper consistantly produces a 1 to 2 dB greater improvement than does the signal-nulling editor (Table 5-1). At first, this is somewhat suprising. However, optimum detection of a signal in nonGaussian noise [1] requires a nonlinear characteristic that transforms the nonGaussian noise into Gaussian noise. The clipper may be a better approximation to such a characteristic than the editor.

Figure 5-8 shows that the variation of improvement with SNR (signal level) is slight. As expected, the improvement increases with the impulsivity of the noise. At the preferred setting of $\tau = 0.178$, average improvements of 16.5, 12.5, and 8.1 dB were obtained for high-level, moderate-level, and low-level noise, respectively. These results compare favorably with the 13.1, 8.9, and 3.9 dB improvements that would be obtained by eliminating the power-Rayleigh component of the ELF noise entirely.

The effect of the nonlinear processing upon Gaussian noise is relatively small, usually only a few decibels improvement or degradation. This is not suprising, since reducing the threshold effectively reduces the number of samples, resulting in a slow increase in the estimation error. In contrast, reducing the threshold rapidly reduces the contributions of the impulsive component of the noise to the estimation error.

5.5 CHARACTERISTICS OF NARROWBAND OUTPUT

The statistical characteristics of the narrowband output of the nonlinear processor are evaluated through a series of simulations based upon the twelve different noise conditions defined in Table 3-3. A 100-Hz input bandwidth is assumed, and the impulsivity and spikiness are obtained from Table 4-1. The wideband ELF signals are generated as discussed in Chapter 3; all components are scaled to be of roughly the same amplitude.

Histogram Analysis

Histograms are compiled for both wideband inputs and narrowband outputs. The histograms of the wideband inputs are similar to those shown in Chapters 3 and 4. The impulsivities of the geology-filter components (i.e, E_x, E_y, and H_z) are similar to the impulsivities of the incident-field components (H_x, H_y, and E_z).

All of the histograms of the narrowband outputs appear to be Gaussian, regardless of the input noise conditions. A typical example is shown in Figure 5-9. Comparison of individual histograms to Gaussian curves (Figure 5-10) shows the agreement between them to be excellent. It therefore appears that a narrowband ANC processor designed to work with Gaussian noise should be satisfactory for dealing with the narrowband output signals.

NOISE CONDITION	PROCESSOR					
	CLIPPER			EDITOR		
	MAXIMUM IMPROVEMENT	MAXIMUM DEGRADATION	AVERAGE IMPROVEMENT	MAXIMUM IMPROVEMENT	MAXIMUM DEGRADATION	AVERAGE IMPROVEMENT
High level	+16.5	0	+13.4	+14.5	0	+11.8
Moderate level	+13.1	0	+12.5	+12.1	0	+ 9.8
Low level	+ 9.7	0	+ 8.1	+ 4.2	-1.8	+ 1.1
Gaussian	+ 7.8	0	+ 6.7	+ 7.8	-5.5	+ 0.7

Notes: $\tau = 0.178$.
All values in decibels.

Table 5-1. Effects of signal-nulling processors.

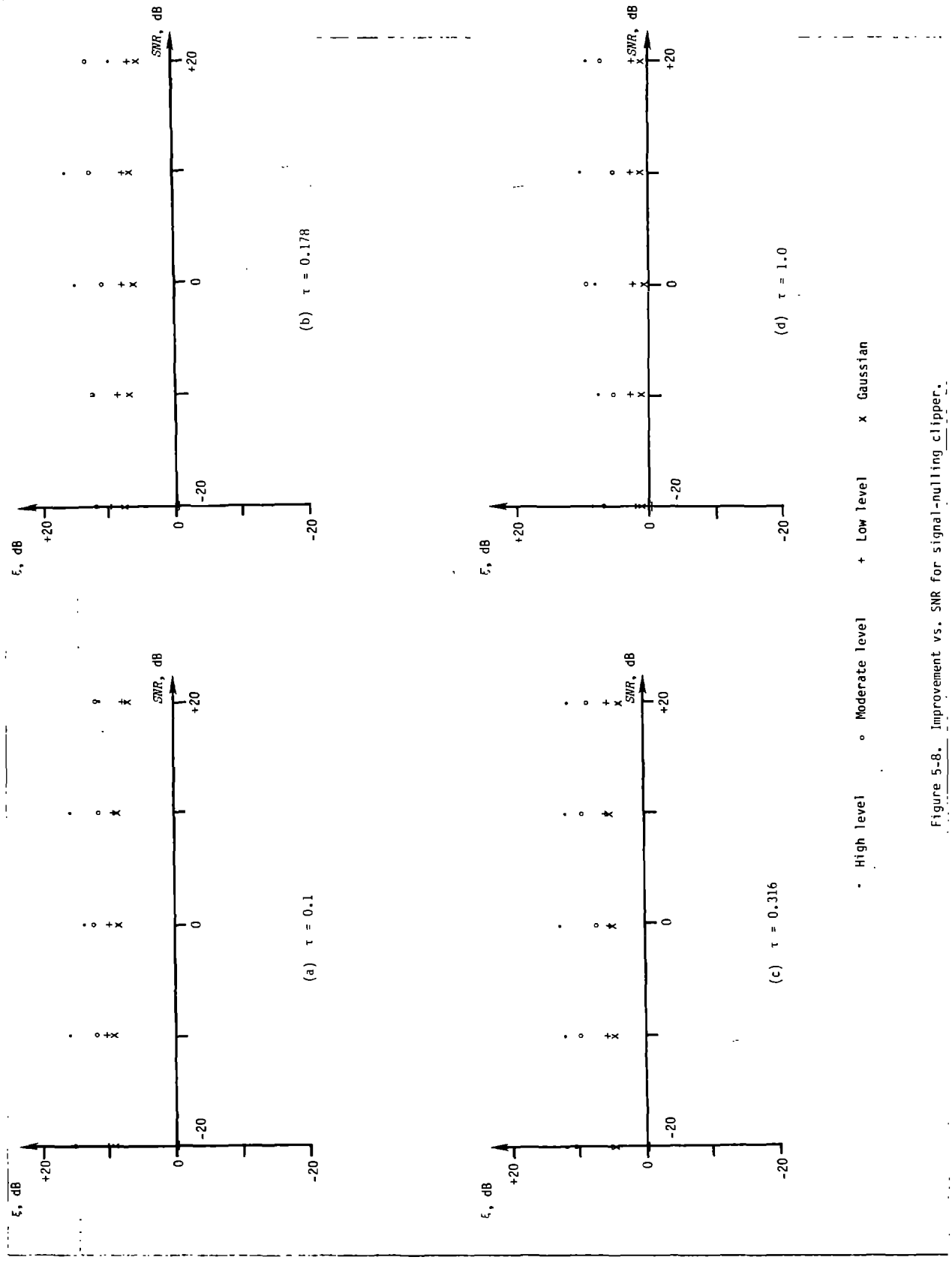

Figure 5-8. Improvement vs. SNR for signal-nulling clipper.

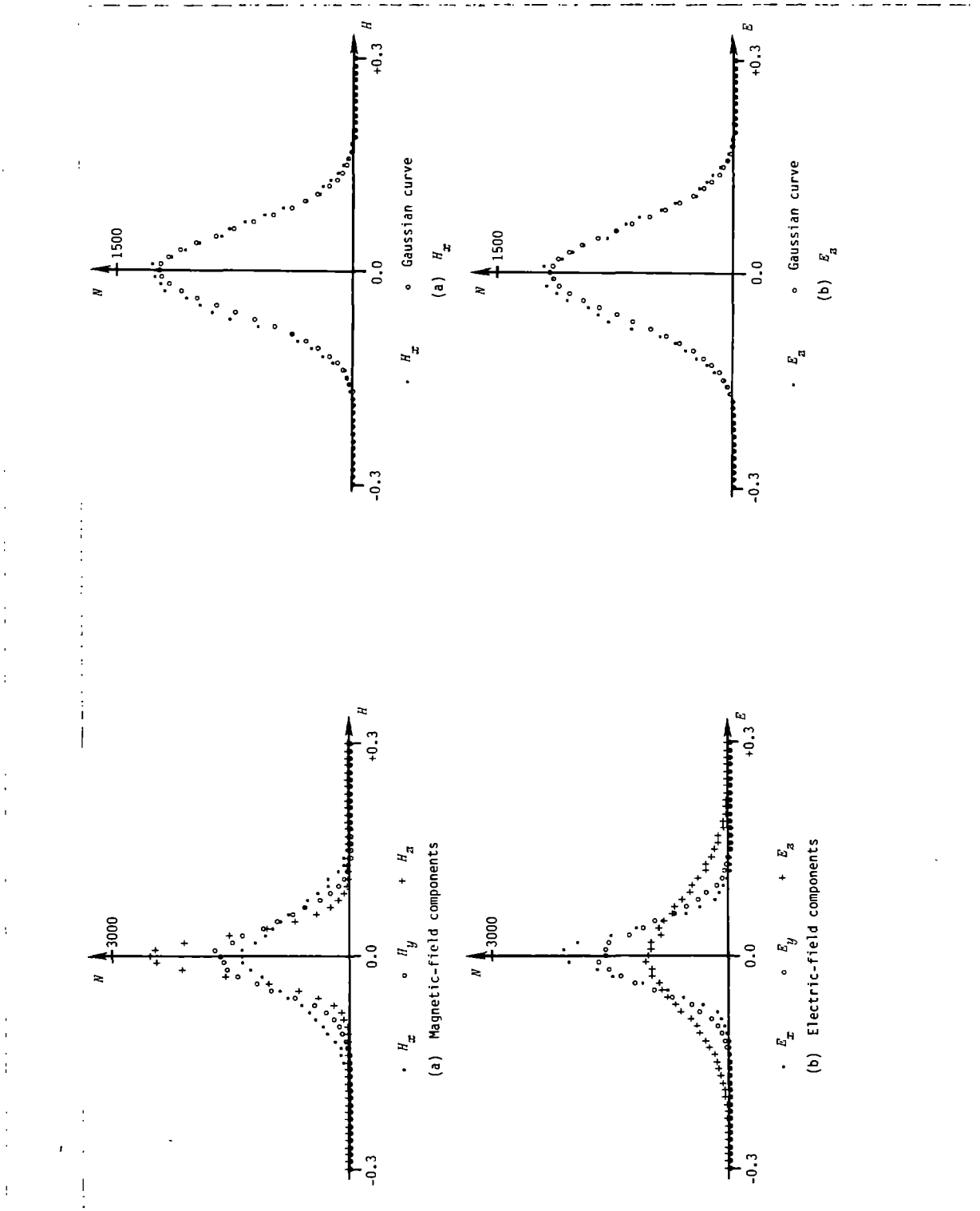

Figure 5-10. Comparison of histograms of narrowband output to Gaussian curve (Test #1).

Figure 5-9. Histograms of narrowband output (Test #6).

Correlation Analysis

The estimation of the covariance matrix of real random variables is discussed in [7]. From (36) of [7], the estimated covariance matrix of the wideband input noise is

$$\hat{C}_W = \frac{1}{K-1} \left\{ \sum_{k=1}^{K} \boldsymbol{z}(k)\, \boldsymbol{z}^T(k) - K\, \bar{\boldsymbol{z}}\, \bar{\boldsymbol{z}}^T \right\} , \tag{26}$$

where K represents the total number of samples.

A 12 × 12 real covariance matrix for the narrowband output could similarly be computed. However, a 6 × 6 complex covariance matrix is much more meaningful as it clearly indicates amplitude and phase relationships.

The relationship between real and complex covariance matrices is given by an isomorphism [8, §E.2]. Let zero-mean complex random vector $\boldsymbol{z}$ be represented by

$$\boldsymbol{z} = \boldsymbol{x} + j\, \boldsymbol{y} \quad . \tag{27}$$

Since the real and imaginary (in-phase and phase-quadrature, or I and Q) parts of $\boldsymbol{z}$ must have similar characteristics, it is necessary that

$$E[\boldsymbol{x}\, \boldsymbol{x}^T] = E[\boldsymbol{y}\, \boldsymbol{y}^T] = \boldsymbol{V} \tag{28}$$

and

$$-E[\boldsymbol{x}\, \boldsymbol{y}^T] = E[\boldsymbol{y}\, \boldsymbol{x}^T] = \boldsymbol{W}. \tag{29}$$

The complex covariance matrix of $\boldsymbol{z}$ is then

$$\boldsymbol{C}_N = E[\boldsymbol{z}\, \boldsymbol{z}^\dagger] = \boldsymbol{V} + j\, \boldsymbol{W} \quad , \tag{30}$$

where $\boldsymbol{z}^\dagger = (\boldsymbol{z}^*)^T$ is the complex conjugate of $\boldsymbol{z}$.

Use of this isomorphism and analogy to (26) yields estimators for the real and imaginary parts of complex covariance matrix for the narrowband output:

$$\hat{\boldsymbol{V}} = \frac{1}{2(K-1)} \left\{ \sum_{k=1}^{K} [\boldsymbol{x}(k)\, \boldsymbol{x}^T(k) + \boldsymbol{y}(k)\, \boldsymbol{y}^T(k)] - K[\bar{\boldsymbol{x}}\, \bar{\boldsymbol{x}}^T + \bar{\boldsymbol{y}}\, \bar{\boldsymbol{y}}^T] \right\} \tag{31}$$

$$\hat{\boldsymbol{W}} = \frac{1}{2(K-1)} \left\{ \sum_{k=1}^{K} [-\boldsymbol{x}(k)\, \boldsymbol{y}^T(k) + \boldsymbol{y}(k)\, \boldsymbol{x}^T(k)] - K[-\bar{\boldsymbol{x}}\, \bar{\boldsymbol{y}}^T + \bar{\boldsymbol{y}}\, \bar{\boldsymbol{x}}^T] \right\} \quad . \tag{32}$$

It is naturally difficult to compare the wideband and narrowband covariance matrices, since the former is real while the latter is complex. To aid in the comparison, the ratios of corresponding elements are computed accord-

ing to

$$R_{ij} = (|C_{Nij}|/C_{Wij})/(|C_{N6,6}|/C_{W6,6}) \quad . \tag{33}$$

Normalization by the ratio of the element corresponding to E_z suppresses the reduction in noise power caused by the reduction in bandwidth.

For elements that are significantly larger than the estimation noise, the ratio is always 0.3 or greater, and is usually 0.5 or greater. Thus the directional correlation characteristics of the narrowband outputs are expected to resemble closely those of the wideband inputs.

5.6 REFERENCES

1. S. S. Rappaport and L. Kurz, "An optimal nonlinear detector for digital data transmission through non-Gaussian noise," *IEEE Transactions on Communications Technology*, vol. COM-14, no. 6, pp. 266 - 274, June 1966.

2. E. C. Field, Jr. and M. Lewinstein, "Amplitude-probability distribution model for VLF/ELF atmospheric noise," *IEEE Transactions on Communications*, vol. COM-26, no. 1, pp. 83 - 87, January 1978.

3. J. W. Modestino, "A model for ELF noise," ESD-TR-71-322 (AD-737,368), Lincoln Laboratory, M.I.T., Lexington, MA, December 16, 1971.

4. T. Kalaith, "A general likelihood-ratio formula for random signals in Gaussian noise," *IEEE Transactions on Information Theory*, vol. IT-15, pp. 350 - 361, May 1969.

5. L. H. Rorden, T. C. Moore, E. C. Fraser, and L. R. Bulduc, "Phase I - Development of system concept for location of trapped miners in deep mines by an electromagnetic method," Final Report, Contract No. J0199009, Develco, Inc., Sunnyvale, CA, October 1979.

6. S. M. Bozic, *Digital and Kalman Filtering*, New York: John Wiley and Sons, 1979.

7. F. H. Raab, "Adaptive-noise-cancellation techniques for through-the-earth electromagnetics, Volume I," Report GMRR TR82-1, Green Mountain Radio Research Company, Burlington, VT, January 1982.

8. R. A. Monzingo and T. W. Miller, *Introduction to Adaptive Arrays*, New York: John Wiley and Sons, 1980.

CHAPTER 6. NARROWBAND ANC ALGORITHMS

Various algorithms for adaptive noise cancellation are reviewed in [1], and the direct-matrix-inversion (DMI) and least-mean-square (LMS) algorithms are identified as most applicable to the through-the-earth electromagnetic location systems. This chapter implements narrowband versions of the two algorithms and then conducts a set of three comparisons involving:

- DMI algorithm with various covariance estimators,
- LMS algorithm with various gains, and
- Best DMI and best LMS algorithms.

6.1 NOISE MODEL AND AVAILABLE INFORMATION

The narrowband-noise generator is somewhat less complicated than the wideband ELF model discussed in Chapter 3. The samples represent the baseband output of a detector, hence the signal appears as a constant rather than a sinewave. The noise is assumed to be Gaussian, to have zero mean, and to be uncorrelated from sample to sample. Correlations corresponding to the various electromagnetic components are obtained by applying a linear transformation to a vector of independent, Gaussian elements, as discussed in Chapter 5 of [1].

The noisy received signal is represented as the vector

$$\boldsymbol{z} = \boldsymbol{s} + \boldsymbol{x} = [z_1, z_2, \ldots, z_{L_s}]^T \quad , \tag{1}$$

where $\boldsymbol{s}$ represents the true signal and $\boldsymbol{x}$ represents the received noise. All three vectors are of length L_s, which represents the number of primary receiving channels. For three-axis magnetic-field reception at two locations, $L_s = 6$.

The noise output from the L_y reference channels is represented as the length-L_y vector

$$\boldsymbol{y} = [y_1, y_2, \ldots, y_{L_y}]^T \quad . \tag{2}$$

The primary-channel and reference-channel noise vectors $\boldsymbol{x}$ and $\boldsymbol{y}$ can be assembled into a single vector

$$\boldsymbol{n} = \begin{bmatrix} \boldsymbol{x} \\ \boldsymbol{y} \end{bmatrix} \quad , \tag{3}$$

whose length is $L_n = L_s + L_y$.

In the absence of an in-band CW signal, it is assumed that

$$E[\boldsymbol{n}] = \mathbf{0} \quad . \tag{4}$$

The covariance of the total-noise vector $\boldsymbol{n}$ is defined as

$$R_{nn} = E[\boldsymbol{n}\,\boldsymbol{n}^T] = \begin{bmatrix} R_{xx} & R_{xy} \\ R_{yx} & R_{yy} \end{bmatrix} \quad , \tag{5}$$

where

$$R_{xy} = E[\boldsymbol{x}\,\boldsymbol{y}^T] = R_{yx}^T \quad , \tag{6}$$

etc. It is also assumed the sampling rate and bandwidth are such that different samples are uncorrelated; i.e.,

$$E[n_i(k)\; n_j(l)] = 0 \quad \text{if} \quad k \neq l \quad . \tag{7}$$

Available Information

Retention of all signal and noise samples requires an inordinate amount of memory. Therefore, the principal statistics available to the ANC processor are sums of samples and products such as

$$\Sigma\boldsymbol{z}(k),\ \Sigma\boldsymbol{y}(k),\ \Sigma\boldsymbol{z}(k)\;\boldsymbol{y}^T(k),\ \text{and}\ \Sigma\boldsymbol{y}(k)\;\boldsymbol{y}^T(k) \quad . \tag{8}$$

Averages such as

$$\overline{\boldsymbol{z}}(K) = \frac{1}{K}\sum_{k=1}^{K} \boldsymbol{z}(k) \tag{9}$$

and

$$\overline{\boldsymbol{y}}(K) = \frac{1}{K}\sum_{k=1}^{K} \boldsymbol{y}(k) \tag{10}$$

are readily derived from the accumulated sums.

6.2 DMI ALGORITHM

A direct-matrix-inversion ANC algorithm based upon a CW signal, narrowband Gaussian noise, and unknown noise covariance is developed. Several candidate covariance estimators are compared by simulation. The best performance is obtained by a recursive computation that alternately improves the signal estimate and then the covariance estimate.

Requirements for Unbiased Estimator

The ANC algorithm forms the estimate $\boldsymbol{s}$ of the signal from a linear combination of the primary and reference inputs, thus

$$\hat{\boldsymbol{s}} = \boldsymbol{T}\,\overline{\boldsymbol{z}} - \boldsymbol{W}\,\overline{\boldsymbol{y}} \quad , \tag{11}$$

where matrices $\boldsymbol{T}$ and $\boldsymbol{W}$ are to be determined.

The position of the subsurface transmitter is estimated directly from the amplitudes of the components of the received magnetic-field vectors [2]. It is therefore highly desirable (if not necessary) that the signal estimator be *unbiased*; i.e.

$$E[\hat{\boldsymbol{s}}] = \boldsymbol{s} \quad , \tag{12}$$

where E[ ] denotes an expected value. This property is called *undistorted* in adaptive-array literature [3].

Application of (12) to (11) produces

$$\boldsymbol{T}\,E[\overline{\boldsymbol{z}}] - \boldsymbol{W}\,E[\overline{\boldsymbol{y}}] = \boldsymbol{s} \quad . \tag{13}$$

From (9), (10), and (4),

$$E[\overline{\boldsymbol{y}}] = E[\overline{\boldsymbol{y}}] = \boldsymbol{0} \tag{14}$$

and

$$E[\overline{\boldsymbol{z}}] = E[\boldsymbol{z}] = \boldsymbol{s} \quad . \tag{15}$$

The insertion of (14) and (15) in (13) yields

$$\boldsymbol{s} = \boldsymbol{T}\,\boldsymbol{s} - \boldsymbol{W}\,\boldsymbol{0} = \boldsymbol{T}\,\boldsymbol{s} \quad . \tag{16}$$

The only general solution to (16) is

$$\boldsymbol{T} = \boldsymbol{I} \quad . \tag{17}$$

The requirement for an unbiased estimate of the signal therefore prohibits combination of the primary inputs (i.e., inputs containing components of the signal). This simplifies the derivation of the ANC estimator somewhat, since the derivation is reduced to L_s separate scalar problems.

DMI Estimator

A DMI ANC algorithm is based upon inversion of the known or estimated noise covariance matrix [1,3]. From the preceding discussion, the DMI estimator has the form

$$\hat{\boldsymbol{s}} = \overline{\boldsymbol{z}} - \boldsymbol{W}\,\overline{\boldsymbol{y}} \quad . \tag{18}$$

The form of weighting matrix $\boldsymbol{W}$ is determined in this section.

It is convenient to break this problem into L_s separate scalar problems. This is accomplished by partitioning weighting matrix $\boldsymbol{W}$ into L_s row vectors,

thus

$$\boldsymbol{W} = \begin{bmatrix} \boldsymbol{w}_1^T \\ \boldsymbol{w}_2^T \\ \cdots \\ \boldsymbol{w}_{L_\varepsilon}^T \end{bmatrix} \quad . \tag{19}$$

Remember that $\boldsymbol{w}_i$ is $L_y \times 1$ while $\boldsymbol{w}^T$ is $1 \times L_y$. Vector equation (18) may now be divided into L_ε scalar equations of the form

$$\hat{\varepsilon} = \overline{z} - \boldsymbol{w}^T \overline{\boldsymbol{y}} \quad ; \tag{20}$$

By use of (1), the estimate of ε becomes

$$\hat{\varepsilon} = \varepsilon + \overline{x} - \boldsymbol{w}^T \boldsymbol{y} \quad , \tag{21}$$

hence the estimation error is

$$\tilde{\varepsilon} = \varepsilon - \hat{\varepsilon} = - \overline{x} + \boldsymbol{w}^T \boldsymbol{y} \quad . \tag{22}$$

The squared estimation error is therefore

$$\tilde{\varepsilon}^2 = \overline{x}^2 - 2\, \overline{x}\, \boldsymbol{w}^T \boldsymbol{y} + \boldsymbol{w}^T \overline{\boldsymbol{y}}\, \overline{\boldsymbol{y}}^T \boldsymbol{w} \quad . \tag{23}$$

The expected mean-squared estimation error (MSE) is obtained by taking the expected value of (23), thus

$$\varepsilon = E[\tilde{\varepsilon}^2] = E[\overline{x}^2] - 2\, \boldsymbol{w}^T E[\overline{x}\, \overline{\boldsymbol{y}}] + \boldsymbol{w}^T E[\overline{\boldsymbol{y}}\, \overline{\boldsymbol{y}}^T]\, \boldsymbol{w} \quad . \tag{24}$$

The first term in (24) is a scalar of the form

$$E[\overline{x}^2] = (1/K)\, E[x^2] = (1/K)\, R_{xx} \quad ; \tag{25}$$

note that this is the (i,i) element of the primary-noise covariance matrix $\boldsymbol{R}_{xx}$. The second term in (24) includes the $L_y \times 1$ vector

$$E[\overline{\boldsymbol{y}}\, \overline{x}] = (1/K)\, E[\boldsymbol{y}\, x] = (1/K)\, \boldsymbol{r}_{yx} \quad , \tag{26}$$

which is the i^{th} column of the cross-covariance matrix

$$R_{yx} = [\boldsymbol{r}_{yx_1}, \boldsymbol{r}_{yx_2}, \cdots, \boldsymbol{r}_{yx_{L_\varepsilon}}] \quad . \tag{27}$$

The third term of (24) contains the $L_y \times L_y$ matrix

$$E[\bar{\boldsymbol{y}}\ \bar{\boldsymbol{y}}^T] = (1/K)\ E[\boldsymbol{y}\ \boldsymbol{y}^T] = (1/K)\ \boldsymbol{R}_{yy} \quad . \tag{28}$$

Insertion of (25), (26), and (28) into (24) yields

$$\varepsilon = (1/K)\ [R_{xx} - 2\ \boldsymbol{w}^T\ \boldsymbol{r}_{yx} + \boldsymbol{w}^T\ R_{yy}\ \boldsymbol{w}] \quad . \tag{29}$$

The desired weighting matrix should minimize the expected mean-squared estimation error. The vector $\boldsymbol{w}_i$ that minimizes the MSE in ε_i is found by determining the gradient of the MSE with respect to $\boldsymbol{w}_i$ and setting the result equal to a zero vector, thus

$$\boldsymbol{0} = \nabla_{\boldsymbol{w}}\ \varepsilon = -\ 2\ \boldsymbol{r}_{yx} + 2\ R_{yy}\ \boldsymbol{w} \quad . \tag{30}$$

From the above, it is apparent that

$$\boldsymbol{w} = R_{yy}^{-1}\ \boldsymbol{r}_{yx} \quad . \tag{31}$$

Note that the same result could be obtained by differentiating (29) with respect to each element of $\boldsymbol{w}_i$ and assembling the resulting L_y scalar equations into a single vector equation.

The transpose of the weighting matrix is given by

$$\begin{aligned} \boldsymbol{W}^T &= [\boldsymbol{w}_1, \boldsymbol{w}_2, \ldots, \boldsymbol{w}_{L_y}] \\ &= R_{yy}^{-1}\ [\boldsymbol{r}_{yx_1}, \boldsymbol{r}_{yx_2}, \ldots, \boldsymbol{r}_{yx_{L_y}}] = R_{yy}^{-1}\ R_{yx} \quad . \end{aligned} \tag{32}$$

Since $\boldsymbol{R}_{yy}$ is symmetric, R_{yy}^{-1} is also symmetric, and

$$\boldsymbol{W} = [R_{yy}^{-1}\ R_{yx}]^T = R_{yx}^T\ [R_{yy}^{-1}]^T = R_{xy}\ R_{yy}^{-1} \quad . \tag{33}$$

The expected estimation error can now be obtained by substituting (31) into (29), which yields

$$\varepsilon_{i,\min} = (1/K)\ [R_{xx(i,i)} - \boldsymbol{r}_{yx_i}^T\ R_{yy}^{-1}\ \boldsymbol{r}_{yx_i}] \tag{34}$$

for a single channel. Combining all channels then yields the total expected MSE

$$\varepsilon_{\min} = (1/K)\ \text{trace}\ (R_{xx}\ R_{yx}^T\ R_{yy}^{-1}\ R_{yx}) \quad . \tag{35}$$

Covariance Estimators

The weighting matrix (33) is derived from the noise covariance matrices $\boldsymbol{R}_{yx}$ and $\boldsymbol{R}_{yy}$. In the TTE EM application, neither of these matrices is known *a priori*, hence estimates must be used in their place. The form of the DMI weighting matrix is therefore

$$\boldsymbol{W} = \hat{\boldsymbol{R}}_{xy}^{T} \; \hat{\boldsymbol{R}}_{yy}^{-1} \quad . \tag{36}$$

The reference input $\boldsymbol{y}$ is assumed to be pure noise and therefore to have a zero mean. The estimator for $\boldsymbol{R}_{yy}$ is therefore [1, Chapter 5]

$$\hat{\boldsymbol{R}}_{yy} = \frac{1}{K} \sum_{k=1}^{K} \boldsymbol{y}(k) \; \boldsymbol{y}^{T}(k) \quad . \tag{37}$$

The expected value of the primary $\boldsymbol{z}$ input is nonzero, the expected value of the reference input $\boldsymbol{y}$ is zero, and signal $\boldsymbol{s}$ is unknown *a priori*. The form of the estimator for $\boldsymbol{R}_{xy}$ is therefore more difficult to determine than that of $\hat{\boldsymbol{R}}_{yy}$. Numerous *ad hoc* estimators are used in adaptive-antenna systems [3].

A simple candidate for the covariance estimator is

$$\hat{\boldsymbol{R}}_{xy}(0) = \frac{1}{K} \sum_{k=1}^{K} \boldsymbol{z}(k) \; \boldsymbol{y}^{T}(k) \quad . \tag{38}$$

The use of (14) and (15) yields

$$\hat{\boldsymbol{R}}_{xy}(0) = (1/K) \; \Sigma \; \boldsymbol{x} \; \boldsymbol{y}^{T} + \boldsymbol{s} \; \overline{\boldsymbol{y}}^{T} \quad , \tag{39}$$

from which it is apparent that

$$E[\hat{\boldsymbol{R}}_{xy}(0)] = E[\boldsymbol{x} \; \boldsymbol{y}^{T}] = \hat{\boldsymbol{R}}_{xy} \quad ; \tag{40}$$

i.e., it is unbiased.

While $\boldsymbol{R}_{xy}(0)$ is unbiased, its second term is the product of a possibly large constant and a random sum and may therefore contribute significantly to the variance of the estimate. A second candidate estimator of the form

$$\hat{\boldsymbol{R}}_{xy}(1) = \frac{1}{K} \sum_{k=1}^{K} \boldsymbol{z}(k) \; \boldsymbol{y}^{T}(k) - \overline{\boldsymbol{z}} \; \overline{\boldsymbol{y}}^{T} \tag{41}$$

is therefore proposed. The use of (14) and (15) yields

$$\hat{\boldsymbol{R}}_{xy}(1) = (1/K) \; \Sigma \boldsymbol{x} \; \boldsymbol{y}^{T} - \overline{\boldsymbol{x}} \; \overline{\boldsymbol{y}}^{T} \quad ; \tag{42}$$

it is apparent that this estimator is also unbiased. Since the second term in (42) is the product of two random sums with expected values of zero, the variance of $\boldsymbol{R}_{xy}(1)$ should be less than that of $\boldsymbol{R}_{xy}(0)$ when there is a significant signal.

The objective of subtracting the product of the two averages in (41) is to estimate and to cancel the contributions of signal-estimation error. It

is therefore reasonable to propose another candidate estimator of the form

$$\hat{R}_{xy}(2) = \frac{1}{K} \sum_{k=1}^{K} \boldsymbol{z}(k)\, \boldsymbol{y}^T(k) - \hat{\boldsymbol{s}}(1)\, \overline{\boldsymbol{y}}^T \quad , \tag{43}$$

where $\hat{\boldsymbol{s}}(1)$ is the signal estimate obtained by the DMI technique with the covariance estimate $R_{xy}(1)$. Equation (43) suggests a recursive process by which a signal estimate is used to improve the covariance estimate, which is in turn used to improve the signal estimate. Higher-order estimators are defined by analogy to (43).

Comparison of Covariance Estimates

The various candidate covariance estimators were compared by simulation. The signal was estimated by the DMI ANC algorithm with covariance estimators $R_{xy}(0)$, $R_{xy}(1)$, $R_{xy}(2)$, and $R_{xy}(3)$. The signal was also estimated by simple averaging (no ANC). The squared error was tabulated for all five estimates of the signal.

The simulations used a 3-element signal vector and a 3-element reference vector. The covariance structure was relatively simple: signal channel #1 was correlated only with reference channel #1, etc. Tests were run with unity noise variance and zero and unity signal levels.

Typical results for unity signal levels are shown in Figure 6-1; in all cases, a maximum of 1000 samples were processed. The results indicate that:

- For correlations below 0.9, the ANC algorithm produces little or no improvement, and form of the covariance estimator has little or no effect.
- At a correlation of 0.9, ANC produces some improvement but the form of the covariance estimator makes little difference.
- For correlations of 0.99 to 0.999, ANC produces significant improvement and $R_{xy}(2)$ produces a slight improvement over $R_{xy}(1)$.
- At a correlation of 1.0, the improvement of the ANC algorithm is (as expected) dramatic, and $R_{xy}(2)$ produces significantly better results than $R_{xy}(1)$. No further improvement is obtained by using $R_{xy}(3)$.

From these results, it is concluded that $R_{xy}(2)$ should be used as the covariance estimator.

The full benefits of an ANC algorithm cannot be obtained without a good estimate of the covariance matrix. Therefore, it appears likely that if more samples were processed, the ANC algorithm would make more significant improvements for correlations in the range of 0.5 to 0.9.

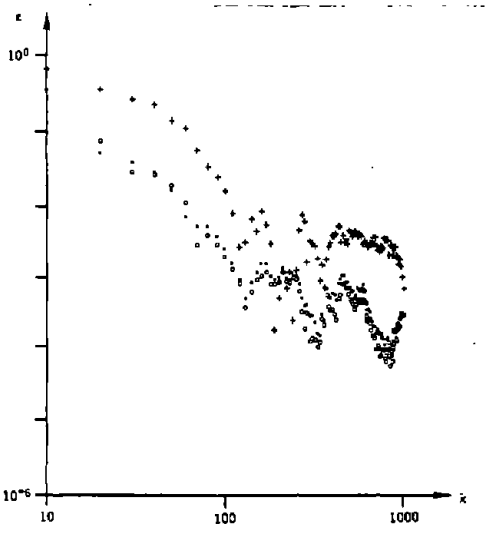

(a) Correlation of 0.9

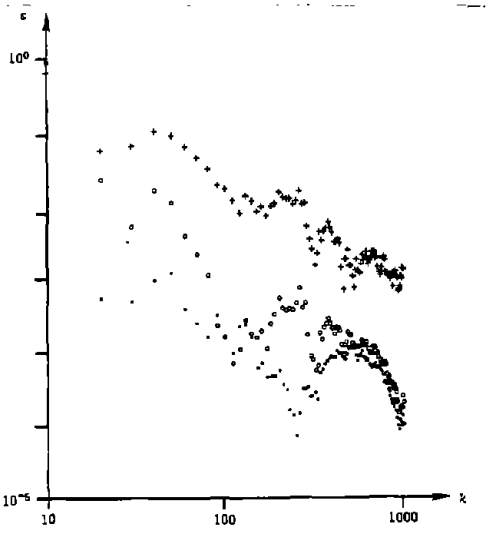

(b) Correlation of 0.99

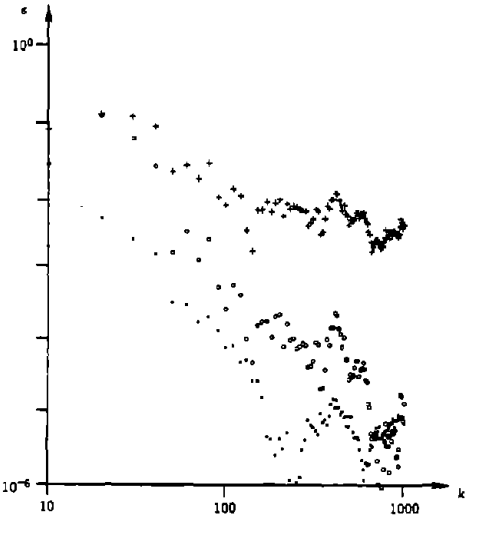

(c) Correlation of 0.999

\+ No ANC ∘ DMI with $\hat{R}_{xy}(0)$ · DMI with $\hat{R}_{xy}(1)$

Figure 6-1. Convergence of DMI algorithm.

6.3 LMS ALGORITHM

The direct-matrix inversion ANC algorithm converges rapidly and makes nearly optimum use of the available information. However, it requires matrix inversion and can therefore be performed infrequently, perhaps only upon completion of the data collection. An alternative ANC technique [3,4] known as "least mean square" or "LMS" requires only relatively simple computations and can therefore be performed in real time as data samples are taken. This section formulates the LMS ANC algorithm for the TTE EM application and tests it through simulation.

Formulation

Many aspects of the formulation of the LMS estimator are similar to those of the DMI estimator. The signal-and-noise model is identical. The requirement for unbiased estimation of signal components prohibits the combination of primary inputs with each other. Again, the estimator is most easily formulated first in terms of separate scalar estimators and then generalized to vector form.

In constrast to the DMI estimator, the LMS estimator operates in real time on a sample-by-sample basis. The *single-sample* estimate produced by the LMS algorithm is therefore represented by

$$u(k) = z(k) + \boldsymbol{w}^T(k)\ \boldsymbol{y}(k) \quad , \tag{44}$$

where $\boldsymbol{w}$ is a weighting vector similar to that used in the DMI algorithm. The *final* or *all-sample* estimate of the signal is obtained by averaging the single-sample estimates, thus

$$\hat{s}(k) = \frac{1}{k} \sum_{j=1}^{k} u(j) \quad . \tag{45}$$

The error in the single-sample estimate $\boldsymbol{u}(k)$ is

$$\tilde{u}(k) = s - u(k) = x(k) - \boldsymbol{w}^T(k)\ \boldsymbol{y}(k) \quad , \tag{46}$$

hence the squared single-sample error is

$$\tilde{u}^2(k) = x^2(k) - 2\ \boldsymbol{w}^T(k)\ \boldsymbol{y}(k)\ x(k) + \boldsymbol{w}^T(k)\ \boldsymbol{y}(k)\ \boldsymbol{y}^T(k)\ \boldsymbol{w}(k) \quad . \tag{47}$$

The expected value of the squared error (MSE) is therefore given by

$$\xi(k) = E[\tilde{u}(k)] = R_{xx} - 2\ \boldsymbol{w}^T(k)\ \boldsymbol{r}_{yx} + \boldsymbol{w}^T(k)\ R_{yy}\ \boldsymbol{w}(k) \quad . \tag{48}$$

This form is identical to that of the DMI estimator (23) except for the factor $1/K$.

Weighting Vector

If the statistics of the noise were known, the weighting vector would be given by a product of the inverse covariance matrix and the cross-covariance matrix, as in (31). The use of estimates of R_{yy} and r_{yx} as in the DMI algorithm would require real-time matrix inversion. Matrix inversion can be avoided by recursive updating of the estimated inverse matrix; however several matrix multiplications are required to process each new sample.

The Widrow LMS algorithm [3,4] uses a simple, *ad-hoc* approach based upon estimation of the gradient of the MSE with respect to the weighting vector. Consider an all-scalar application and suppose that an estimate $w(k)$ of the weighting constant is available and that an improved estimate $w(k+1)$ is desired. The derivative $\partial\xi/\partial w$ indicates the direction in which to change $w(k)$ to obtain $w(k+1)$ with a lower ξ.

The multi-dimensional analogy is

$$\boldsymbol{w}(k+1) = \alpha(k)\,\boldsymbol{w}(k) - \beta(k)\,\boldsymbol{g}(k) \quad , \tag{49}$$

where the gradient vector is given by

$$\boldsymbol{g}(k) = \nabla_{w}\,\xi = R_{yy}\,\boldsymbol{w}(k) - \boldsymbol{r}_{yx} \tag{50}$$

when the noise characteristics are known. Time constants $\alpha(k)$ and $\beta(k)$ are discussed subsequently.

Since the covariance matrices are unknown *a priori*, the gradient vector must be estimated. The single-sample squared error

$$\hat{\xi}(k) = \tilde{u}^2(k) \tag{51}$$

provides a convenient estimate of the expected MSE. The estimated gradient vector is therefore

$$\hat{g}(k) = \nabla_{w}\,\tilde{u}^2(k) = 2\,\tilde{u}(k)\,\nabla_{w}\,\tilde{u}(k) \tag{52}$$

$$= 2\,\tilde{u}(k)\,\nabla_{w}[x(k) - \boldsymbol{w}^{T}(k)\,\boldsymbol{y}(k)] = -\,2\,\tilde{u}(k)\,\boldsymbol{y}(k) \quad . \tag{53}$$

Since s is not known, the estimate $\hat{s}$ is used in its place, thus

$$\tilde{u}(k) \cong \hat{s}(k-1) - u(k) \tag{54}$$

is used in (53).

The usual formulation of the LMS algorithm uses time constants of the form

$$\alpha(k) = 1$$

$$\beta(k) = \text{constant} \quad . \tag{55}$$

Such a set of constants corresponds to a filter with a fixed bandwidth. Consequently, the effects of a particular sample decrease with time and the variance of the gradient estimate becomes constant after a sufficient number of samples has been processed.

The constant-bandwidth filter is well suited to time-varying signals or nonstationary noise characteristics. However, when the signal is constant and the noise is stationary (as in the present application), the use of a constant-bandwidth filter (55) may limit the accuracy of the estimate of the gradient vector (and therefore also limit the accuracy of the estimate of the signal). An alternative that may prove useful in this application is

$$\beta(k) = 1/k$$

$$\alpha(k) = 1 - \beta(k) = (k - 1)/k \quad . \tag{56}$$

The use of (56) provides an always decreasing bandwidth by weighting all single-sample estimates (k=1, ..., K) equally.

Since the quality of the all-sample signal estimate $\hat{s}$ improves with time, the quality of the gradient estimate $\hat{g}$ also improves with time. Consequently, the equal-weight approach of (56) may not be optimum, and a stepped gain algorithm may be useful. In this approach, β is decreased in steps as the number of samples increases; for example:

$$\beta = \begin{cases} \beta_0, & 1 < k \leq 10 \\ \beta_0/10, & 10 < k \leq 100 \\ \beta_0/100, & 100 < k \leq 1000 \\ \cdots & \end{cases} \quad , \tag{57}$$

Vector Estimator

The vector form of the LMS estimator can be derived by analogy to the scalar form derived above. As for the DMI estimator,

$$\boldsymbol{W}(k) = \begin{bmatrix} \boldsymbol{w}_1^T(k) \\ \boldsymbol{w}_2^T(k) \\ \cdots \\ \boldsymbol{w}_{L_s}^T(k) \end{bmatrix} \quad . \tag{58}$$

The single-sample estimate and error vectors are given by

$$\tilde{\boldsymbol{u}}(k) = [u_1(k),\ u_2(k),\ \ldots\ ,\ u_{L_s}(k)]^T = \boldsymbol{z}(k) - \boldsymbol{W}(k)\ \boldsymbol{y}(k) \tag{59}$$

and

$$\tilde{\boldsymbol{u}}(k) = \hat{\boldsymbol{s}}(k - 1) - \boldsymbol{u}(k) \quad . \tag{60}$$

The all-sample estimate of the signal vector is given by

$$\hat{\boldsymbol{s}}(k) = \frac{1}{k} \sum_{j=1}^{k} \boldsymbol{u}(k) = \frac{k - 1}{k}\ \hat{\boldsymbol{s}}(k - 1) + \frac{1}{k}\ \boldsymbol{u}(k) \quad . \tag{61}$$

The L_s length-L_y gradient vectors are assembled into the gradient matrix

$$\hat{G}(k) = \begin{bmatrix} \hat{\boldsymbol{g}}_1^T(k) \\ \hat{\boldsymbol{g}}_2^T(k) \\ \cdots \\ \hat{\boldsymbol{g}}_{L_s}^T(k) \end{bmatrix} = \tilde{\boldsymbol{u}}(k)\ \boldsymbol{y}^T(k) \quad , \tag{62}$$

and the weighting matrix is therefore given by

$$\boldsymbol{W}(k + 1) = \alpha(k)\ \boldsymbol{W}(k) + \beta(k)\ \hat{\boldsymbol{G}}(k) \quad . \tag{63}$$

Simulation Results

The three proposed versions of the LMS ANC algorithm were tested by simulation. The noise-correlation structures were the same as those used with the DMI algorithm. While 10,000 samples were used in two of the simulations, all others used 1000 samples.

For the conventional, constant-gain LMS algorithm, $\beta = 0.1$ usually produces the smallest total squared error. The value of β is not critical, and the results appear to be nearly the same for $0.0316 \leq \beta \leq 0.316$. Values of $\beta > 0.5$ produce instability. The instability is consistant with the requirement [1,3,4] that β be less than the largest eigenvalue of the noise covariance matrix. Figure 6-2 illustrates the convergence of the LMS algorithm with various values of β.

The stepped-gain algorithm consistantly produces larger squared errors than the constant-gain algorithm. The estimates produced by the conventional and average-gradient versions appear to have the same accuracy.

The advantage of ANC is apparent when noise correlation is high. For correlations of 0.999 and 0.99, the constant-gain LMS algorithm effectively reduces the noise level by an average of about 17 dB. The noise reduction achieved by the LMS algorithm does not appear to be as great as that achieved by the DMI algorithm.

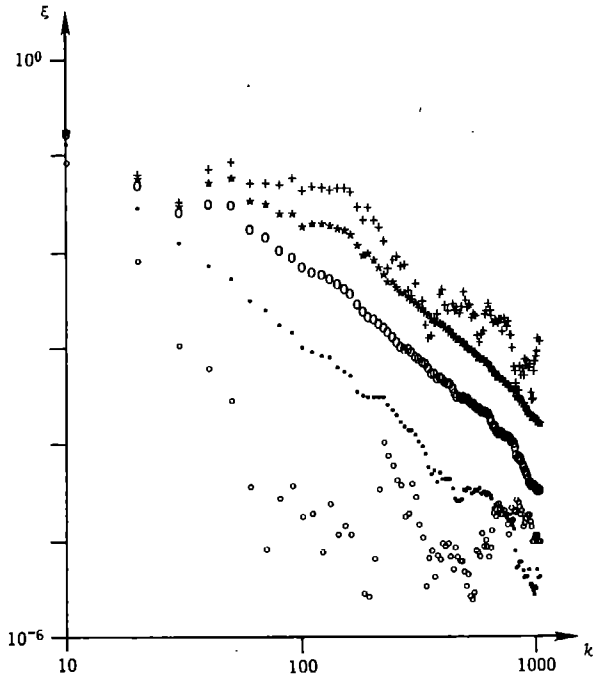

\+ No ANC * β = 0.01 o β = 0.0316
• β = 0.1 ∘ β = 0.3160

(a) Correlation of 0.999

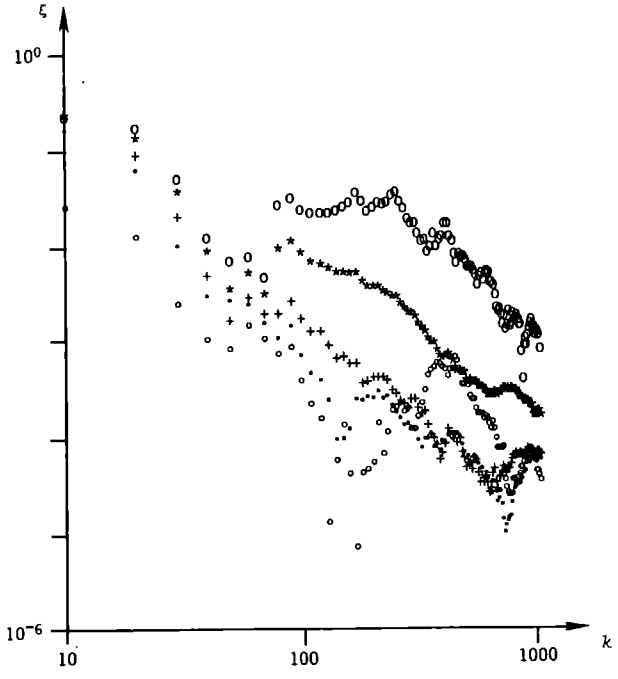

o No ANC * β = 0.01 + β = 0.0316
• β = .1 ∘ β = .3160

(b) Correlation of 0.99

Figure 6-2. Convergence of LMS algorithm.

Conclusions

The conclusions drawn from the preceding analysis and simulation results are:

- The constant-gain (conventional) LMS algorithm is preferred over the other candidates,
- The value of β is not critical. It should be approximately 0.1 times the largest eigenvalue of the best *a priori* estimate of noise covariance matrix.

6.4 COMPARISON OF ALGORITHMS

The preferred forms of the DMI and LMS ANC algorithms for narrowband Gaussian noise are compared by simulation. Comparable noise reductions are achieved for correlations in the range of 0.9 to 0.99. For correlations greater than 0.999, the DMI algorithm achieves significantly greater noise reduction. The noise reduction achieved is close to that achievable when the noise covariance characteristics are known. For correlations less than 0.9, neither algorithm produces significant noise reduction.

Figure 6-3 illustrates typical convergence characteristics. For small values of k, the DMI algorithm clearly yields greater noise reduction. However, by $k = 500$, the LMS algorithm has achieved a good estimate of the gradient vector (hence optimum weighting matrix).

In most cases, the DMI and LMS algorithms produce comparable noise reductions, provided there are a sufficient number of samples ($k \geq 500$) to allow convergence of the LMS gradient estimate. The simulations show that this is true for up to 10,000 samples.

The noise reduction achieved in the simulations is plotted as a function of correlation in Figure 6-4. For a correlation of 0.5 or less, neither algorithm is effective. However, the results would be similar even if the noise covariance were known *a priori*, since there is little noise that can be cancelled.

For correlations between about 0.9 and 0.99, the DMI and LMS algorithms produce similar noise reductions. However, for correlations of 0.999 and higher, the DMI algorithm is clearly superior. The noise cancellation achieved by the DMI algorithm (and the LMS algorithm for correlations between 0.9 and 0.99) is nearly that which can be obtained when the noise covariance matrix is known *a priori*. For example, if $\rho = 0.99$, the effective noise power can be reduced to approximately 1 percent of that in the output of the primary antenna.

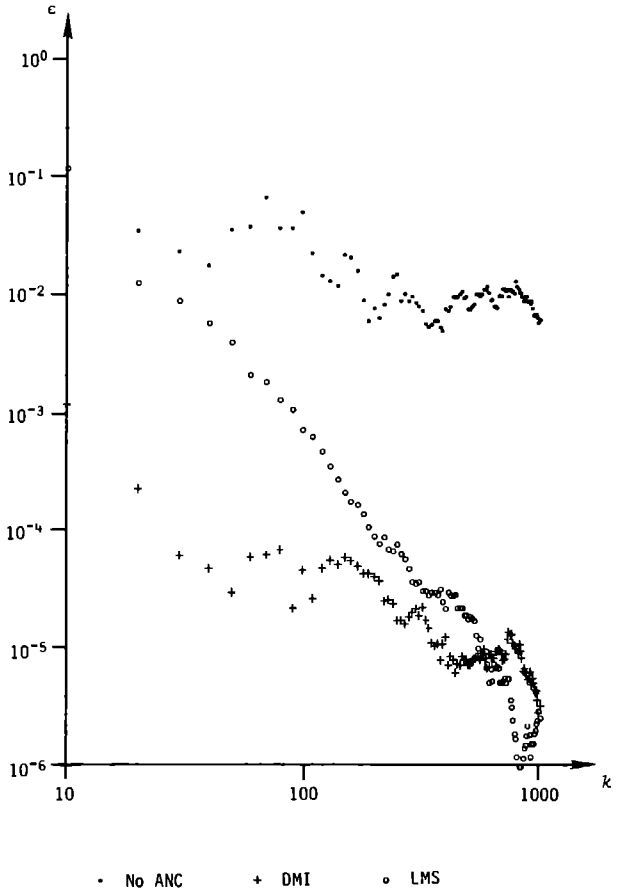

Figure 6-3. Convergence of ANC algorithms with noise correlation of 0.999.

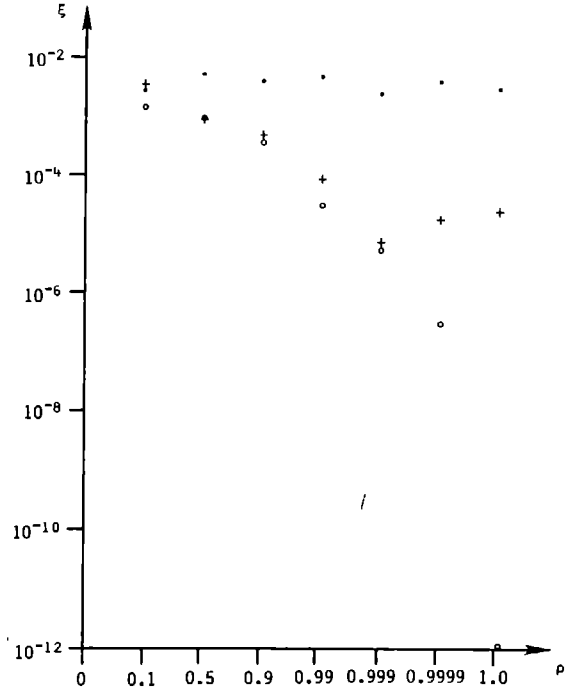

Figure 6-4. Mean-square error as a function of correlation.

6.5 SIMULATION

The simulations discussed here test the two narrowband ANC algorithms under conditions resembling those in the real world. The objectives of these simulations include observation of the effects of

- Electric-field vs. magnetic-field reference antennas,
- Atmospheric noise vs. local (instrumentation) noise,
- Various numbers of atmospheric-noise sources, and
- Various geological (ground) conditions.

Formulation

The simulation programs discussed here use only real quantities, corresponding to the in-phase components of the signals. This is an oversimplification of the real-world, since complex variables or twice as many real variables are required to include the phase-quadrature components of each signal.

In both simulation programs, the primary received signal is represented by the three-element vector

$$\boldsymbol{z} = [H_x, H_y, H_z]^T \quad . \tag{64}$$

The reference signal is also represented as a three-element vector. The total noise vector is therefore a six-element vector, which is attributed to both local- and atmospheric-noise sources by

$$\boldsymbol{n} = \boldsymbol{B}_L \, \boldsymbol{g}_L + \boldsymbol{B}_A \, \boldsymbol{g}_A \quad . \tag{65}$$

The atmospheric-noise driving matrix $\boldsymbol{B}_A$ is composed of geologic effects ($\boldsymbol{G}$) and atmospheric effects ($\boldsymbol{H}$) according to

$$\boldsymbol{B}_A = \boldsymbol{G}\,\boldsymbol{H} \quad ; \tag{66}$$

the forms of the $\boldsymbol{G}$ and $\boldsymbol{H}$ matrices are different for electric and magnetic reference antennas and are given subsequently.

The atmospheric-noise power σ_A^2 is the sum of the power in up to six allowable atmospheric-noise sources; i.e.,

$$\sigma_A^2 = \sigma_1^2 + \sigma_2^2 + \ldots + \sigma_6^2 \quad . \tag{67}$$

The total noise power in the primary antenna is

$$\sigma_T^2 = \sigma_L^2 + \sigma_A^2 \quad , \tag{68}$$

where σ_L^2 is the total local-noise power entering the primary antenna. All of the simulation results presented here use uncorrelated local noise produced by

$$B_L = \sigma_L \, I/3^{1/2} \quad . \tag{69}$$

For all of the tests, $\sigma_T^2 = 1$, and the ratio of atmospheric-noise power to local-noise power is varied. The tests use various combinations of three atmospheric-noise sources corresponding to the principal thunderstorm areas of the world.

Electric-Field Reference Antenna

For an electric-field reference antenna,

$$y = [E_x/n, \; E_y/n, \; E_z/n]^T \quad . \tag{70}$$

Normalization by the free-space impedance is used so that both electric- and magnetic-field signals are of roughly the same magnitude.

Each atmospheric noise source produces a vertical electric-field component and a horizontal magnetic-field component transverse to the direction of propagation. Local geology determines how the vertical magnetic and horizontal electric fields are related to the incident horizontal magnetic fields [1]. The atmospheric-noise matrix therefore has the form

$$\boldsymbol{G}\,\boldsymbol{H} = \begin{bmatrix} 1 & 0 & 0 & 0 & 0 & 0 \\ 0 & 1 & 0 & 0 & 0 & 0 \\ Z_{zx} & Z_{zy} & 0 & 0 & 0 & 0 \\ Z_{xx} & Z_{xy} & 0 & 0 & 0 & 0 \\ Z_{yx} & Z_{yy} & 0 & 0 & 0 & 0 \\ 0 & 0 & 0 & 0 & 0 & 1 \end{bmatrix} \begin{bmatrix} -\sigma_1 \sin\psi_1 & -\sigma_2 \sin\psi_2 & \cdots & -\sigma_6 \sin\psi_6 \\ \sigma_1 \cos\psi_1 & \sigma_2 \cos\psi_2 & \cdots & \sigma_6 \cos\psi_6 \\ 0 & 0 & \cdots & 0 \\ 0 & 0 & \cdots & 0 \\ 0 & 0 & \cdots & 0 \\ \sigma_1 & \sigma_2 & \cdots & \sigma_6 \end{bmatrix} \tag{71}$$

where σ_i is the rms output and ψ is the azimuth of the i^{th} noise source.

Magnetic-Field Reference Antenna

For a remote magnetic-field reference antenna,

$$y = [H_{xr}, \; H_{yr}, \; H_{zr}]^T \quad . \tag{72}$$

In this simulation, the $\boldsymbol{H}$ matrix is used to produce only the incident horizontal magnetic-field components at the primary antenna. The $\boldsymbol{G}$ matrix produces the vertical magnetic field at the primary antenna and all three components of the magnetic field at the reference antenna. The forms of the $\boldsymbol{G}$

and H matrices are therefore

$$G\,H = \begin{bmatrix} 1 & 0 & 0 & 0 & 0 & 0 \\ 0 & 1 & 0 & 0 & 0 & 0 \\ G_{31} & G_{32} & 0 & 0 & 0 & 0 \\ G_{41} & G_{42} & 0 & 0 & 0 & 0 \\ G_{51} & G_{52} & 0 & 0 & 0 & 0 \\ G_{61} & G_{62} & 0 & 0 & 0 & 0 \end{bmatrix} \begin{bmatrix} 1 & 0 & 0 & 0 & 0 & 0 \\ 0 & 1 & 0 & 0 & 0 & 0 \\ Z_{zx} & Z_{zy} & 0 & 0 & 0 & 0 \\ Z_{xx} & Z_{xy} & 0 & 0 & 0 & 0 \\ Z_{yx} & Z_{yy} & 0 & 0 & 0 & 0 \\ 0 & 0 & 0 & 0 & 0 & 0 \end{bmatrix} . \quad (73)$$

Results

The results are summarized in Table 6-1 and Figure 6-5. The effects of noise correlation (ratio of atmospheric to total noise power) are apparent. No improvement occurs for ratios of less than 0.1 (as expected). For ratios of 0.5, a decibel or two of noise reduction is achieved. For noise-power ratios between 0.9 and 0.999 the improvement is clear and varies steadily with increased correlation (decreased uncorrelated local-noise power). For correlations of 0.999 (σ_L^2/σ_t^2 = -30 dB), the DMI algorithm achieves noise reductions between 25 and 30 dB. In all cases, the noise reduction achieved by the DMI algorithm is within 5 dB of what could be achieved with perfect *a priori* knowledge of the noise covariance matrix.

The averages shown in Table 6-1 and Figure 6-5 appear to indicate that ANC performance is degraded by perfect noise correlation. Inspection of the results of individual tests shows that the degradation is often catastrophic. The cause is a noninvertable noise covariance matrix. The problem can be avoided by including in the ANC algorithm a check of the determinant of the noise-covariance matrix. If the determinant is too low, the algorithm could eliminate one or more reference input to obtain an invertable covariance matrix. It is, of course, doubtful that perfect correlation will occur under realistic conditions, so the determinant check may be unnecessary.

The results show that the DMI algorithm is clearly superior to the LMS algorithm. In most cases, the noise reduction (in decibels) is twice as great with the DMI algorithm as it is with the LMS algorithm. The LMS algorithm outperforms the DMI algorithm only in rare cases or when the noise-covariance matrix is noninvertable. It should be noted that noninvertability of the noise covariance matrix (occuring because of perfect correlation) can produce erratic results from either or both algorithms, hence the LMS algorithm offers little under these conditions.

The results are similar for electric and magnetic reference antennas, as well as ideal and nonideal ground, given the same ratio of atmospheric to local noise power. The only significant difference observed between the various noise-source conditions was a greater tendency toward poor conver-

ALGORITHM	REFERENCE	GROUND	AVERAGE EFFECTIVE NOISE REDUCTION IN DECIBELS σ_A^2/σ_T^2						
			0.0	0.1	0.5	0.9	0.99	0.999	1.0
DMI	Electric	I	-	0.1	2.4	8.5	17.5	27.7	4.2
		N	-	-	2.8	8.4	17.7	29.2	28.1
	Magnetic	I	0.1	0.1	2.1	7.4	16.5	25.1	24.0
		N	-	-	1.7	5.5	18.9	26.5	20.4
	Average	I & N	0.1	0.1	2.25	7.45	17.65	27.13	19.18
LMS	Electric	I	-1.0	-0.4	2.1	5.8	10.2	15.4	10.8
		N	-	-	1.7	5.8	9.6	15.0	2.1
	Magnetic	I	-2.2	0.1	1.6	6.1	18.9	8.8	1.6
		N	-	-	0.9	3.8	9.2	11.0	0.3
	Average	I & N	-1.6	-0.2	1.58	5.38	9.48	12.55	3.7

I: Ideal N: Nonideal

Table 5-1. Average effective noise reduction.

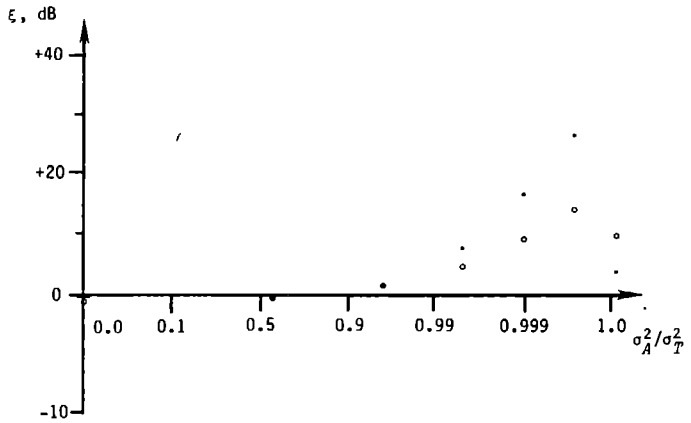

(a) Electric reference, ideal ground

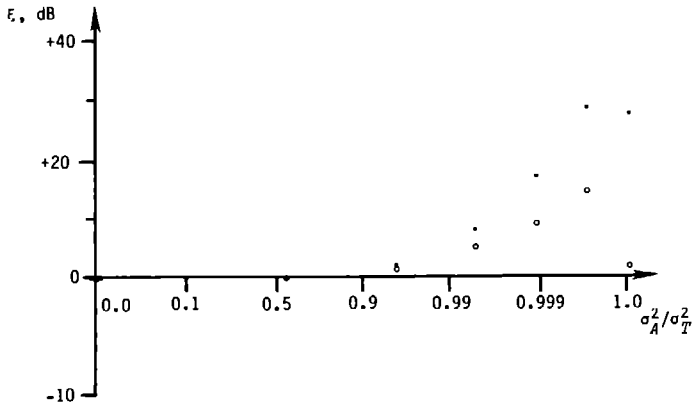

(b) Electric reference, nonideal ground

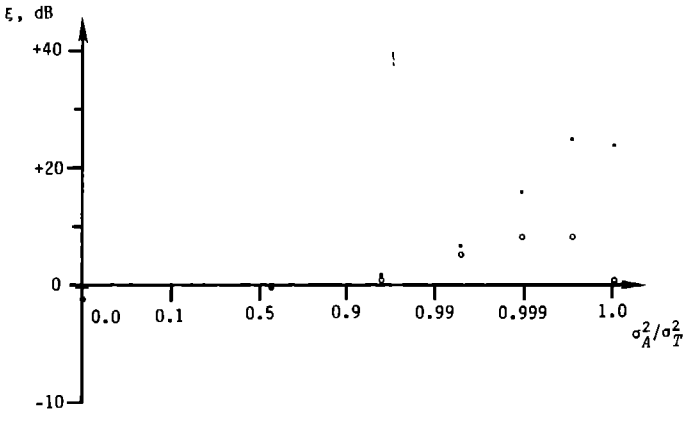

(c) Magnetic reference, ideal ground

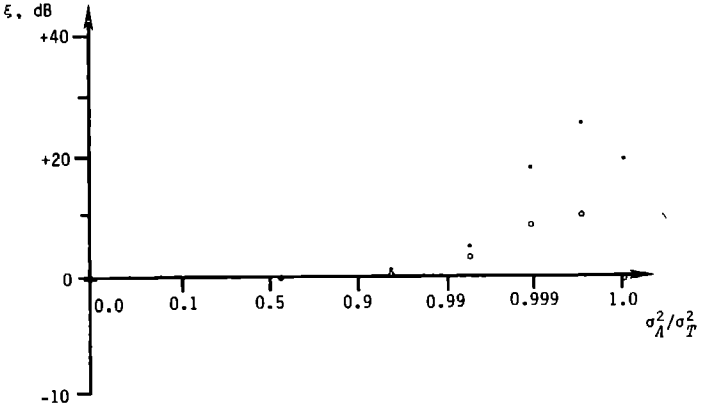

(d) Magnetic reference, nonideal ground

∘ LMS · DMI

Figure 6-5. Average noise reduction.

gence (given perfect correlation) when there was only a single noise source. This is to be expected, since it can reduce the rank of the noise-covariance matrix.

6.6 REFERENCES

1. F. H. Raab, "Adaptive-noise-cancellation techniques for through-the-earth electromagnetics, Vol. I," Final Report GMRR TR82-1, Green Mountain Radio Research Company, Burlington, VT, January 1982.

2. L. H. Rorden, T. C. Moore, E. C. Fraser, and L. R. Bulduc, "Phase I - Development of system concept for location of trapped miners in deep mines by an electromagnetic method," Final Report, Contract No. J0199009, Develco, Inc., Sunnyvale, CA, October 1979.

3. R. A. Monzingo and T. W. Miller, *Introduction to Adaptive Arrays*, New York: John Wiley and Sons, 1980.

4. B. Widrow, et al., "Adaptive noise cancelling: principles and application," *Proceedings of the IEEE*, vol. 63, no. 12, pp. 1692 - 1716, December 1976.

CHAPTER 7. WIDEBAND SIGNAL-PROCESSING ALGORITHM

A considerable portion of the power in ELF noise is contained in discrete impulses. The effective signal-to-noise ratio is therefore increased by initial wideband reception (to preserve impulse sharpness) followed by nonlinear processing to excise the impulses. The ANC algorithm developed in Chapter 6 has a narrow and ever-decreasing bandwidth. While it is capable of cancelling correlated noise of any bandwidth, it cannot act fast enough to reduce the noise power contributed by individual impulses. Adaptive noise cancellation for TTE EM applications is therefore implemented by applying the ANC algorithm to the narrowband outputs from a set of nonlinear processors/demodulators (Chapter 5).

The ANC algorithm presented in Chapter 6 processes only real quantities. However, the narrowband outputs from the nonlinear processor/demodulator are most readily represented as complex quantities. The DMI ANC algorithm is therefore modified to process complex quantities. (The LMS ANC algorithm is shown in Chapter 6 to be markedly inferior to the DMI algorithm and is therefore not included here).

A complete simulation program (Appendix B) is developed to test the nonlinear processor and ANC algorithm in a real-world environment. This program includes:

- Multi-component incident ELF-noise generator (Chapter 3),
- Ground filter (Chapter 3),
- Choice of electric-field or magnetic-field reference antenna,
- Nonlinear processor/demodulator (Chapter 5),
- Direct-matrix inversion ANC algorithm (Chapter 6), and
- Gaussian local noise.

The simulation program was used extensively to evaluate the performance of the wideband signal-processing algorithm. The principal areas of evaluation included:

- Performance of the linear ANC subsystem,
- Performance of the nonlinear-processing (NLP) subsystem, and
- Performance of the combined NLP/ANC system.

7.1 FORMULATION OF ALGORITHM

The basic form of the ANC algorithm for complex quantities is identical to that for all-real quantities. The signal $\boldsymbol{s}$, noise $\boldsymbol{x}$, and received signal $\boldsymbol{z}$ are represented by three-element complex vectors and are related by

$$\boldsymbol{z} = \boldsymbol{s} + \boldsymbol{x} \quad . \tag{1}$$

The estimated signal is given by

$$\hat{\boldsymbol{s}} = \overline{\boldsymbol{z}} - \boldsymbol{W}\overline{\boldsymbol{y}} \quad , \tag{2}$$

where $\bar{\boldsymbol{y}}$ represents the average of reference (remote-antenna) input $\boldsymbol{y}$, which is also a complex three-element vector.

The weighting matrix $\boldsymbol{W}$ can be divided into three complex three-element vectors; i.e.,

$$\boldsymbol{W} = \begin{bmatrix} \boldsymbol{w}_1^T \\ \boldsymbol{w}_2^T \\ \boldsymbol{w}_3^T \end{bmatrix} \quad , \tag{3}$$

which implies that the vector-ANC problem is equivalent to three scalar-ANC problems. If the true noise statistics were known *a priori*, the weighting vectors would be given by

$$\boldsymbol{w} = \boldsymbol{R}_{yy}^{-1} \, \boldsymbol{r}_{yx} \quad . \tag{4}$$

However, since the noise statistics are not known *a priori*, estimated correlation and cross-correlation must be used in (5). As in the all-real formulation, it is convenient to use a single cross-correlation matrix rather than three cross-correlation vectors, thus

$$\boldsymbol{W} = \hat{\boldsymbol{R}}_{xy} \, \hat{\boldsymbol{R}}_{yy}^{-1} \quad . \tag{5}$$

Complex Correlation Estimator

For complex variables, the correlation matrix is [1, §6.9]

$$\boldsymbol{R}_{yy} = E[\boldsymbol{y}\boldsymbol{y}^\dagger] \quad , \tag{6}$$

where $\boldsymbol{y}^\dagger = (\boldsymbol{y}^*)^T$. In the absence of CW signals (bias in the demodulator output), the estimator for the correlation matrix is therefore

$$\hat{\boldsymbol{R}}_{yy} = \frac{1}{K} \sum_{k=1}^{K} \boldsymbol{y}(k) \, \boldsymbol{y}^\dagger(k) \quad , \tag{7}$$

where K is the total number of samples. If CW signals may be present in the reference signal, a slightly better estimate of $\hat{\boldsymbol{R}}_{yy}$ is given by

$$\hat{\boldsymbol{R}}_{yy} = \frac{1}{K-1} \left[\sum_{k=1}^{K} \boldsymbol{y}(k) \, \boldsymbol{y}^\dagger(k) - K \, \overline{\boldsymbol{y}\boldsymbol{y}}^T \right] \quad . \tag{8}$$

Complex Cross-Correlation Estimator

For complex random variables, the optimum cross-correlation vector is (from [1], §6.9)

$$\boldsymbol{r}_{yx} = E[\boldsymbol{y}\, x^*] \quad . \tag{9}$$

The analogous form of $\hat{R}_{xy}$ (See Chaper 6) is therefore

$$R_{xy} = E[\boldsymbol{x}^*\, \boldsymbol{y}^T] \quad , \tag{10}$$

and a simple cross-correlation estimator is

$$\hat{R}_{xy} = \frac{1}{K} \sum_{k=1}^{K} \boldsymbol{z}^*(k)\, \boldsymbol{y}^T(k) - \overline{\boldsymbol{z}}^*\, \overline{\boldsymbol{y}}^T \quad . \tag{11}$$

Recursive Implementation

The accuracy of the signal and cross-correlation estimates ($\hat{\boldsymbol{s}}$ and $\hat{R}_{xy}$) are interrelated and interdependent. Simulations of the narrowband algorihtm (Chapter 6) show that the errors due to interdependence can be eliminated and the estimation accuracy therefore significantly improved by recursively estimating the two unknowns.

The recursive process is started by setting

$$\hat{\boldsymbol{s}}(0) = \overline{\boldsymbol{z}} \quad . \tag{12}$$

The recursive process then repeats the following three steps:

$$\hat{R}_{xy}(n) = \frac{1}{K} \sum_{k=1}^{K} \boldsymbol{z}^*(k)\, \boldsymbol{y}^T(k) - \hat{\boldsymbol{s}}^*(n-1)\overline{y}^T \tag{13}$$

$$\boldsymbol{W}(n) = \hat{R}_{xy}(n)\, \hat{R}_{yy}^{-1} \tag{14}$$

$$\hat{\boldsymbol{s}}(n) = \overline{\boldsymbol{z}} - \boldsymbol{W}(n)\, \overline{\boldsymbol{y}} \quad . \tag{15}$$

Previous simulations have shown that maximum noise cancellation is achieved after only two or three iterations.

7.2 EFFECT OF DEMODULATOR BANDWIDTH

The combined nonlinear-processor / ANC algorithm requires the selection of a number of signal-processing parameters. One of these is the bandwidth of the demodulator output.

If ANC were not used, the demodulator output bandwidth would be of little consequence, since the demodulator output subsequently averages over a time interval considerably longer than the inverse of the bandwidth. However, the effect of bandwidth upon the performance of the ANC algorithm is

not as obvious. A simple analogy is used to show that the bandwidth does not degrade the accuracy of the covariance estimates, and therefore does not affect ANC performance.

Wideband Samples

Suppose that a set of samples of a Gaussian random variable are characterized by

$$E[x(k)] = 0 \quad , \tag{16}$$

$$\text{var}[x(k)] = E[x^2(k)] = v \quad , \tag{17}$$

and

$$E[x(j)\ x(k)] = 0, \ j \neq k \quad . \tag{18}$$

The estimator for the variance v of x is

$$\hat{v} = \frac{1}{K} \sum_{k=1}^{K} x^2(k) \quad . \tag{19}$$

From Chapter 5 of [2],

$$E[\hat{v}] = v \tag{20}$$

and

$$\text{var}[\hat{v}] = (2/K)\ v^2. \tag{21}$$

Note that (21) is the variance of the variance estimator, not the variance of x.

Effect of Bandwidth Reduction

Now suppose that bandwidth is reduced prior to observation of the random variable. The bandwidth reduction is roughly equivalent to averaging several of the wideband samples. The narrowband filter output might therefore be represented by

$$y(k) = \frac{1}{N} \sum_{n=k}^{k+N} x(n) \quad . \tag{22}$$

Since y is also a Gaussian random variable,

$$u = \text{var}[y(k)] = v/N \quad . \tag{23}$$

If the variance of y is estimated by averaging M samples of y, then by analogy to (21),

$$\text{var}[\hat{u}] = (2/M)\ u^2 = 2\ v^2/(MN^2) \quad . \tag{24}$$

Since each sample of the narrowband variable y comprises N samples of the wideband variable x,

$$K = MN \quad . \tag{25}$$

Insertion of the above into (24) yields

$$\text{var}[\hat{u}] = 2\ v^2/(KN) = \text{var}[\hat{v}]/N \quad . \tag{26}$$

The quality factor or "signal-to-noise ratio" for the estimate $\hat{v}$ can be defined as the ratio

$$Q_{\hat{v}} = v/\text{var}[v] \quad . \tag{27}$$

The quality factor for the estimate $\hat{u}$ is similarly

$$Q_{\hat{u}} = u/\text{var}[u] = (v/N)/(\text{var}[v]/N) = Q_v \quad . \tag{28}$$

Equation (28) implies that the quality of the variance estimate is unchanged by the reduction in bandwidth. A similar relationship should hold for the covariance estimates. The demodulator bandwidth therefore should not affect the performance of the ANC system.

7.3 LINEAR-PROCESSING SIMULATION

A variety of simulations were conducted to verify proper operation of the wideband signal-processing system and to determine the optimum settings of various linear-system parameters. The parameters tested include:

- Convergence,
- Bandwidth,
- Sampling rate,
- Iterations, and
- Signal level.

In all of these tests, the clipping threshold was set at 10^8 times the estimated noise power so that only the linear processing was exercised.

Acceptance Tests

A battery of "acceptance" tests was conducted in addition to the four groups mentioned above. The acceptance tests were shorter than the other tests and provided a quick verification of proper system operation.

The acceptance tests showed that the previously presented ground-filter model can cause H_z to be linearly dependent upon H_x and H_y regardless of the number of atmospheric-noise sources. The resultant noninvertable covariance

matrix prevents the ANC algorithm from improving the signal estimate even when the primary and reference noises are well correlated. The ground filter was therefore modified to include E_z directly; i.e.,

$$H_z = Y_{zx} E_x + Y_{zy} E_y + Y_{zz} E_z \quad . \tag{29}$$

This modification allows a noninvertable covariance matrix when there are three or more atmospheric-noise sources.

Convergence

A series of eight tests was conducted to verify covergence of the ANC algorithm to proper operation. All tests ran for 300 seconds, sampled the converter output at 100 Hz, and used a 1-Hz post-conversion bandwidth. All used a magnetic reference antenna and a unit-element signal vector.

The performance-evaluation criterion is the effective reduction in noise level. The effective noise reduction is most easily found by comparing the mean-square estimation error with ANC to that without ANC; i.e.,

$$\xi = \varepsilon^2_{\mathrm{ANC}(n)} / \varepsilon^2_{\mathrm{NO\ ANC}} \quad , \tag{30}$$

where n is the number of iterations. The simulation program computes the no-ANC estimate as well as ANC estimates for n = 0, 1, and 2.

Figure 7-1 shows the effects of local noise level upon the convergence and effective noise reduction from τ = 0 to τ = 300 s. A single atmospheric noise source (Africa) of unit power was used in all six tests, and the noise series were identical. It is apparent that the noise reduction increases with increasing correlation of the primary and reference signals (decreasing local-noise level). Similar results were produced by other test series.

Bandwidth

A series of nine tests was conducted to determine the effects of post-conversion bandwidth upon the performance of the ANC system. Three different noise series and three different bandwidths (1, 3.16, and 10 Hz) were used. All tests used a single atmospheric-noise source of unit power and P_L = 0.01.

The results are shown in Table 7-1 and Figure 7-2. It is quite apparent that the effects of reasonable variations in bandwidth are negligible, as predicted in the previous section of this report.

Sampling Frequency

The effects of the choice of sampling frequency were evaluated by a series of twelve tests. These tests used three different noise series and four different sampling frequencies (100, 33.3, 10, and 3.3 Hz). The sampling frequency in question is that of the narrowband converter output; note that the simulation frequency of 100 Hz remains fixed. All tests were con-

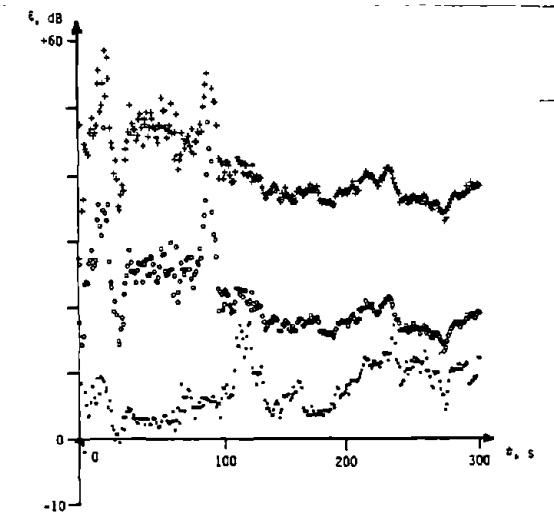

· P_L = 1.0 ∘ P_L = 0.01 + P_L = 0.0001

P_1 = 1.0, P_2 = P_3 = P_4 = 0

Y_1 = Y_2 = Y_3 = Y_4 = 0

a_1 = a_2 = a_3 = a_4 = N/A

I_{xx} = 0.6, I_{xy} = 0.4, I_{xz} = 0.0

e = [1, 1, 1]^T, Magnetic reference antenna

f_{samp} = 100 Hz, B = 1 Hz, n = 2

Figure 7-1. Effect of local-noise level.

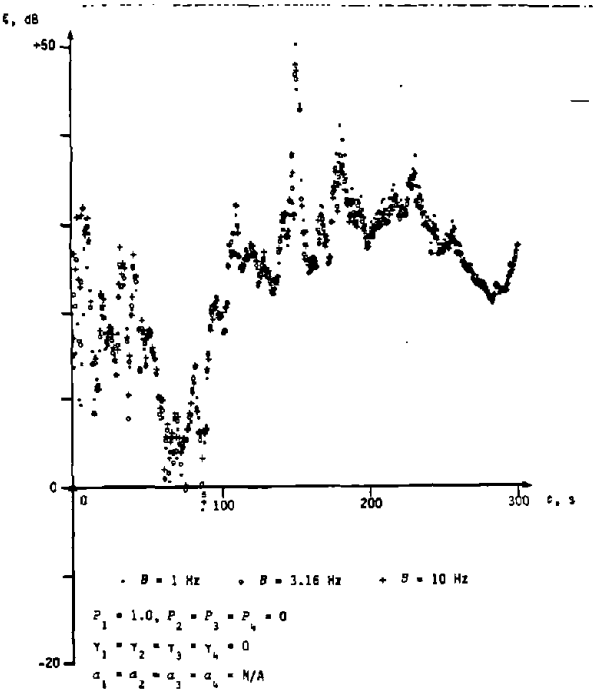

· B = 1 Hz ∘ B = 3.16 Hz + B = 10 Hz

P_1 = 1.0, P_2 = P_3 = P_4 = 0

Y_1 = Y_2 = Y_3 = Y_4 = 0

a_1 = a_2 = a_3 = a_4 = N/A

I_{xx} = 0.6, I_{xy} = 0.4, I_{xz} = 0.0

P_L = 0.01, e = [1, 1, 1]^T, Magnetic reference antenna

f_{samp} = 100 Hz, n = 0

Seeds: 11, 25

Figure 7-2. Effects of bandwidth, noise series #1.

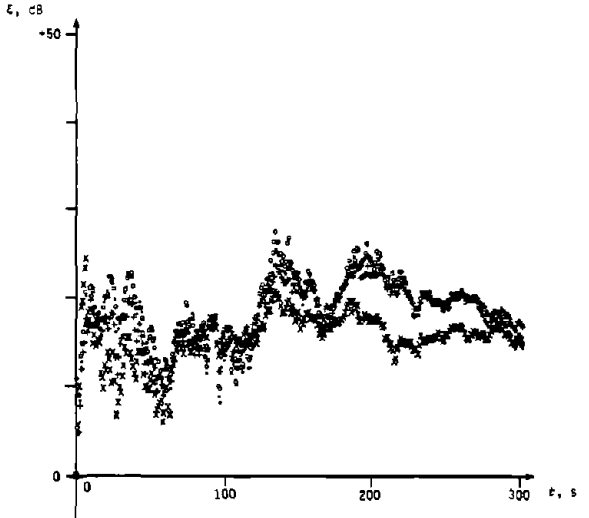

P_1 = 1.0, P_2 = P_3 = P_4 = 0

Y_1 = Y_2 = Y_3 = Y_4 = 0

a_1 = a_2 = a_3 = a_4 = N/A

I_{xx} = 0.6, I_{xy} = 0.4, I_{xz} = 0.0

P_L = 0.01, e = [1, 1, 1]^T, Magnetic reference antenna

B = 1 Hz, n = 0

Seeds: 19, 25

Sampling frequency: · 100 Hz ∘ 33.3 Hz + 10 Hz x 3.3 Hz

Figure 7-3. Effects of sampling frequency, noise series #3.

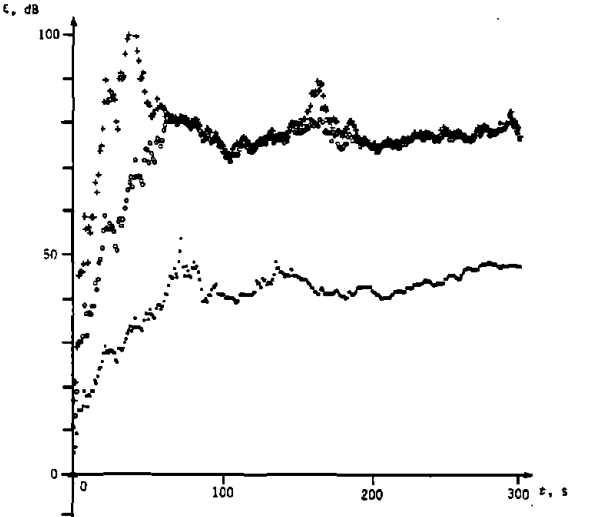

· n = 0 ∘ n = 1 + n = 2

P_1 = P_2 = P_3 = 0.3333, P_4 = 0

Y_1 = Y_2 = Y_3 = Y_4 = 0

a_1 = a_2 = a_3 = a_4 = N/A

I_{xx} = 0.6, I_{xy} = 0.4, I_{xz} = 0.0

P_L = 0, e = [1, 1, 1]^T, Magnetic reference antenna

f_{samp} = 1, B = 1 Hz

Seeds: 24, 2

Figure 7-4. Effects of iteration, P_L = 0.

Noise Series	Seeds	Average Improvement $\overline{\xi}$ in Decibels		
		B = 1 Hz	B = 3.16 Hz	B = 10 Hz
#1	11,25	29.6	28.8	28.4
#2	18,2	29.1	29.1	29.1
#3	19,25	20.3	20.4	20.6

Table 7-1. Effect of bandwidth.

Noise Series	Seeds	Average Improvement $\overline{\xi}$ in Decibels			
		f_s = 100	f_s = 33.3	f_n = 10	f_n = 3.3
#1	11,25	29.6	30.6	23.4	19.8
#2	18,2	29.1	29.0	26.7	25.5
#3	19,25	20.3	20.6	20.3	16.5

Table 7-2. Effect of sampling frequency.

Noise Series	Seeds	n	Average Improvement $\overline{\xi}$ in Decibels		
			P_L = 0.0	P_L = 0.00001	P_L = 0.0001
#1	24,2	0	43.9	41.6	36.2
		1	76.8	48.0	38.0
		2	77.8	48.0	38.0
#2	3,9	0	62.9	44.8	34.7
		1	68.4	44.4	34.6
		2	68.4	44.4	34.6
#3	3,17	0	46.0	44.0	36.9
		1	76.8	47.0	37.0
		2	75.6	47.0	37.0

Table 7-3. Effect of iteration.

Noise Series	Seeds	Average Improvement $\overline{\xi}$ in Decibels		
		P_s = -3 dB	P_n = -13 dB	P_s = -23 dB
#1	11,25	29.6	29.6	29.6
#2	18,2	29.1	29.1	29.1
#3	19,25	20.3	20.3	20.3

Table 7-4. Effect of signal level.

ducted with a single atmospheric-noise source and B = 1 Hz.

The results are shown in Table 7-2 and Figure 7-3. Reduction of the sampling frequency from 100 to 33 Hz has negligible effect. Some degradation is noticable at 10 Hz, and considerable degradation can occur at 3.3 Hz.

The results suggest that oversampling is desirable. This result is not suprising, since small errors in the estimate of the noise-covariance matrix can produce rather large changes in the amount of noise reduction, especially when the local-noise level is low.

DMI Iteration

The benefits of iterative signal/covariance estimation were evaluated by a set of nine tests. To avoid noninvertible covariance matrices, three atmospheric-noise sources and E_z-to-H_z coupling were used. Three different noise series were used with local-noise power levels of 0, 10^{-5}, and 10^{-4}.

The results are shown in Table 7-3 and Figure 7-4 to 7-6. In all cases, the second iteration produces little or no improvement over the first iteration for $\tau > 1$ s. In the absence of local noise, the first iteration produces considerable improvement (e.g., 40 dB) over the initial (no-iteration) DMI estimate. For $P_L = 10^{-5}$, the additional improvement drops to a few decibels, and for $P_L = 10^{-4}$, there additional improvement is hardly noticable.

For large integration times and normal operating conditions, it appears that iteration gives little improvement in the estimate. However, when the noise is very well correlated, iteration can produce significant additional noise reduction. One iteration should be sufficient.

Signal Level

The effects of signal level were evaluated by a set of nine simulations that used three different noise series and three different signal levels. The results (Table 7-4 and Figure 7-7) show that signal level has a negligible effect upon ANC system performance.

7.4 NONLINEAR-PROCESSING SIMULATION

The nonlinear-processing portion of the ANC system was evaluated by a series of simulation tests similar to those used to evaluate the linear portion of the system. The primary objectives of these tests were

- To evaluate the interaction between the nonlinear processing (NLP) and ANC algorithms, and
- To determine the best adaptive-clipper threshold settings.

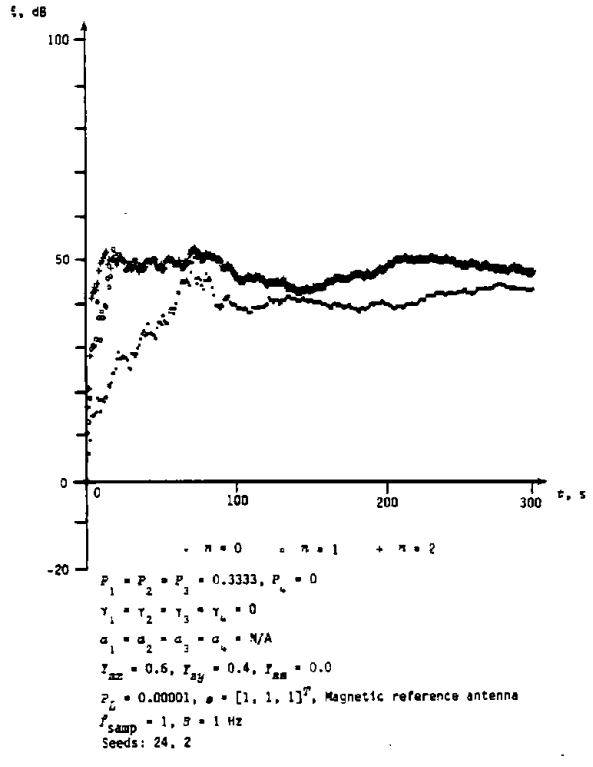

Figure 7-5. Effects of iteration, P_L = 0.00001.

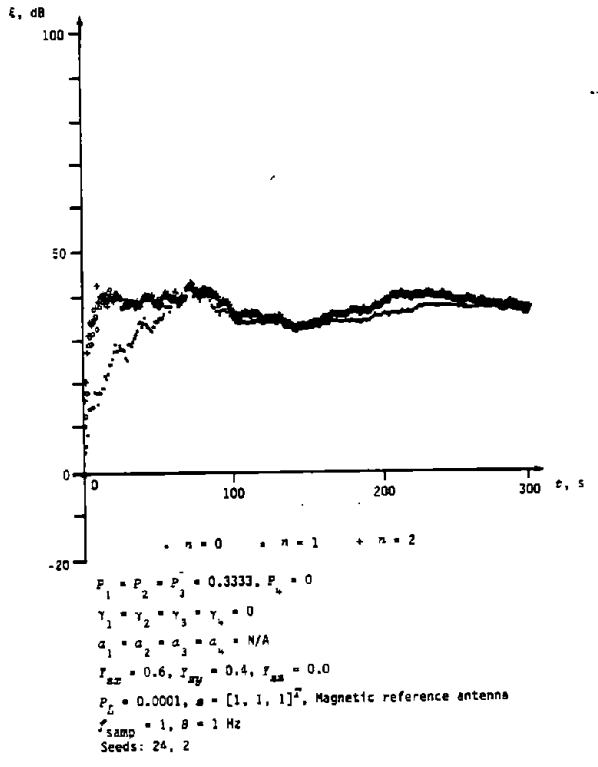

Figure 7-6. Effects of iteration, P_L = 0.0001.

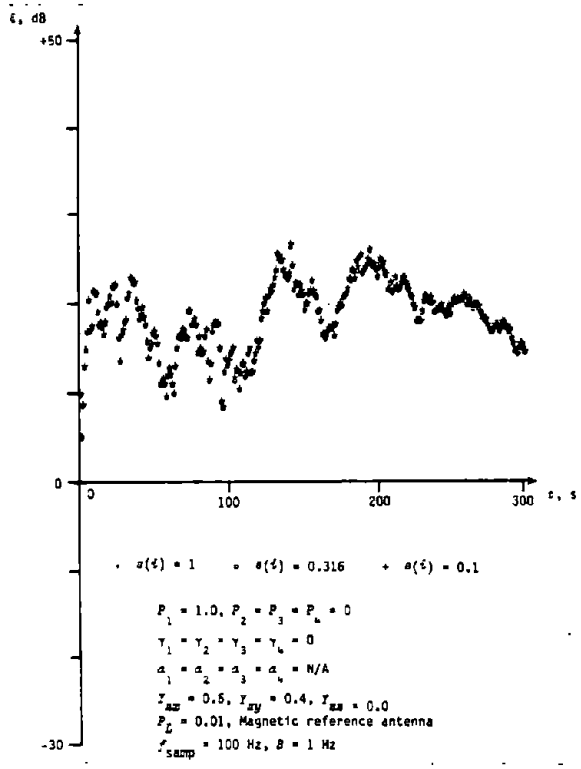

Figure 7-7. Effect of signal level.

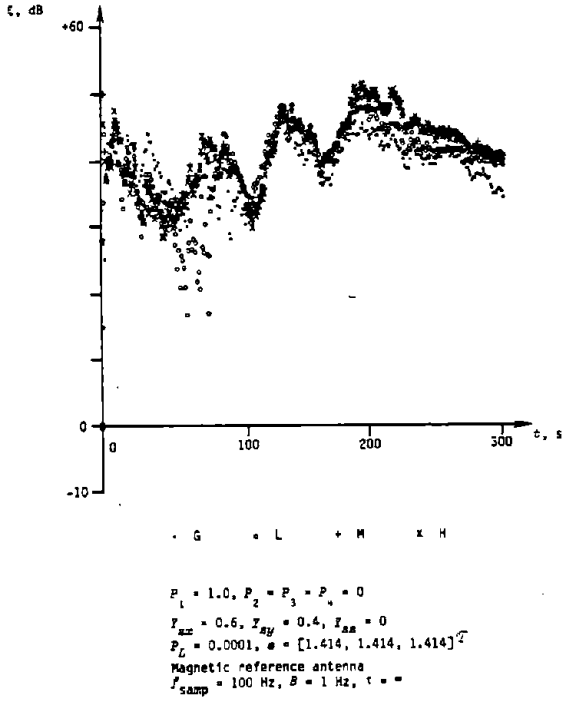

Figure 7-8. Effect of noise type, linear processing.

The results of these tests are presented in this section.

Impulsive Atmospheric Noise

The majority of the tests deal with impulsive atmospheric noise and pure, Gaussian local noise.

Convergence

Figure 7-8 shows the convergence of the ANC algorithm for four different noise types (Gaussian, low-level, moderate-level, and high-level) based upon the same noise (random-number) series. Nonlinear processing is disabled by setting $\tau = \infty$. It is apparent in the figure and in Table 7-5 that the convergence and final results are similar for all noise types.

The effects of activating the nonlinear processing by lowering the threshold are shown in Figures 7-9 to 7-12. Convergence becomes both slower and steadier. The effective noise reduction achieved by ANC also decreases as τ decreases.

Effect of Threshold

The effect of threshold setting upon performance can be seen in Table 7-5 and Figures 7-13 to 7-17. The improvements achieved by nonlinear processing alone are similar to those presented in Chapter 5. With Gaussian atmospheric noise, performance is degraded when $\tau < 2$. For low-level atmospheric noise, a maximum improvement of 2.4 dB is achieved (at $\tau = 1.8$) and a maximum degradation of about 3 dB occurs when the clipping level is set too low. For moderate- and high-level noise, improvements of 11.3 and 13.6 dB, respectively, are achieved by proper threshold settings ($\tau = 1$ and $\tau = 0.56$, respectively). For these noise conditions, performance is not degraded (with respect to a linear system) if the threshold is 0.1 or more.

The effects of combined NLP and ANC can be seen in the upper set of curves in Figure 7-13. When the atmospheric noise is Gaussian, performance is little affected unless $\tau < 0.56$. For low-level noise, a maximum improvement of 43.2 dB occurs at $\tau = 1$. For moderate-level noise, a maximum improvement of 45.2 dB occurs at $\tau = 0.56$, and for high-level noise, a maximum improvement of 48.1 dB occurs at $\tau = 0.32$. In all cases, setting τ too low results in a significant *decrease* in the total noise reduction achieved by the system.

It is apparent that the use of both NLP and ANC is beneficial. However, it is also apparent that the benefits are not additive and performance can be degraded significantly if the clipping threshold is set at too low a value.

PARAMETER	NOISE TYPE	THRESHOLD τ							
		0.1	0.1778	0.3162	0.5623	1.0	1.778	3.162	∞
$\lvert\epsilon\rvert \cdot 10^{-3}$ NO ANC	G	10.49	10.57	9.898	9.548	7.686	4.958	4.378	4.416
	L	10.56	10.20	9.638	8.312	6.902	5.838	6.145	7.702
	M	3.214	3.308	3.172	2.821	2.169	2.181	3.023	7.991
	H	2.068	2.267	2.094	1.617	1.668	1.655	2.390	7.711
$\lvert\epsilon\rvert \cdot 10^{-3}$ ANC $n=2$	G	1.587	0.5668	0.1272	0.09723	0.06479	0.05597	0.07335	0.08133
	L	1.462	0.3073	0.08914	0.07408	0.05349	0.06065	0.07169	0.07959
	M	0.2838	0.08676	0.06807	0.04379	0.05104	0.06613	0.06238	0.07470
	H	0.1920	0.06014	0.03047	0.05762	0.05838	0.06375	0.06353	0.07093
ξ_{NLP} dB	G	- 7.5	- 7.6	- 7.0	- 6.7	- 4.8	- 1.0	0.1	0.0
	L	- 2.7	- 2.4	- 1.9	- 0.7	1.0	2.41	2.0	0.0
	M	7.9	7.7	8.0	9.0	11.3	11.3	8.4	0.0
	H	11.4	10.6	11.3	13.6	13.3	13.4	10.2	0.0
ξ_{ANC} dB	G	16.4	25.4	37.8	39.8	41.5	38.9	35.5	34.7
	L	17.2	30.4	40.7	41.0	42.2	39.7	38.7	39.7
	M	21.1	31.6	33.4	36.2	32.6	30.4	33.7	40.6
	H	20.6	31.5	36.7	29.0	29.1	28.3	31.5	40.7
ξ_{TOTAL} dB	G	5.2	17.8	30.8	33.1	36.7	37.9	35.6	34.7
	L	14.4	28.0	38.7	40.3	43.2	42.1	40.6	39.7
	M	29.0	39.3	41.4	45.2	43.9	41.4	42.2	40.6
	H	32.1	42.2	48.1	42.5	42.4	41.7	41.7	40.8

G: $\gamma = 0$ L: $\gamma = 1.2$, $\alpha = 0.63$ M: $\gamma = 2.6$, $\alpha = 0.28$ H: $\gamma = 4.4$, $\alpha = 0.28$

$\beta = [1.414, 1.414, 1.414]^T$, $P_1 = 1.0$, $P_2 = P_3 = P_4 = 0.0$, $P_L = 0.0001$, Seeds: 19.25

Table 7-5. Combined ANC and nonlinear processor with impulsive atmospheric noise.

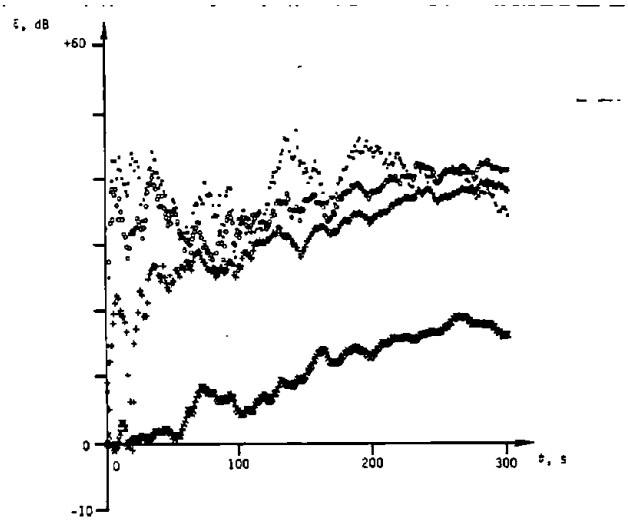

Figure 7-9. Effect of threshold, Gaussian atmospheric noise.

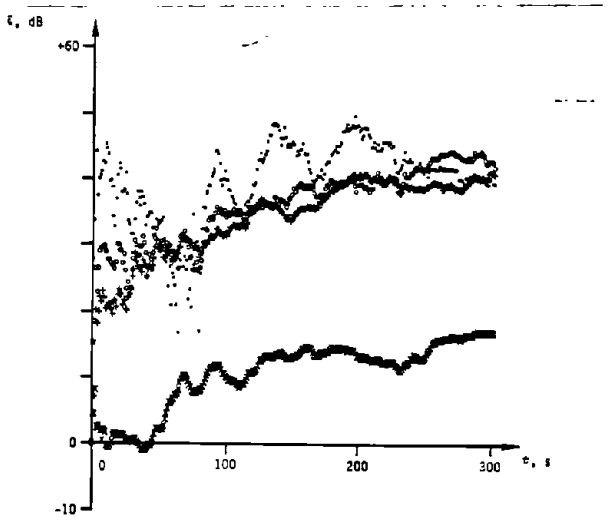

Figure 7-10. Effect of threshold, low-level atmospheric noise.

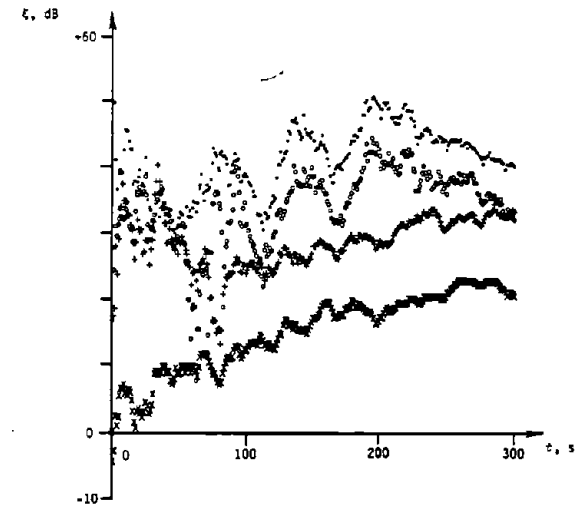

Figure 7-11. Effect of threshold, moderate-level atmospheric noise.

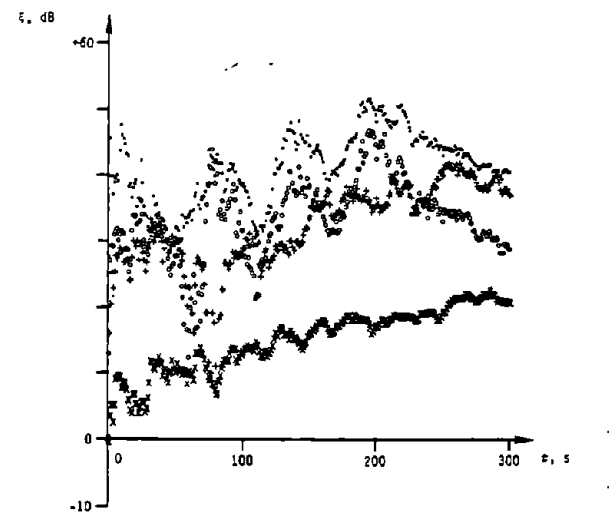

Figure 7-12. Effect of threshold, high-level atmospheric noise.

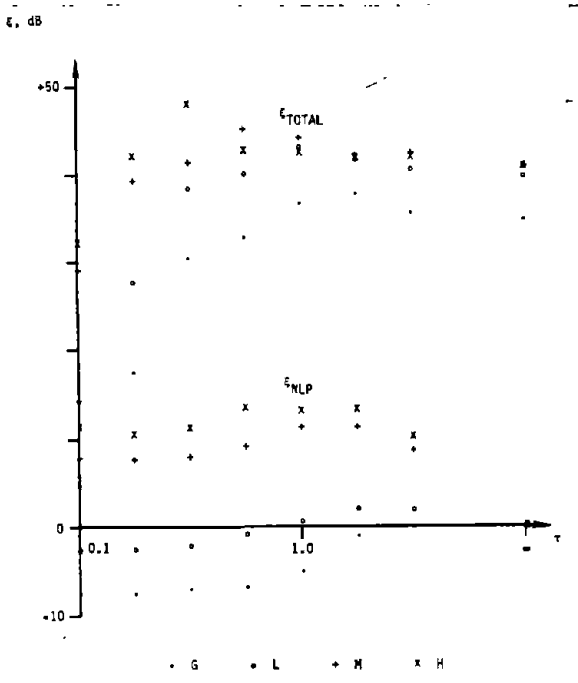

Figure 7-13. Improvement vs. threshold.

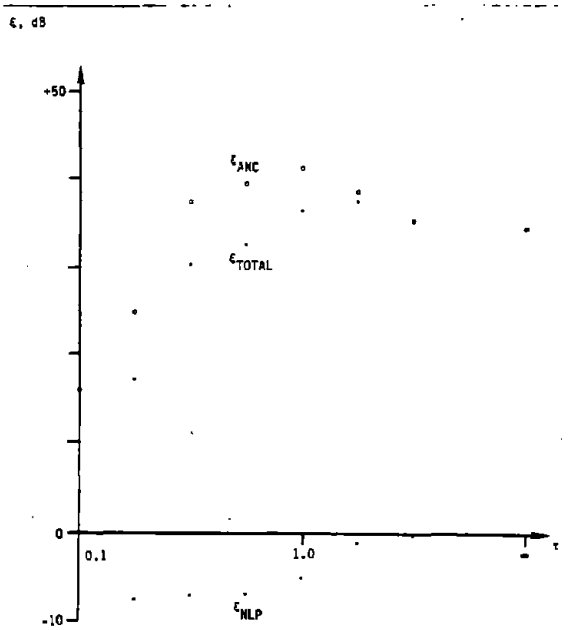

Figure 7-14. Improvement for Gaussian noise.

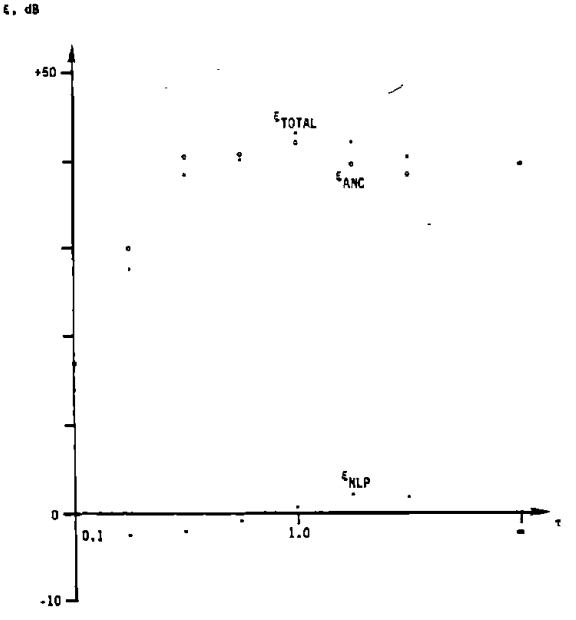

Figure 7-15. Improvement for low-level noise.

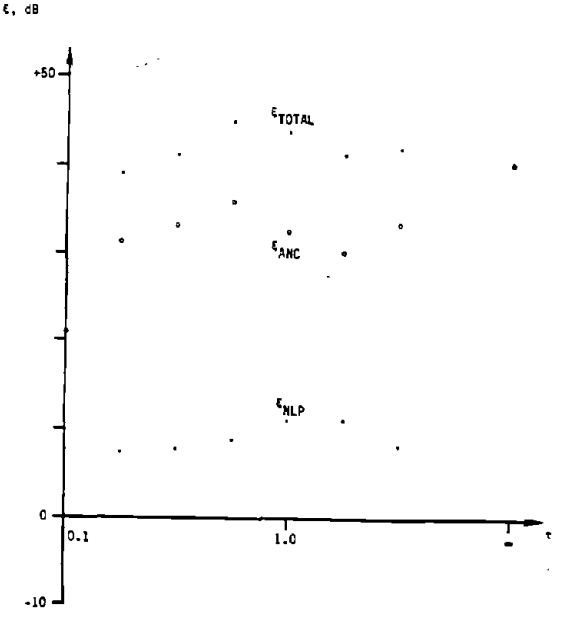

Figure 7-16. Improvement for moderate-level noise.

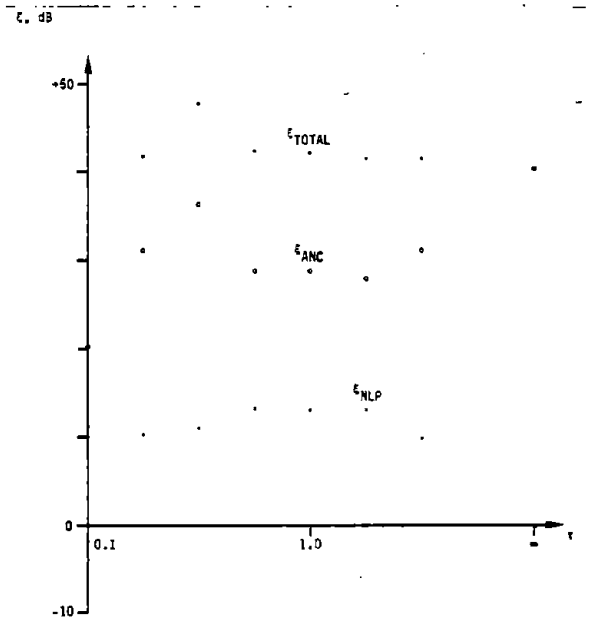

Figure 7-17. Improvement for high-level noise.

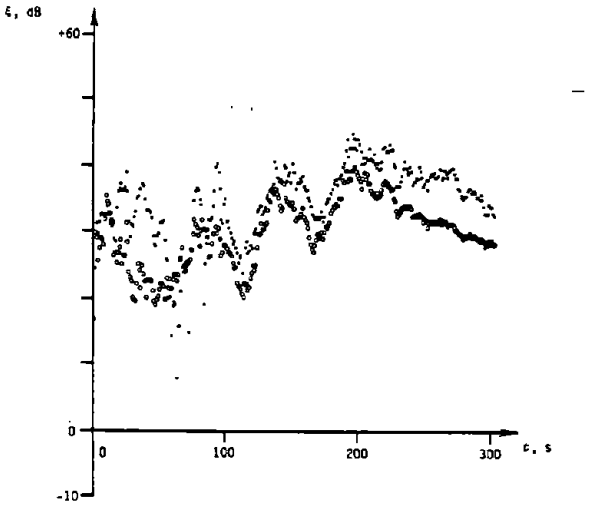

- $\tau = 1.0$, $P_1 = 1.0$
- $\tau = \infty$, $P_1 = 0.07751$

$P_2 = P_3 = P_4 = 0$
$\gamma_{xx} = 0.6$, $\gamma_{xy} = 0.4$, $\gamma_{ss} = 0$
$P_L = 0.0001$, $a = [1.414, 1.414, 1.414]^T$
Magnetic reference antenna
$f_{samp} = 100$ Hz, $B = 1$ Hz

Figure 7-18. Comparison of nonlinear processing and noise-power reduction, moderate-level noise.

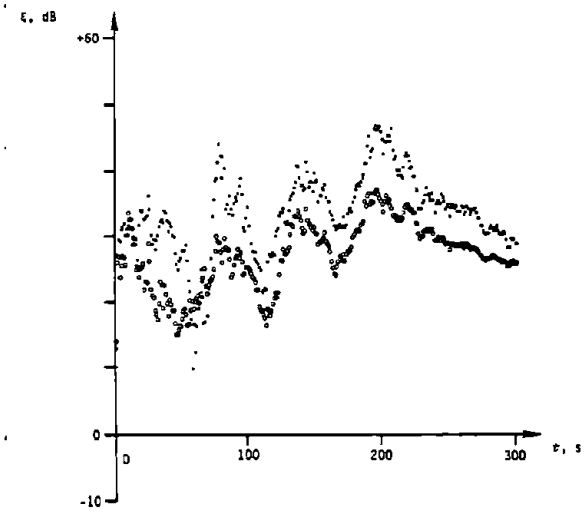

- $\tau = 1.0$, $P_1 = 1.0$
- $\tau = \infty$, $P_1 = 0.04679$

$P_2 = P_3 = P_4 = 0$
$\gamma_{xx} = 0.6$, $\gamma_{xy} = 0.4$, $\gamma_{ss} = 0$
$P_L = 0.0001$, $a = [1.414, 1.414, 1.414]^T$
Magnetic reference antenna
$f_{samp} = 100$ Hz, $B = 1$ Hz

Figure 7-19. Comparison of nonlinear processing and noise-power reduction, high-level noise.

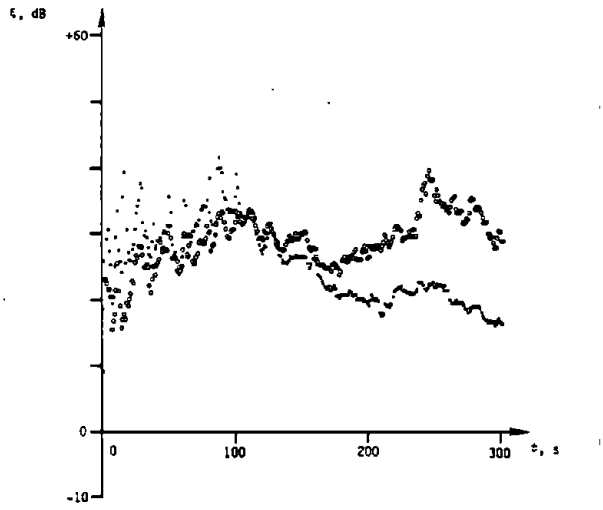

- $\tau = \infty$ - $\tau = 1$

$P_1 = 1.0$, $P_2 = P_3 = P_4 = 0$
$\gamma_{xx} = 0.6$, $\gamma_{xy} = 0.4$, $\gamma_{ss} = 0$
$a = [1.414, 1.414, 1.414]^T$
Magnetic reference antenna
$f_{samp} = 100$ Hz, $B = 1$ Hz
$P_L = 0.01$, $\gamma_L = 4.4$, $a_L = 0.28$

Figure 7-20. Effect of clipping upon high-level local noise.

Effect of NLP upon ANC

In addition to the total noise reduction achieved, Figures 7-14 to 7-17 plot the noise reductions achieved by NLP and ANC alone. It is apparent that the primary effect of setting the clipping level too low is a marked decrease in the performance of the ANC algorithm.

Additional insight into the interaction of the NLP and ANC algorithms can be obtained by comparing a system with nonlinear processing to a system with purely linear processing and an appropriately reduced atmospheric-noise level. Similar errors for the no-ANC estimates are obtained in both cases (Table 7-6). However, the ANC improvement decreases by 3 to 4 dB when nonlinear processing is used. It is clear from the convergence patterns (Figures 7-18 and 7-19) that nonlinear processing effectively reduces noise correlation as well as noise level.

Impulsive Local Noise

The effects of combined NLP and ANC upon impulsive local noise were evaluated by simulation. In this series of tests, the atmospheric noise was Gaussian.

The results are summarized in Table 7-7 and Figures 7-20 and 7-21. For moderate- and high-level local noise, inclusion of nonlinear processing allows significantly better ANC performance. The increased noise reduction (10 to 15 dB) due to ANC overcomes the small degradation (1 dB) due to clipping of the atmospheric noise. The inclusion of nonlinear processing has little effect upon low-level local noise, and can cause a significant degradation of performance (10 dB) when the local noise is Gaussian.

The significant improvement obtained by including nonlinear processing is not suprising, since it effectively reduces the local-noise power, thereby increasing the correlation of the primary and reference signals. In addition, omission of nonlinear processing allows the noise spikes to have an excessive influence upon the averages from which correlations are estimated.

Conclusions

The inclusion of both nonlinear processing and adaptive noise cancellation is desirable. However, the benefits of the two systems are not additive.

For impulsive atmospheric noise, NLP effectively decreases the atmospheric-noise level, allowing the local noise to be more significant. It also reduces the correlation between the primary and reference signals.

For impulsive local noise, NLP effectively decreases the local-noise level, thereby increasing the correlation between primary and reference signals. ANC performance is therefore increased.

The optimum value of the clipping threshold depends upon the type of noise. If the noise conditions are known *a priori*, τ should be selected from

NOISE TYPE	τ	P_1	$\|\varepsilon\|\cdot10^{-3}$ NO ANC	$\|\varepsilon\|\cdot10^{-3}$ ANC, π=2	ξ_{NLP}, dB	ξ_{ANC}, dB	$\Delta\xi_{TOTAL}$, dB
M	1.0	1.0	2.169	0.05104	11.3	32.6	0
	∞	0.07751	2.227	0.08250	0	28.6	-4.0
H	1.0	1.0	1.668	0.05838	13.3	29.1	0
	∞	0.04679	1.669	0.08211	0	26.2	-2.9

Table 7-6. Comparison of nonlinear processing and noise-power reduction.

LOCAL NOISE		τ	ξ_{NLP}, dB	ξ_{ANC}, dB	ξ_{TOTAL}, dB
POWER	TYPE				
0.01	G	∞ 1	0 -1.1	27.1 18.2	27.1 17.1
	L	∞ 1	0 -1.1	22.2 22.1	22.2 21.0
	M	∞ 1	0 -1.1	16.9 30.0	16.9 28.9
	H	∞ 1	0 -1.1	16.6 29.1	16.6 27.9
0.001	G	∞ 1	0 -1.1	38.5 27.8	38.5 26.7
	L	∞ 1	0 -1.1	32.0 33.5	32.0 32.4
	M	∞ 1	0 -1.1	26.6 43.6	26.6 42.5
	H	∞ 1	0 -1.1	26.3 40.0	26.3 38.9

Seeds: 9,19 $\quad P_1 = 1, P_2 = P_3 = P_4 = 0$

Table 7-7. Impulsive local noise.

Noise Type	τ
Gaussian	∞
Low level	1.0
Moderate level	0.56
High level	0.32

Table 7-8. Optimum threshold values.

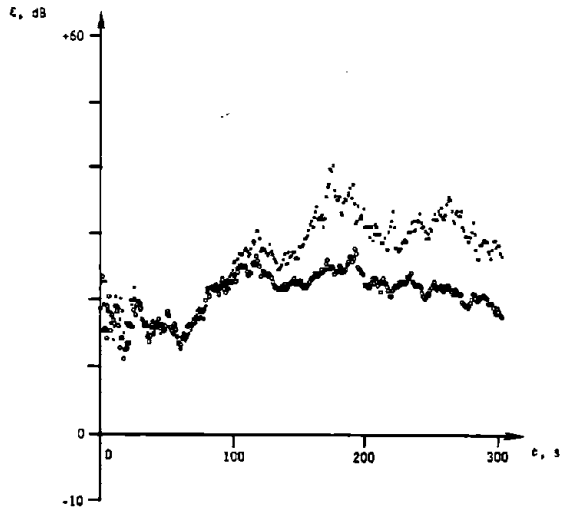

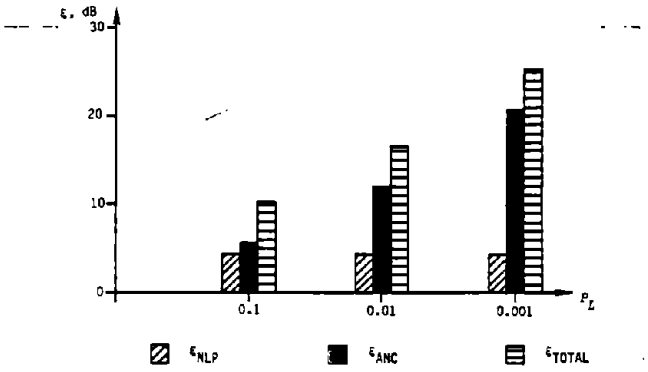

Figure 7-22. Average improvements for typical atmopsneric conditions.

$P_1 = 1.0, P_2 = P_3 = P_4 = 0$
$\gamma_{xx} = 0.6, \gamma_{xy} = 0.4, \gamma_{xz} = 0$
$a = [1.414, 1.414, 1.414]^T$
Magnetic reference antenna
$f_{samp} = 100$ Hz, $B = 1$ Hz
$P_L = 0.01, \gamma_L = 0$

Figure 7-21. Effect of clipping upon Gaussian local noise.

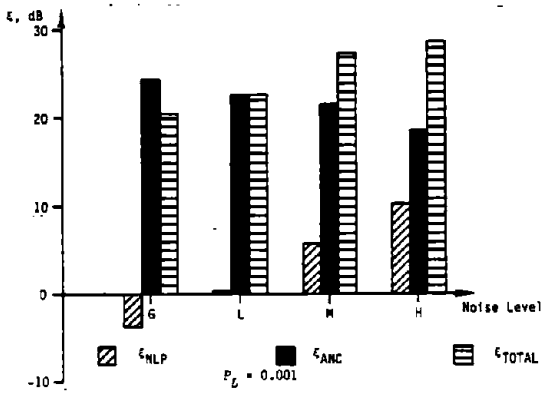

Figure 7-23. Improvements as a function of noise level.

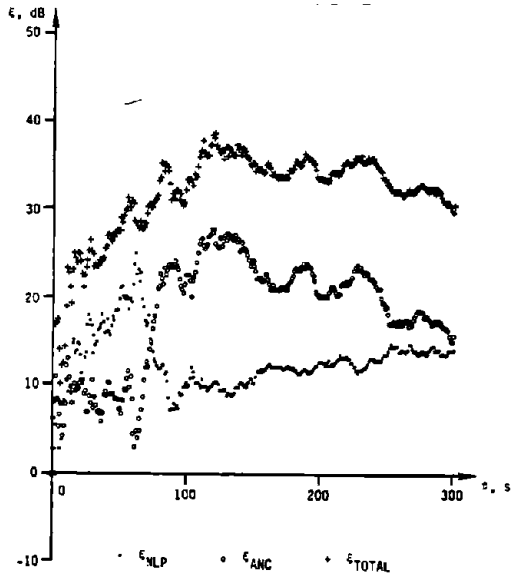

$P_1 = P_3 = 0.5, P_2 = P_4 = 0.0, P_L = 0.001$
$\gamma_1 = \gamma_3 = 4.4, \alpha_1 = \alpha_3 = 0.28$
$\gamma_{xx} = 0.6, \gamma_{xy} = 0.4, \gamma_{xz} = 0.0$
$a = [0.1414, 0.1414, 0.1414]^T$
Magnetic reference antenna
$f_{samp} = 100$ Hz, $B = 1$ Hz
Seeds: 16379, 16656

Figure 7-24. Example convergence plot.

Table 7-7.

If the noise conditions are not known *a priori*, caution must be used in selecting τ, since performance degrades rapidly when τ is set below the value shown in Table 7-8. In general, atmospheric noise is somewhat impulsive (low-level, moderate-level, or high-level), rather than Gaussian. It is therefore desirable to set τ between 0.56 and 1. A suitable value is τ = 0.707, which means that the threshold is set at -3 dB below the estimated rms noise level.

7.5 ATMOSPHERIC-NOISE SIMULATION

Operation of the combined nonlinear processing and adaptive-noise-cancellation algorithm is tested by simulation. The twelve noise conditions specified in Table 7-9 include various combinations of impulsivity, power, and direction. The ELF spikiness parameter α corresponds to a 100-Hz bandwidth (Table 4-1).

Each test run includes 30,000 samples, which corresponds to 300 seconds of real-world signal processing. All test runs use a magnetic reference antenna. Signals are sampled at a rate of 100 Hz and the clipping threshold is set at 0.707 of the estimated rms noise level. The input noise power is set at unity. For all tests, the signal is

$$\boldsymbol{s} = [0.1414,\ 0.1414,\ 0.1414]^T \quad , \tag{31}$$

which is 20 dB below the input noise level and 25 dB above the output noise level in a system with neither nonlinear processing nor ANC. All tests use a 100-element ground filter with Y_{zx} = 0.6 and Y_{zy} = 0.4 to simulate nonhomogeneous ground.

The simulation program (Appendix B) provides for comparison of the outputs from three different processors:

- Linear ANC processing,
- Nonlinear processing, and
- Combined nonlinear processing and ANC.

Results

Test results are summarized in Table 7-9. The noise reduction achieved by nonlinear processing is consistant with that of earlier tests. For high-level noise, the improvement ranges from 8 to 12 dB (average 9.9 dB). For moderate-level, low-level, and Gaussian noise, the improvements are approximately 5, 0, and -4 dB, respectively. The only case in which nonlinear processing effectively raises the noise level involves purely Gaussian atmospheric noise, which is not a likely real-world ELF noise condition.

The overall average noise reductions achieved by the linear ANC algorithm are 19.8 dB for P_L = 0.001, 11.1 dB for P_L = 0.01, and 4.9 for P_L =

Atmospheric-Noise Conditions (Power/Level)					P_L = 0.001			P_L = 0.01			P_L = 0.1		
#	A	S	I	R	ξ_{NLP}	ξ_{ANC}	ξ_{TOTAL}	ξ_{NLP}	ξ_{ANC}	ξ_{TOTAL}	ξ_{NLP}	ξ_{ANC}	ξ_{TOTAL}
1	0	0	1.0 H	0	10.6	20.1	30.7	10.6	10.1	20.7	10.6	2.5	13.1
2	0	0	0	1.0 H	12.0	15.5	27.4	12.0	8.0	20.0	12.0	3.4	15.4
3	0	0.5 H	0.5 H	0	8.6	20.4	29.0	8.6	12.7	21.3	8.6	7.8	16.4
4	0.5 H	0.5 H	0	0	8.0	14.9	22.9	8.0	6.0	14.0	8.0	0.2	8.1
5	0.5 H	0	0.5 H	0	10.2	17.2	27.3	10.2	9.6	19.7	10.2	5.6	15.7
6	0.33 H	0.33 H	0.33 H	0	10.2	18.7	28.8	10.2	8.8	18.9	10.2	2.5	12.6
7	0.33 M	0.33 M	0.33 M	0	5.9	21.5	27.4	5.9	13.8	19.8	5.9	9.1	15.1
8	0.33 L	0.33 L	0.33 L	0	0.2	22.6	22.8	0.2	12.5	12.7	0.2	3.7	3.9
9	0.33 G	0.33 G	0.33 G	0	-3.7	24.4	20.7	-3.7	15.9	12.2	-3.7	7.3	3.6
10	0.33 M	0.33 L	0.33 H	0	3.1	22.7	25.8	3.1	13.6	16.8	3.1	6.8	9.9
11	0.22 M	0.07 M	0.71 M	0	6.7	19.8	26.5	6.7	11.1	17.8	6.7	4.7	11.4
12	0.09 M	0.01 M	0.90 M	0	3.5	19.9	23.4	3.5	11.4	15.0	3.5	5.4	8.9
Average: All					6.3	19.8	26.1	6.3	11.1	17.4	6.3	4.9	11.2
Average: #1 - #6 (high-level)					9.9	17.8	27.7	9.9	9.2	19.1	9.9	3.7	13.6
Average: #10 - #12 (typical)					4.4	20.8	25.2	4.4	12.0	16.5	4.4	5.6	10.1

Notes: A: Africa S: South America I: Indonesia R: Random ($-110° \leq \psi \leq -160°$)

H: $\gamma = 4.4$ and $\alpha = 0.28$ M: $\gamma = 2.6$ and $\alpha = 0.28$ L: $\gamma = 1.2$ and $\alpha = 0.63$ G: $\gamma = 0$.

Table 7-9. Results of atmospheric-noise simulations.

0.1. The last three conditions (various impulsivities or power levels) are probably the most typical. The average noise reductions for these three conditions are 20.8, 12.0, and 5.6 dB, for P_L = 0.001, 0.01, and 0.1, respectively. When the 4.4-dB average improvement from nonlinear processing is added to the average improvement from ANC, the total improvements are 25.2, 16.5, and 10.1 dB for these "typical" conditions (Figure 7-22).

It is apparent that ANC achieves greater noise reduction when processing Gaussian noise than when processing impulsive noise. For example (Figure 7-23), the average improvement due to ANC in conditions #6 - #9 with P_L = 0.001 varies from 24.4 dB (Gaussian noise) to 18.7 dB (high-level noise). The decrease in ANC effectiveness is, however, more than offset by the reduction in the effective noise level; in the same set of tests, average total improvement varies from 20.7 dB (Gaussian) to 28.8 dB (high-level). The complementary relationship between the improvements from nonlinear processing and ANC can also be seen in the convergence plot of Figure 7-24.

The results of the simulations are consistant with theoretical predictions and design goals. They demonstrate proper operation of the wideband ANC/nonlinear-processing algorithm as well as its usefulness in ELF reception.

7.6 REFERENCES

1. R. A. Monzingo and T. W. Miller, *Introduction to Adaptive Arrays*, New York: John Wiley and Sons, 1980.

2. F. H. Raab, "Adaptive-noise-cancellation techniques for through-the-earth electromagnetics, Volume I," Final Report GMRR TR82-1, Green Mountain Radio Reserach Company, Burlington, VT, January 1982.

CHAPTER 8. CONCLUSIONS AND RECOMMENDATIONS

The extension of through-the-earth electromagnetic location techniques to deep-mine depths (1-km) requires more noise reduction than can be achieved (in an acceptable amount of time) by simple signal integration. Intrinsic-safety requirements preclude significant increases in the power of the underground transmitter. The development of a signal-processing technique such as adaptive noise cancellation is therefore clearly necessary.

Phase I of this program included an investigation of ELF-noise characteristics and ANC techniques. The nature of the multicomponent ELF-noise model was defined. The available noise-correlation data suggested that 10 to 40 dB of noise reduction could be achieved through ANC techniques. DMI and LMS techniques were identified as candidate ANC algorithms.

Phase II of this program was a detailed simulation and comparison of techniques. Its major accomplishments include:

- Implementation of a multicomponent ELF-noise model that incorporates FLM impulsive noise, direction of arrival, and geology effects;
- Development of a method for conversion of the FLM ELF-noise parameters to allow for the effects of a bandwidth reduction;
- Implementation and comparison of nonlinear processors for ELF noise;
- Implementation, optimization, and comparison of DMI and LMS ANC algorithms; and
- Implementation and testing of a signal processor that combines both nonlinear processing and adaptive noise cancellation.

The major findings of the Phase-II research are:

- The adaptive clipper is the preferred nonlinear processing technique.
- The clipping threshold should be set between 0.5 and 1.0 times the estimated rms noise level.
- Recursive estimation of correlation and application of noise cancellation increases the noise reduction achieved by the DMI algorithm, especially for high correlations.
- The DMI ANC algorithm is far superior to the LMS ANC algorithm.
- The benefits of nonlinear processing and ANC are not additive.
- The greatest noise reduction is achieved by employing both nonlinear processing and ANC.
- Under typical conditions, the total noise reduction varies from 5 to 25 dB as the local noise level varies from -10 to -30 dB with respect to the atmospheric-noise level.

Adaptive noise cancellation for through-the-earth EM location systems appears to be both feasible and desirable. The simulated tests show that it can provide the additional 20 dB or so needed for operation at deep-mine (1-km) depths.

Evaluation of the ANC algorithms with real ELF-noise data is therefore recommended. The major components of the Phase-III investigation are:

- Digitization of analog ELF-noise data,
- Processing the data with the combined NLP/ANC system, and
- Evaluation of the multicomponent noise model.

(The analog ELF-noise data has already been recorded as part of another program). The results of the Phase-III effort will both validate the ANC concept for TTE EM systems and optimize its parameters.

APPENDIX A. ANALOGIES FOR COMPLEX MATRIX COMPUTATIONS

Computations for complex vectors and matrices can be implemented with real-number arithmetic by the use of appropriate analogies. Let

$$R = A + jB \quad , \tag{A.1}$$

$$S = C + jD \quad , \tag{A.2}$$

and

$$R^{-1} = E + jF \quad , \tag{A.3}$$

where R and S represent complex matrices or vectors, and A, B, C, D, E, and F represent real matrices or vectors of the same dimensions.

Multiplication of complex matrices is directly analogous to multiplication of complex scalars, thus

$$R\,S = (A\,C - B\,D) + j(B\,C + A\,D) \quad . \tag{A.4}$$

Inversion of complex matrices is most readily accomplished (in this application) by using the isomorphism given by Monzingo and Miller [1, Problem 9, p. 318]. To invert R, form the all-real double-size matrix

$$G = \begin{bmatrix} A & B \\ -B & A \end{bmatrix} \quad . \tag{A.5}$$

Inversion of G produces

$$G^{-1} = \begin{bmatrix} E & F \\ -F & E \end{bmatrix} \quad . \tag{A.5}$$

This analogy is applicable to all invertable complex matrices, is readily implemented, and requires no "IF" statements in the subroutine. In some special cases, the use of a double-size matrix can be avoided. While speed may be increased, restrictions are imposed and the subroutine is considerably more complicated.

A.1 REFERENCE

1. R. A. Monzingo and T. W. Miller, *Introduction to Adaptive Arrays*, New York: John Wiley and Sons, 1980.

APPENDIX B. PROGRAM LISTINGS

B.1 RANDOM-VARIABLE GENERATORS

```
C  Program # FHR-300-, 03/07/83
C  Uniform, Gaussian, and Power-Rayleigh random-number generators


      SUBROUTINE GAUSS(IR2,IR1,MU,SIGMA,G)
C  Modified version of program #FHR-249-
C  Gaussian random variable by nonlinear transformation of
C  uniform random variable
      INTEGER X(28)
      REAL MU, Y(28)
C  Principal points in nonlinear function
      DATA X(1),  Y(1)  /0,     0.0/
      DATA X(2),  Y(2)  /2608,  0.1/
      DATA X(3),  Y(3)  /5197,  0.2/
      DATA X(4),  Y(4)  /7726,  0.3/
      DATA X(5),  Y(5)  /10184, 0.4/
      DATA X(6),  Y(6)  /12550, 0.5/
      DATA X(7),  Y(7)  /14978, 0.6/
      DATA X(8),  Y(8)  /16908, 0.7/
      DATA X(9),  Y(9)  /18881, 0.8/
      DATA X(10), Y(10) /20703, 0.9/
      DATA X(11), Y(11) /22367, 1.0/
      DATA X(12), Y(12) /23875, 1.1/
      DATA X(13), Y(13) /25225, 1.2/
      DATA X(14), Y(14) /26424, 1.3/
      DATA X(15), Y(15) /27473, 1.4/
      DATA X(16), Y(16) /28390, 1.5/
      DATA X(17), Y(17) /29177, 1.6/
      DATA X(18), Y(18) /29845, 1.7/
      DATA X(19), Y(19) /30415, 1.8/
      DATA X(20), Y(20) /30887, 1.9/
      DATA X(21), Y(21) /31280, 2.0/
      DATA X(22), Y(22) /31857, 2.2/
      DATA X(23), Y(23) /32231, 2.4/
      DATA X(24), Y(24) /32460, 2.6/
      DATA X(25), Y(25) /32598, 2.8/
      DATA X(26), Y(26) /32683, 3.0/
      DATA X(27), Y(27) /32755, 3.5/
      DATA X(28), Y(28) /32767, 4.0/
C  GET UNIFORM RANDOM NUMBER 0 <= IR0<= +32,767
      CALL RANDU(IR2,IR1)
      IR0=IABS(IR1)
      N=1
C  SEARCH FOR ADJACENT POINTS ON CURVE
   10 IF(IR0.EQ.X(N)) GO TO 200
      NP=N+1
      IF(IR0.LT.X(NP)) GO TO 100
      IF(NP.EQ.28) GO TO 100
      N=NP
      GO TO 10
C  INTERPOLATE
  100 CONTINUE
      G=Y(N) + (Y(NP) - Y(N)) * (IR0 - X(N)) / (X(NP) - X(N))
      GO TO 250
C  IR0 EQUALS X(N)
  200 G=Y(N)
C  GET SIGN
  250 IF(IR1.LT.0) G=-G
C     NOW E[G] = 0 , VAR[G] = 1.0
  300 G=G*SIGMA+MU
C     NOW E[G] = MU , VAR[G] = SIGMA**2
      RETURN
      END
```

```
      SUBROUTINE PWRRAY(IR2,IR1,R,A,Y)
C  Modified version of Program # FHR-25Ø-
C  Power-Rayleigh random variable
C  See GMRR TR82-1 and GMRR RN82-37
C
C  Get uniform random number, 1 <= IRØ <= 32767
   1Ø CALL RANDU(IR2,IR1)
      IRØ=IABS(IR1)
      IF(IRØ.EQ.32767) GO TO 1Ø
      Y = R * ( - ALOG(1.Ø - IRØ/32767.Ø) ) ** (1.Ø/A)
C
C  Restore sign
      IF(IR1.LT.Ø) Y=-Y
      RETURN
      END


      SUBROUTINE RANDU(IR2,IR1)
C  Uniform random-variable generator (16-bit integer)
C  -32767 <= IR1 <= +32767
C  Use IR1 as output;  call RANDU twice after seeding IR1 and IR2
      IMPLICIT INTEGER (A-Z)
      LOGICAL L
      DATA M1, M2, LB, Z /-3Ø751,-15384, 32767, X'8ØØØ'/
C  Z = -32768 = 8ØØØH, M1 = 87E1H, M2 = C3E8H
   1Ø CONTINUE
      DO 1ØØ L=1, 16
C
C  Compute feedback bit
      J1=IR1.AND.M1
      J2=IR2.AND.M2
      C=1
      P=Ø
      DO 5Ø N=1,16
      IF((J1.AND.C).NE.Ø) P=P+1
      IF((J2.AND.C).NE.Ø) P=P+1
      C=C*2
   5Ø CONTINUE
C
C  Shift IR1
      IR1=IR1.AND.(-2)
      IR1=IR1/2
C
C  Load high bit of IR1
      IR1=(IR1.AND.LB).OR.((IR2.AND.1)*Z)
C
C  Shift IR2
      IR2=IR2.AND.(-2)
      IR2=IR2/2
C
C  Load high bit of IR2
      HB=(P.AND.1)
      IR2=(IR2.AND.LB).OR.((P.AND.1)*Z)
C
  1ØØ CONTINUE
C
C  Eliminate output of -32768
      IF(IR1.EQ.Z) GO TO 1Ø
      RETURN
      END
```

B.2 WIDEBAND SIMULATION PROGRAM

```
C  Program # FHR-311-, Ø5/Ø7/83
C  DMI ANC algorithm with ELF noise input
```

```
C
      IMPLICIT LOGICAL (L)
      DIMENSION P(4),GAMMAL(4),A(4),CHX(4),CHY(4),PSI(4),R(4),
     >  SIGX(4), HXOLD(1ØØ), HYOLD(1ØØ), FW(1ØØ),
     >  SR(3), SI(3), ZW(3), YW(3), ZR(3), ZI(3), YR(3), YI(3),
     >  PHATZ(3), PHATY(3), NNLZ(3), NNLY(3),
     >  ZBARR(3), ZBARI(3), YBARR(3), YBARI(3),
     >  SIGZR(3), SIGZI(3), SIGYR(3), SIGYI(3),
     >  SIGYYR(3,3), SIGYYI(3,3), SIGZYR(3,3), SIGZYI(3,3),
     >  RYYR(3,3), RYYI(3,3), RZYR(3,3), RZYI(3,3),
     >  CONJ(3), DUM1(3,3), DUM2(3,3), DUM3(3,3),
     >  SHATR(3), SHATI(3), RXYR(3,3), RXYI(3,3),
     >  DUM4(6,6), DUM5(6,6), DUM6(6,6), RINVR(3,3), RINVI(3,3),
     >  WR(3,3), WI(3,3),ZRL(3),YRL(3),ZIL(3),YIL(3),
     >  SIGZRL(3),  SIGYRL(3), SIGZIL(3), SIGYIL(3),
     >  ZBARRL(3), ZBARIL(3), YBARRL(3), YBARIL(3)
      COMMON /BLOCK1/ IR2,IR1,P,A,CHX,CHY,PSI,R,SIGX,PSIMIN,PSID
      COMMON /BLOCK2/ NFILT, FW
      COMMON /FLTR/ FGAIN, FTHR, TOTSMP, COSWAV, SINWAV
      DATA PSI(1),PSI(2),PSI(3),PSI(4) /45.Ø,135.Ø,-7Ø.Ø,Ø.Ø/
   1Ø FORMAT(' DMI ANC algorithm with ELF noise, ',
     >  'Program # FHR-311-',/)
C
C  Fixed parameters and constants
C  If total number of wideband samples will exceed 32,767, FSAMP must be
C  integer multiple of FSIG and KMOD=FSAMP.
C
      DR=Ø.Ø17453293
      TWOPI=6.2831852
      SIGMAG=1.Ø
      KMOD=1ØØ
      FSAMP=1ØØ.Ø
      CFILT=1.Ø
      FSIG=1Ø.Ø
      ILS=3
      ILY=3
      ILY2=ILY*2
C
C  Announce name and get other parameters
C
      WRITE(3,1Ø)
   9Ø WRITE(3,1ØØ)
  1ØØ FORMAT(' INPUT:  Noise-source parameters',/,
     >  '  #',2X,'P, Gamma, A, Psimin, Psimax (degrees)')
      DO 12Ø I=1, 4
      WRITE(3,11Ø) I
  11Ø FORMAT(' ',I2,2X)
      CALL ATR(P(I),IERR)
      IF(IERR.EQ.27) GO TO 9Ø
      CALL ATR(GAMMAL(I),IERR)
      IF(IERR.EQ.27) GO TO 9Ø
      CALL ATR(A(I),IERR)
      IF(IERR.EQ.27) GO TO 9Ø
  12Ø CONTINUE
      CALL ATR(PSIMIN,IERR)
      IF(IERR.EQ.27) GO TO 9Ø
      CALL ATR(PSIMAX,IERR)
      IF(IERR.EQ.27) GO TO 9Ø
      PSID=PSIMAX-PSIMIN
C
C  Type of reference
      WRITE(3,13Ø)
  13Ø FORMAT(/,' Reference (E or M) ? ')
      READ(3,135) LREF
  135 FORMAT(A1)
      LREF=LUPPER(LREF)
C
C  Local noise level
      WRITE(3,14Ø)
  14Ø FORMAT(' Plocal = ')
      CALL ATR(PLOCAL,IERR)
```

```
      SIGLCL=SQRT(PLOCAL)
C
C  Signal parameters
      WRITE(3,160)
  160 FORMAT(/,' In-phase signal components x,y,z =   ')
      CALL ATR(SR(1),IERR)
      CALL ATR(SR(2),IERR)
      CALL ATR(SR(3),IERR)
      WRITE(3,170)
  170 FORMAT(' Quadrature signal components x,y,z = ')
      CALL ATR(SI(1),IERR)
      CALL ATR(SI(2),IERR)
      CALL ATR(SI(3),IERR)
C
C  Other parameters
      WRITE(3,200)
  200 FORMAT(/,' Nsamp, Nw, Kout = ')
      CALL ATI(NSAMP,IERR)
      CALL ATI(NW,IERR)
      CALL ATI(KOUT,IERR)
      WRITE(3,210)
  210 FORMAT(' Nset, F3dB, Thresh = ')
      CALL ATI(NSET,IERR)
      CALL ATR(F3DB,IERR)
      CALL ATR(FTHR,IERR)
      KMAX=NSAMP+NSET
      WRITE(3,220)
  220 FORMAT(' Nfilter, Yzx, Yzy, Yzz = ')
      CALL ATI(NFILT,IERR)
      CALL ATR(YZX,IERR)
      CALL ATR(YZY,IERR)
      CALL ATR(YZZ,IERR)
      WRITE(3,230)
  230 FORMAT(' Number of runs = ')
      CALL ATI(NRUN,IERR)
      WRITE(3,240)
  240 FORMAT(' Seeds = ')
      CALL ATI(ISEED1,IERR)
      CALL ATI(ISEED2,IERR)
      IF((ISEED1.NE.0).AND.(ISEED2.NE.0)) GO TO 250
      CALL SEED(ISEED1)
      CALL SEED(ISEED2)
  250 IR1=ISEED1
      IR2=ISEED2
C
C  Write parameters and headings to output files
C
      CALL FOPENO(7,IERR)
      WRITE(3,300)
  300 FORMAT(23X,'Noise-Source Data',/,'    I',5X,'P',9X,'Gamma',9X,
     >  'A',6X,'Psi/Psimin',2X,'Psimax',/)
      WRITE(7,10)
      WRITE(7,300)
      DO 340 I=1,4
      IF(I.EQ.4) GO TO 320
      WRITE(3,310) I, P(I), GAMMAL(I), A(I), PSI(I)
  310 FORMAT(' #',I2,3G12.4,F8.1,2X,F8.1)
      WRITE(7,310) I, P(I), GAMMAL(I), A(I), PSI(I)
      GO TO 330
  320 WRITE(3,310) I, P(I), GAMMAL(I), A(I), PSIMIN, PSIMAX
      WRITE(7,310) I, P(I), GAMMAL(I), A(I), PSIMIN, PSIMAX
  330 CONTINUE
      PSI(I)=PSI(I)*DR
      CHX(I)=-SIN(PSI(I))
      CHY(I)=COS(PSI(I))
  340 CONTINUE
      PSIMIN=PSIMIN*DR
      PSIMAX=PSIMAX*DR
      PSID=PSID*DR
      PT=0.0
      DO 345 I=1,4
```

```
      PT=PT+P(I)
  345 CONTINUE
      PT4=PT*4.Ø
      PT9=PT*9.Ø
      WRITE(3,346) PT
      WRITE(7,346) PT
  346 FORMAT(' T  ',G12.4)
      IF(LREF.EQ.69) GO TO 351
      WRITE(7,35Ø), PLOCAL
  35Ø FORMAT(/,' Magnetic reference antenna, Plocal = ',G12.4)
      GO TO 355
  351 WRITE(7,352), PLOCAL
  352 FORMAT(/,' Electric reference antenna, Plocal = ',G12.4)
  355 CONTINUE
      WRITE(7,37Ø) (SR(I), I=1,3), (SI(I), I=1,3)
  37Ø FORMAT(/,' Re(S) = ',3G12.4,/,' Im(S) = ',3G12.4)
      WRITE(7,39Ø) NSAMP, NW, KOUT
  39Ø FORMAT(/,' Nsamp = ',I6,'  Nw = ', I6,' Kout = ',I6)
      WRITE(7,391) NSET, F3DB, FTHR
  391 FORMAT(' Nset = ',I6,' F3dB = ',F5.2, '  Thresh = ',G12.4)
      WRITE(7,395) NFILT, YZX, YZY, YZZ
  395 FORMAT(' Nfilter = ',I3,'  Yzx = ',G12.4,'  Yzy = ',G12.4,
     >  '  Yzz = ',G12.4)
C
C  Start run
C
      DO 9ØØØ NR=1, NRUN
      WRITE(3,4ØØ) NR
      WRITE(7,4ØØ) NR
  4ØØ FORMAT(/,' ',8Ø('-'),/,' Run # ',I3)
C
C  Output headings
C
      WRITE(3,4Ø5)
      WRITE(7,4Ø5)
  4Ø5 FORMAT(/,5X,'T',6X,'MSEL',8X,'MSEN',8X,'MSEA',
     >  9X,'Gn',6X,'Ga',6X,'Gt',/)
C
C  Initialize parameters
C
      ISEED1=IR1
      ISEED2=IR2
      CALL RANDU(IR2,IR1)
      CALL RANDU(IR2,IR1)
      DO 41Ø I=1,4
      IF(P(I).GT.Ø.Ø) CALL ELFPRM(P(I),GAMMAL(I),A(I),SIGX(I),R(I))
  41Ø CONTINUE
      DO 43Ø J=1,3
      ZRL(J)=Ø.Ø
      ZIL(J)=Ø.Ø
      YRL(J)=Ø.Ø
      YIL(J)=Ø.Ø
      ZR(J)=Ø.Ø
      ZI(J)=Ø.Ø
      YR(J)=Ø.Ø
      YI(J)=Ø.Ø
      SIGZR(J)=Ø.Ø
      SIGZI(J)=Ø.Ø
      SIGYR(J)=Ø.Ø
      SIGYI(J)=Ø.Ø
      SIGZRL(J)=Ø.Ø
      SIGZIL(J)=Ø.Ø
      SIGYRL(J)=Ø.Ø
      SIGYIL(J)=Ø.Ø
      DO 42Ø I=1,3
      SIGYYR(I,J)=Ø.Ø
      SIGYYI(I,J)=Ø.Ø
      SIGZYR(I,J)=Ø.Ø
      SIGZYI(I,J)=Ø.Ø
  42Ø CONTINUE
      PHATZ(J)=Ø.Ø
```

```
      NNLZ(J)=Ø
      PHATY(J)=Ø.Ø
      NNLY(J)=Ø
  43Ø CONTINUE
      DO 44Ø J=1,NFILT
      HXOLD(J)=Ø.Ø
      HYOLD(J)=Ø.Ø
      FW(J)=PR(CFILT,J)
  44Ø CONTINUE
      FGAIN=2.Ø * TWOPI * F3DB / FSAMP
      OD=TWOPI*FSIG/FSAMP
      KS=Ø
      K=Ø
      GØAVG=Ø.Ø
      G1AVG=Ø.Ø
      G2AVG=Ø.Ø
      NG=Ø
      TOTSMP=Ø.Ø
C
C  Begin narrowband-sample loop
C
      DO 7ØØØ KN=1, KMAX
C
C  Begin wideband-sample loop
C
      DO 1ØØØ KW=1, NW
      KS=KS+1
      IF(KS.EQ.KMOD) KS=Ø
      CALL INTRPT(LINT)
      IF(LINT.EQ.27) GO TO 9999
      OMEGAT=OD*KS
      COSWAV=COS(OMEGAT)
      SINWAV=SIN(OMEGAT)
C
C  Begin noise generation
      TOTSMP=TOTSMP + 1.Ø
C
C  Generate incident noise fields
      CALL ELFINC(ZW(1),ZW(2),EZ)
C
C  Horizontal electric fields
      YW(1)=FILTER(ZW(2),HYOLD)
      YW(2)=FILTER(ZW(1),HXOLD)
C
C  Vertical magnetic field
      ZW(3)=YZX*ZW(1) + YZY*ZW(2) + YZZ*EZ
C
C  Vertical electric field
      YW(3)=EZ
C
C  Magnetic reference antenna?
      IF(LREF.EQ.69) GO TO 51Ø
      DO 5ØØ I=1,3
      YW(I)=ZW(I)
  5ØØ CONTINUE
  51Ø CONTINUE
C
C  Generate and add local noise
C
      DO 52Ø I=1, 3
      CALL GAUSS(IR2,IR1,Ø.Ø,SIGLCL,GN)
      YW(I)=YW(I) + GN
  52Ø CONTINUE
C
C  Add signal
      DO 55Ø I=1, 3
      ZW(I)=ZW(I) + SR(I)*COSWAV + SI(I)*SINWAV
  55Ø CONTINUE
C
C  Detect without nonlinear processing
      DO 6ØØ I=1,3
```

```
      CALL LP(ZW(I),ZRL(I),ZIL(I))
      CALL LP(YW(I),YRL(I),YIL(I))
  6ØØ CONTINUE
C
C Apply nonlinear processing and obtain narrowband waveforms
C
      DO 61Ø I=1,3
      CALL NLP(ZW(I),PHATZ(I),NNLZ(I),ZR(I),ZI(I))
      CALL NLP(YW(I),PHATY(I),NNLY(I),YR(I),YI(I))
  61Ø CONTINUE
C
C End wideband sample
C
 1ØØØ CONTINUE
C
C Settled?
C
      IF(KN.LE.NSET) GO TO 697Ø
      K=K+1
C
C Begin narrowband sample
C
C Accumulate measurement statistics
C
C Bias Zbarl
      CALL MADD(3,1,SIGZRL,ZRL,SIGZRL)
      CALL MADD(3,1,SIGZIL,ZIL,SIGZIL)
C Bias Ybarl
      CALL MADD(3,1,SIGYRL,YRL,SIGYRL)
      CALL MADD(3,1,SIGYIL,YIL,SIGYIL)
C Bias Zbar
      CALL MADD(3,1,SIGZR,ZR,SIGZR)
      CALL MADD(3,1,SIGZI,ZI,SIGZI)
C Bias Ybar
      CALL MADD(3,1,SIGYR,YR,SIGYR)
      CALL MADD(3,1,SIGYI,YI,SIGYI)
C
C Covariance (z*) * (yT)
      CALL SMULT(ILS,1,ZI,-1.Ø,CONJ)
      CALL CMVMLT(ILS,1,ILY,ZR,CONJ,YR,YI,DUM1,DUM2,DUM3)
      CALL MADD(ILS,ILY,SIGZYR,DUM1,SIGZYR)
      CALL MADD(ILS,ILY,SIGZYI,DUM2,SIGZYI)
C
C Covariance (y*) * (yT)
      CALL SMULT(ILY,1,YI,-1.Ø,CONJ)
      CALL CMVMLT(ILY,1,ILY,YR,CONJ,YR,YI,DUM1,DUM2,DUM3)
      CALL MADD(ILY,ILY,SIGYYR,DUM1,SIGYYR)
      CALL MADD(ILY,ILY,SIGYYI,DUM2,SIGYYI)
C
C Time to make estimate?
      IF(K/KOUT*KOUT.NE.K) GO TO 699Ø
C
C Estimate bias and covariances
C
      CK=1.Ø/K
C
C Bias vectors
      CALL SMULT(3,1,SIGZRL,CK,ZBARRL)
      CALL SMULT(3,1,SIGZIL,CK,ZBARIL)
      CALL SMULT(3,1,SIGYRL,CK,YBARRL)
      CALL SMULT(3,1,SIGYIL,CK,YBARIL)
C
C Bias vectors
      CALL SMULT(3,1,SIGZR,CK,ZBARR)
      CALL SMULT(3,1,SIGZI,CK,ZBARI)
      CALL SMULT(3,1,SIGYR,CK,YBARR)
      CALL SMULT(3,1,SIGYI,CK,YBARI)
C
C Covariance Ryy
      CALL SMULT(3,3,SIGYYR,CK,RYYR)
```

```
      CALL SMULT(3,3,SIGYYI,CK,RYYI)
C
C  Covariance Rzy
      CALL SMULT(3,3,SIGZYR,CK,RZYR)
      CALL SMULT(3,3,SIGZYI,CK,RZYI)
C
C  Linear estimate
C
      CALL MSE(ILS,SR,SI,ZBARRL,ZBARIL,RMSEL)
C
C  No-ANC estimate
C
      CALL SMULT(ILS,1,ZBARR,1.Ø,SHATR)
      CALL SMULT(ILS,1,ZBARI,1.Ø,SHATI)
      CALL MSE(ILS,SR,SI,SHATR,SHATI,RMSEN)
C
C  Invert estimated covariance Ryy of reference
C
      CALL CMI(ILY,ILY2,RYYR,RYYI,RINVR,RINVI,DUM4,DUM5,DUM6,DET)
      IF(DET.NE.Ø.Ø) GO TO 56ØØ
      CALL MZERO(3,3,RINVR)
      CALL MZERO(3,3,RINVI)
 56ØØ CONTINUE
C
C  DMI estimate #Ø
C
      CALL DMI(ILS,ILY,ILY2,RZYR,RZYI,ZBARR,ZBARI,
     >  YBARR,YBARI,RXYR,RXYI,SHATR,SHATI,WR,WI,DUM3,
     >  DUM4,DUM5,DUM6,RINVR,RINVI)
      CALL MSE(ILS,SR,SI,SHATR,SHATI,RMSEØ)
C
C  DMI estimate #1
C
      CALL DMI(ILS,ILY,ILY2,RZYR,RZYI,ZBARR,ZBARI,
     >  YBARR,YBARI,RXYR,RXYI,SHATR,SHATI,WR,WI,DUM3,
     >  DUM4,DUM5,DUM6,RINVR,RINVI)
      CALL MSE(ILS,SR,SI,SHATR,SHATI,RMSE1)
C
C  DMI estimate #2
C
      CALL DMI(ILS,ILY,ILY2,RZYR,RZYI,ZBARR,ZBARI,
     >  YBARR,YBARI,RXYR,RXYI,SHATR,SHATI,WR,WI,DUM3,
     >  DUM4,DUM5,DUM6,RINVR,RINVI)
      CALL MSE(ILS,SR,SI,SHATR,SHATI,RMSE2)
C
C  Compute improvement and output results
      T=((1.Ø * K) * NW)/FSAMP
      GØ=Ø.Ø
      G1=Ø.Ø
      G2=Ø.Ø
      IF(RMSEL.EQ.Ø.Ø) GO TO 676Ø
      IF(RMSEN.EQ.Ø.Ø) GO TO 674Ø
C  Improvement due to clipping
      GØ=2Ø.Ø * ALOG1Ø(RMSEL/RMSEN)
 674Ø IF(RMSE2.EQ.Ø.Ø) GO TO 676Ø
C  Improvement added by ANC
      G1=2Ø.Ø * ALOG1Ø(RMSEN/RMSE2)
C  Total Improvement
      G2=GØ + G1
 676Ø IF(K.LT.(KMAX/2)) GO TO 677Ø
C
C  Average Improvements over last half of test
C
      NG=NG+1
      GØAVG=GØAVG + GØ
      G1AVG=G1AVG + G1
      G2AVG=G2AVG + G2
 677Ø WRITE(3,68ØØ) T, RMSEL, RMSEN, RMSE2, GØ, G1, G2
      WRITE(7,68ØØ) T, RMSEL, RMSEN, RMSE2, GØ, G1, G2
 68ØØ FORMAT(' ',F7.2,3G12.4,3F8.1)
C
```

```
      GO TO 6990
C
C  Reset NLP counters at end of settling period
C
 6970 IF(K.NE.NSET) GO TO 6990
      DO 6980 I=1,3
      NNLZ(I)=0
      NNLY(I)=0
 6980 CONTINUE
 6990 CONTINUE
 7000 CONTINUE
C
C  Output final averages and covariances
C
      G0AVG=G0AVG/NG
      G1AVG=G1AVG/NG
      G2AVG=G2AVG/NG
      WRITE(3,7900) G0AVG, G1AVG, G2AVG
      WRITE(7,7900) G0AVG, G1AVG, G2AVG
 7900 FORMAT('     AVG',37X,3F8.1)
      WRITE(7,8000)
 8000 FORMAT(/,' Zbar = ')
      WRITE(7,8010) (ZBARR(I), I=1,3), (ZBARI(I), I=1,3)
 8010 FORMAT(' [',3G12.4,'] +j [',3G12.4,']')
      WRITE(7,8020)
 8020 FORMAT(/,' Ybar = ')
      WRITE(7,8010) (YBARR(I), I=1,3), (YBARI(I), I=1,3)
      WRITE(7,8100)
 8100 FORMAT(/,' Ryy = ')
      DO 8130 I=1,ILY
      WRITE(7,8010) (RYYR(I,J), J=1,3), (RYYI(I,J), J=1,ILY)
 8130 CONTINUE
      WRITE(7,8140) DET
 8140 FORMAT(/,' Det(Ryy) = ',G12.4)
      WRITE(7,8200)
 8200 FORMAT(/,' Rxy = ')
      DO 8230 I=1,ILS
      WRITE(7,8010) (RXYR(I,J), J=1,ILY), (RXYI(I,J), J=1,ILY)
 8230 CONTINUE
      WRITE(7,8300)
 8300 FORMAT(/,' W = ')
      DO 8310 I=1,ILS
      WRITE(7,8010) (WR(I,J), J=1,ILY), (WI(I,J), J=1,ILY)
 8310 CONTINUE
      WRITE(7,8330) ISEED1, ISEED2
 8330 FORMAT(/,' Seeds = ',2I8)
C
 9000 CONTINUE
C
C
 9999 ENDFILE 7
      STOP
      END


      SUBROUTINE DMI(ILS,ILY,ILY2,RZYR,RZYI,ZBARR,ZBARI,YBARR,YBARI,
     >  RXYR,RXYI,SHATR,SHATI,WR,WI,DUM3,DUM4,DUM5,DUM6,RINVR,RINVI)
C  Estimate of signal using DMI ANC algorithm
      DIMENSION RZYR(ILS,ILY), RZYI(ILS,ILY),
     >  ZBARR(ILS), ZBARI(ILS), YBARR(ILY),
     >  YBARI(ILY), SHATR(ILS), SHATI(ILS), WR(ILS,ILY),
     >  WI(ILS,ILY), DUM4(ILY2,ILY2), DUM5(ILY2,ILY2),
     >  DUM6(ILY2,ILY2), RINVR(ILY,ILY), RINVI(ILY,ILY)
C
C  Initial estimate of covariance Rxy (WR and WI are dummies)
C
      CALL SMULT(ILS,1,SHATI,-1.0,SHATI)
      CALL CMVMLT(ILS,1,ILY,SHATR,SHATI,YBARR,YBARI,WR,WI,DUM3)
      CALL SMULT(ILS,ILY,WR,-1.0,WR)
      CALL SMULT(ILS,ILY,WI,-1.0,WI)
      CALL MADD(ILS,ILY,RZYR,WR,RXYR)
```

```
      CALL MADD(ILS,ILY,RZYI,WI,RXYI)
C
C  Compute weighting matrix W
C
      CALL CMVMLT(ILS,ILY,ILY,RXYR,RXYI,RINVR,RINVI,WR,WI,DUM3)
C
C  Calculate improvement vector
C
      CALL CMVMLT(ILS,ILY,1,WR,WI,YBARR,YBARI,SHATR,SHATI,DUM3)
C
C  Estimate
C
      CALL SMULT(ILS,1,SHATR,-1.Ø,SHATR)
      CALL SMULT(ILS,1,SHATI,-1.Ø,SHATI)
      CALL MADD(ILS,1,SHATR,ZBARR,SHATR)
      CALL MADD(ILS,1,SHATI,ZBARI,SHATI)
      RETURN
      END


      SUBROUTINE MSE(I,SR,SI,ER,EI,RMSE)
C  Mean-square error in estimate of complex vector
      DIMENSION SR(I), SI(I), ER(I), EI(I)
      RMSE=Ø.Ø
      DO 1Ø J=1,I
      RMSE=RMSE + (SR(J) - ER(J))**2
      RMSE=RMSE + (SI(J) - EI(J))**2
   1Ø CONTINUE
      RMSE=SQRT(RMSE/I)
      RETURN
      END


      SUBROUTINE ELFINC(HX,HY,EZ)
C  INCIDENT ELF FIELDS
      DIMENSION P(4),A(4),CHX(4),CHY(4),PSI(4),R(4),
     >  SIGX(4)
      COMMON /BLOCK1/ IR2,IR1,P,A,CHX,CHY,PSI,R,SIGX,PSIMIN,PSID
  1ØØ HX=Ø.Ø
      HY=Ø.Ø
      EZ=Ø.Ø
      DO 31Ø I=1,4
      IF(P(I).LE.Ø.Ø) GO TO 3ØØ
      IF(I.LT.4) GO TO 2ØØ
C  GET RANDOM AZIMUTH ANGLE FOR SOURCE #4
      CALL RANDU(IR2,IR1)
      IØ=IABS(IR1)
      PSI(4)=(IØ/32767.Ø)*PSID + PSIMIN
      CHX(4)=-SIN(PSI(4))
      CHY(4)=COS(PSI(4))
C
C  COMPUTE, DECOMPOSE, AND SUM OUTPUTS FROM NOISE SOURCES
C  ELF noise via FLM model
  2ØØ CALL GAUSS(IR2,IR1,Ø.Ø,SIGX(I),Z)
      CALL PWRRAY(IR2,IR1,R(I),A(I),Y)
      H=Z+Y
C  Incident fields
      HX=HX+H*CHX(I)
      HY=HY+H*CHY(I)
      EZ=EZ+H
  3ØØ CONTINUE
  31Ø CONTINUE
      RETURN
      END


      SUBROUTINE ELFPRM(PZ,GAMMAL,A,SIGMAX,R)
C  CALCULATION OF PARAMETERS FOR SUBROUTINE ELFNSE
C  FOR GAUSSIAN COMPONENT
C  GAMMAL=IMPUSLIVITY; GAMMA=GAMMA FUNCTION
      PX=PZ/(1.Ø + GAMMAL**2)
```

```
      SIGMAX=SQRT(PX)
C  FOR POWER=RAYLEIGH COMPONENT
      R=SQRT((PZ-PX)/GAMMA(1.Ø + 2.Ø/A))
      RETURN
      END


      FUNCTION FILTER(H,HOLD)
      DIMENSION HOLD(1ØØ), FW(1ØØ)
      COMMON /BLOCK2/ NFILT, FW
C  SAVE H
      DO 1Ø J=2,NFILT
      JM=J-1
      HOLD(J)=HOLD(JM)
   1Ø CONTINUE
      HOLD(1)=H
C  COMPUTE RESPONSE
      FILTER=Ø.Ø
      DO 2Ø J=1,NFILT
      FILTER=FILTER + HOLD(J)*FW(J)
   2Ø CONTINUE
      RETURN
      END


      FUNCTION PR(C,K)
C  PULSE RESPONSE OF FLAT, HOMOGENEOUS CONDUCTING GROUND
      IF(K.GE.2) GO TO 2ØØ
      IF(K.EQ.1) GO TO 1ØØ
C  K <= Ø
      PR=Ø.Ø
      RETURN
C  K = 1
  1ØØ PR=C
      RETURN
C  K >= 2
  2ØØ PR=C*(1.Ø/(1.Ø*K)**Ø.5 - 1.Ø/(1.Ø*K-1.Ø)**Ø.5)
      RETURN
      END


      SUBROUTINE NLP(VI,PHAT,NNL,SIHAT,SQHAT)
      COMMON /FLTR/ GAIN, T, TOTSMP, COSWAV, SINWAV
C  Signal-nulling loop with clipper
C
C  Null signal using previous estimates
      VIN=VI - SIHAT*COSWAV - SQHAT*SINWAV
C
C  Average power, find rms, set threshold
      PHAT=PHAT + VIN**2
      RMS=SQRT(PHAT/TOTSMP)
      TAUP= RMS*T
      TAUN=-RMS*T
C
C  Clip input and increment nonlinear event counter
      IF(VIN.LT.TAUP) GO TO 1Ø
      VIN=TAUP
      NNL=NNL+1
      GO TO 1ØØ
   1Ø IF(VIN.GT.TAUN) GO TO 1ØØ
      VIN=TAUN
      NNL=NNL+1
      GO TO 1ØØ
C
C  Estimate I and Q components of signal
  1ØØ SIHAT=SIHAT + VIN*COSWAV*GAIN
      SQHAT=SQHAT + VIN*SINWAV*GAIN
      RETURN
      END
```

```
      SUBROUTINE LP(VI,SIHAT,SQHAT)
      COMMON /FLTR/ GAIN, T, TOTSMP, COSWAV, SINWAV
C  Signal-nulling loop without clipper
C
C  Null signal using previous estimates
      VIN=VI - SIHAT*COSWAV - SQHAT*SINWAV
C
C  Estimate I and Q components of signal
  1ØØ SIHAT=SIHAT + VIN*COSWAV*GAIN
      SQHAT=SQHAT + VIN*SINWAV*GAIN
      RETURN
      END


      SUBROUTINE CMVMLT(I,J,K,A,B,C,D,E,F,DUM)
C  Multiplication of complex matrices
C  E + jF = (A + jB) * (C + jD)
      DIMENSION A(I,J), B(I,J), C(J,K), D(J,K), E(I,K), F(I,K),
     >  DUM(I,K)
C  Real part
      CALL MVMLT(I,J,K,A,C,E)
      CALL MVMLT(I,J,K,B,D,DUM)
      CALL SMULT(I,K,DUM,-1.Ø,DUM)
      CALL MADD(I,K,E,DUM,E)
C  Imaginary part
      CALL MVMLT(I,J,K,A,D,F)
      CALL MVMLT(I,J,K,B,C,DUM)
      CALL MADD(I,K,F,DUM,F)
      RETURN
      END


      SUBROUTINE CMI(N,N2,A,B,E,F,G,DUM1,DUM2,DET)
C  Inversion of complex matrix
C  R = A + jB;  Inverse(R) = E + jF
C  Scratch arrays: G, DUM1, DUM2; dimensions N2*N2, N2=N*2
      DIMENSION A(N,N), B(N,N), E(N,N), F(N,N),
     >  G(N2,N2), DUM1(N2,N2), DUM2(N2,N2)
C
C  Load G
C
      DO 2Ø I=1, N
      DO 1Ø J=1, N
      I1=N + I
      J1=N + J
      G(I,J)=A(I,J)
      G(I1,J1)=A(I,J)
      G(I,J1)=B(I,J)
      G(I1,J)=-B(I,J)
   1Ø CONTINUE
   2Ø CONTINUE
C
C  Invert G
C
      CALL INVERT(G,N2,DET,DUM1,DUM2)
C
C  Recover E and F
C
      DO 12Ø I=1,N
      DO 11Ø J=1,N
      J1=J+N
      E(I,J)=G(I,J)
      F(I,J)=G(I,J1)
  11Ø CONTINUE
  12Ø CONTINUE
      RETURN
      END
```